INFORMATION TO USERS

This manuscript has been reproduced from the microfilm master. UMI films the text directly from the original or copy submitted. Thus, some thesis and dissertation copies are in typewriter face, while others may be from any type of computer printer.

The quality of this reproduction is dependent upon the quality of the copy submitted. Broken or indistinct print, colored or poor quality illustrations and photographs, print bleedthrough, substandard margins, and improper alignment can adversely affect reproduction.

In the unlikely event that the author did not send UMI a complete manuscript and there are missing pages, these will be noted. Also, if unauthorized copyright material had to be removed, a note will indicate the deletion.

Oversize materials (e.g., maps, drawings, charts) are reproduced by sectioning the original, beginning at the upper left-hand corner and continuing from left to right in equal sections with small overlaps.

Photographs included in the original manuscript have been reproduced xerographically in this copy. Higher quality 6" x 9" black and white photographic prints are available for any photographs or illustrations appearing in this copy for an additional charge. Contact UMI directly to order.

Bell & Howell Information and Learning
300 North Zeeb Road, Ann Arbor, MI 48106-1346 USA
800-521-0600

The Design and Control of Scout I, A Simple Quadruped Robot

by

Kenneth S. Yamazaki

Department of Mechanical Engineering
McGill University, Montréal

A Thesis submitted to the Faculty of Graduate Studies and Research in partial fulfillment of the requirements of the degree of Master of Engineering

February 1999

To my family

Abstract

A new type of quadruped robot has been developed, the Scout class. Each leg utilizes only one actuated degree of freedom (as opposed to a typical three) to reduce complexity and cost. The design of the first of these robots, Scout I is presented. In modelling Scout, impacts are assumed instantaneous with angular momentum being conserved about the impacting toe. Stance phases are modelled as a double inverted pendulum with one input and a pin joint with the ground. Walking controllers requiring a minimum of sensing are then developed and examined both in simulation and experiments. Small errors in impact modelling coupled with high setpoint sensitivity are found to result in discrepancies. However, despite this stable open loop walking is achieved in all cases examined. Additional behaviors for Scout are presented, including turning, side stepping, sitting and laying down, and step and stair climbing.

Résumé

Un nouveau type de robot-quadrupède est en développement: la catégorie Scout. Chaque jambe utilise uniquement un seul (par opprosition à trois) degré de liberté afin de réduire la complexité et le coût. Le design du premier de ces robots, Scout I, est présenté. En développant le modèle de Scout, les impacts sont supposés instantanés et possédés une conservation de l'inertie angulaire autour du pied d'impact. Les phases de position sont modelées avec un double pendule inversé possédant une entrée ainsi qu'un contact ponctuel avec le sol. Des contrôleurs de marche nécessitant un minimum de capacité sensorielle sont développés puis examinés en simulation et d'une façon expérimentale. De petites erreurs dans la modélisation de l'impact couplées à une grande sensibilité des données recueillies causent des divergences dans les résultats. Cependant, en dépit de cela, la marche en boucle ouverte est accomplie dans tous les cas examinés. D'autres comportements de Scout sont présentés: tourner, marcher de côté, s'asseoir, se coucher et monter une marche et des escaliers.

Acknowledgements

Firstly, I would like to thank my supervisor Martin Buehler for providing me with the opportunity to work in such an unusual and exciting field and for the funding he provided me at the expiry of my original scholarship. His theoretical knowledge in the area of legged locomotion and his extensive practical experience was a great resource for me. I have gained an invaluable amount of knowledge and experience working in his lab.

I would also like to extend my appreciation to the Natural Sciences and Engineering Council of Canada for making this work possible by granting me an NSERC PGSA scholarship.

All of the students at the Ambulatory Robotics Laboratory (ARL) have to some extent contributed to the work in this thesis. Much of the modelling and analysis of the Scout I robot was a continuation of the work done by Anca Cocosco. My task would have been much more difficult if she had not provided a solid basis from which to work from. Nadim El-fata designed and Dave McMordie did much of the development work for the SPP/SPI system that served as the nervous system for the Scout I robot. Sami Obaid developed the gyro sensor which was critical in the experimental analyses in the thesis. Marc LeBlanc and later Geoff Hawker maintained the lab PC's and QNX, which served as the "brains" of Scout I. Geoff Hawker also assisted me in the step climbing experiments described in the thesis and Robert Battaglia designed and built some of the early components for Scout I. Martin de Lasa assisted in the initial attempts to track down impact modelling errors and helped to develop a controller that

improved leg tracking. Mojtaba Ahmadi was always available to explain how things worked in the lab, especially with the Unix system and Latex. Joseph Sarkis did some initial investigations into the accuracy of one of the simulation packages used in this thesis. Finally, Iyad Abdul-baki, Katja Dauster, Liana Mitrea, Gregory Petryk, and Shervin Talebinejad while perhaps not providing concrete support certainly helped to make ARL such a good environment to work and learn in.

I would also like to thank the staff at the Centre for Intelligent Machines (CIM), particularly Marlene Gray, Kathleen VanderNoot, Ornella Cavaliere, and Jan Binder for keeping everything running smoothly, thus allowing me to concentrate on my work. Finally, I would like to thank Alain Domercq for providing the French translation of my abstract and Kathleen VanderNoot for finding my errors when I entered it into Latex.

Contents

List of Figures

List of Tables

Chapter 1

Introduction

1.1 Motivation

Mobile robots have the potential to perform a wide variety of roles for the benefit of society. Indeed, they have already seen limited deployment in performing hazardous or tedious tasks such as bomb disposal, nuclear power plant inspection and maintenance, forest management, and space exploration, to name a few. However, issues such as cost, reliability, adequate payload, endurance, navigation, sensing, and sufficient mobility have and continue to plague these machines.

This work focuses primarily on the mobility issue. While wheeled or tracked vehicles excel in relatively flat areas, animals are capable of traversing virtually any terrain. This extraordinary feat is achieved by the use of arms and legs instead of tracks and wheels. It is primarily for this reason that legged locomotion is studied. With sufficient development, a legged robot has the potential to traverse much more rugged terrain than current wheeled or tracked platforms. In addition to enhanced mobility, legged robots also tend to be very visually appealing. This fact opens up entertainment applications for legged robots in the forms of toys or as theme park attractions. However, for these objectives to become a reality work must focus on the development of stable, autonomous, agile, and cheap robots.

1.2 Historical Background

The desire to develop a legged machine has existed for hundreds of years. However, it has only been in the last half century with the advances of technology that this goal has become achievable. A large number of legged robots have been built to date, and only the most relevant will be listed. They will be divided into static and dynamic machines.

1.2.1 Static Machines

The problem of stability can be solved by keeping the center of mass of the machine within the polygon of support formed by the supporting feet and keeping speeds low enough to minimize dynamic effects. This approach is termed static locomotion and it typically requires that the robot have at least four legs so that three can provide support while one moves. By incorporating feet to provide a base of support, it is possible to reduce the number of legs to (as little) as two.

The earliest machines, lacking computer technology coordinated their legs by employing a fixed gait. That is the motion of the legs followed a repeating pattern. McGhee's four-legged Phony Pony built in 1967 and described by Rosheim [40] utilized an electronic sequencer made of flip-flops to coordinate this motion while Morrison's eight-legged Iron Mule Train [31] regulated walking with a cam-driven lever system. These early attempts could only harness a small fraction of the potential of legged locomotion; marginally increased mobility at the cost of a great deal of speed and efficiency. With the advent of computer control, the use of a completely fixed gait was abandoned, although robots such as Melcrab-1, Melcrab-2 [20] and Dante II [47] have successfully utilized a partially fixed gait. In July of 1994, the eight legged robot Dante II successfully descended into the volcano Mount Spurr in Alaska (Figure 1.1).

Figure 1.1: The Dante II Robot

One notable exception in the 1960's to using a fixed gait was the GE Quadruped developed by Mosher [32]. The robot's "controller" was a human operator that rode inside the vehicle. The limbs of the quadruped were teleoperated and instrumented with force feedback to give the operator a better feel for the machine. With such a sophisticated "controller", the 1350 kg machine displayed remarkable agility (Figure 1.2). However, the quadruped required intense concentration to use and resulted in rapid operator fatigue.

Figure 1.2: The GE Quadruped

In 1979, Hirose [15, 39] developed one of the first computer controlled quadrupeds, PV-II. This 10 kg robot was able to walk on flat ground using a static gait and negotiate a flight of shallow stairs using a simple reflex-type motion (Figure 1.3).

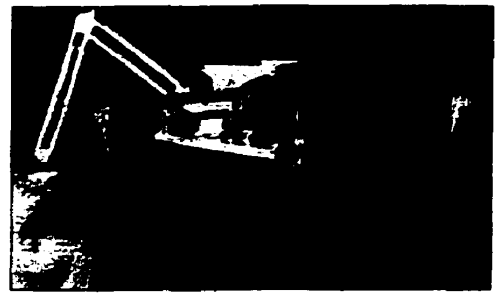

Figure 1.3: The PV-II Robot

During the 1980's, a large number of computer controlled robots employing a static gait were developed. Machines such as the 450 kg Odetics hexapods [5, 6, 40] were demonstrated in indoor environments by walking, climbing stairs, and getting in and out of the back of a pickup truck. At Ohio State University the Adaptive Suspension Vehicle [40, 45, 46], a six-legged 2700 kg robot was developed for outdoor use with an operator providing supervisory control. Figure 1.4 details one of the Odetics hexapods and the Adaptive Suspension Vehicle.

Figure 1.4: An Odetics Hexapod (Left) and the Adaptive Suspension Vehicle (Right)

During the 1990's as computers and control methods became more sophisticated, bipeds were developed that could negotiate stairs using a static gait, such as the SD-2

[12]. New types of machines employing a static walking gait such as the ParaWalker-II [35] continue to be developed to this day.

1.2.2 Dynamic Machines

Walking robots employing a static gait can harness many of the advantages of legged locomotion. However, to maintain balance they must by necessity be slow and often employ the use of a large number of legs, increasing mechanical complexity. An alternate approach is to move dynamically where the upright body acts like an inverted pendulum and must be continuously controlled to remain upright. This is the mode of operation of all mammals when moving at anything but a very slow walk. Based on the unstable dynamics of the system, increased mobility is possible with fewer (less complicated) legs. This, however is at the cost of more complex control for active balance.

The first actively balanced hopper was developed by Matsuoka in 1980 [24, 39]. It was a planar one-legged hopping machine that operated by sliding on a plane that was inclined at 10 deg (0.175 rad) with the horizontal. In 1981, Miura and Shimoyama [30, 39] developed the first 3D actively balanced robot. This biped walked on stiff legs, resembling a human on stilts.

Much of the early work in dynamic legged locomotion was done by Raibert at MIT. During the 1980's, he developed one-, two-, and four-legged hydraulically powered hopping robots that could balance and locomote on flat ground based on variations of a very simple three part control algorithm [39, 40]. He also investigated the negotiating of simple obstacles, such as stairs (Hogins and Raibert 1991 [17]). Figure 1.5 details the quadruped developed by Raibert.

Figure 1.5: The MIT Quadruped

By utilizing dynamic gaits, biped robots became more feasible and many two-legged machines were developed. At Wasada University, a series of bipeds were created by Kato. His WL-10RD [40, 43] was an 80 kg robot with six actuated degrees of freedom per leg. In 1984, it became the first of the series to walk dynamically. During single leg support, it moved by keeping its zero moment point (the point on the ground where the angular momentum of the robot is zero) within the footprint of the supporting foot. Leg transition was accomplished having the robot fall forwards and impact on its other foot. Dunn and Howe [9, 10] developed a biped which moved with a constant body height. During impacts with the ground, the angular momentum about the impacting leg was assumed to be conserved. In 1996, Honda introduced the most impressive biped to date, the P2 (Figure 1.6). This 1.8 m tall 210 kg robot was demonstrated walking, turning, and climbing a flight of stairs. Very little literature currently exists on the control of this robot, although it is speculated to be based on zero momentum point (ZMP).

Quadrupeds capable of dynamic walking also continue to be developed. Hirose's Titan VI [16] built around 1995 utilized four actuated degrees of freedom per leg plus a one actuated degree of freedom back to assist in stair climbing. Scamper [11], also developed around 1995 utilzed an actuated rotary knee and hip (eight actuated

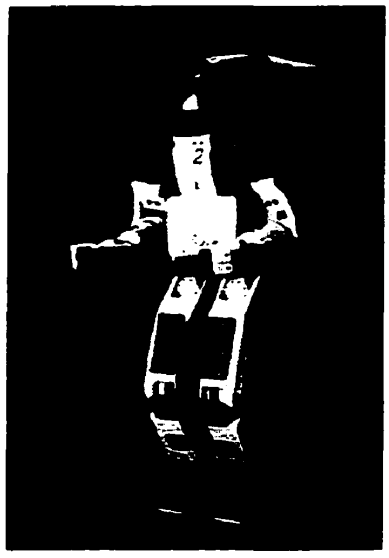

Figure 1.6: The Honda Biped Robot, P2

degrees of freedom total) to realize a bounce gait. Figure 1.7 details the Scamper robot.

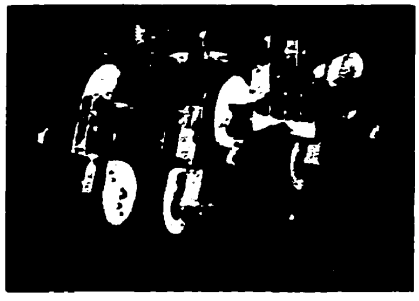

Figure 1.7: The Scamper Robot

1.3 Work at the Ambulatory Robotics Laboratory

The Ambulatory Robotics Laboratory (ARL) at McGill University's Centre for Intelligent Machines (CIM) was founded in 1991 by Martin Buehler. Research at this lab has focused on the final goal of developing a fully autonomous and affordable legged platform. All of the robots developed have been dynamic machines.

The first robot developed was the ARL Monopod I [13, 14], which borrowed heavily from Raibert's work. Research on this machine and its successor, the ARL Monopod II [1, 2] focused on reducing energy consumption by incorporating electric actuation and hip compliance to the original Raibert design. The ARL Monopod II (Figure 1.8) is currently the most energy efficient electrically actuated legged robot in the world, consuming an average mechanical power of 68 W at 1.25 $\frac{m}{s}$.

The Compliant Articulated Robotic Leg (CARL) [27, 28] was the second leg developed at ARL. Work here focused on the development of new mechanical technologies for legged locomotion, particularly in the area of light-weight transmission systems. Figure 1.8 details this robot.

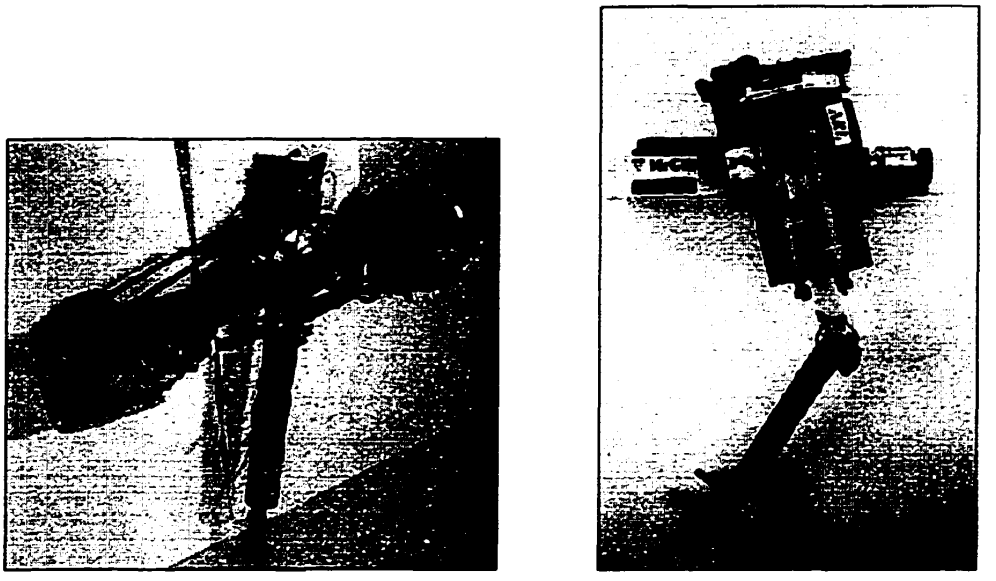

Figure 1.8: The Monopod II (Left) and CARL (Right) Developed at ARL

Current work at ARL revolves around two new quadrupeds, Scout I (Figure 2.1) and Scout II (Figure 1.9) [7, 8]. These robots employ a mechanically simple design, having only one actuated degree of freedom per leg. This idea is in contrast to many of the current quadrupeds in existence which typically utilize three actuated degrees of freedom per leg or twelve in total. The reduced degrees of freedom should work to reduce cost while also increasing mechanical reliability. Research is currently focused

on developing a wide range of behaviors for the robots using a variety of different leg types. Using simple stiff legs, walking and stair climbing is being examined. Walking and running controllers are being developed using legs with a compliant prismatic joint. Finally, trotting with legs utilizing a lockable passive knee joint is being developed.

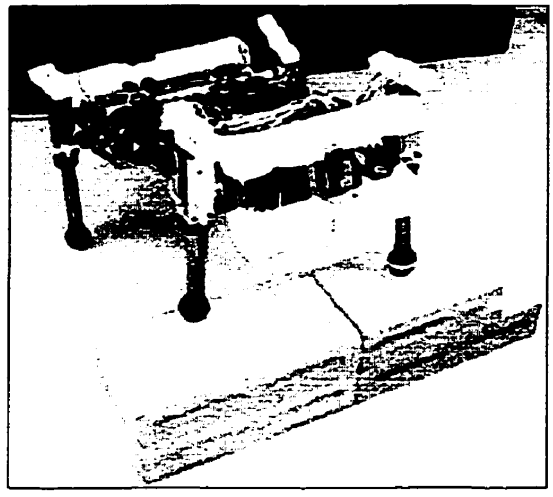

Figure 1.9: The Scout II Robot

1.4 Contributions and Thesis Organization

This thesis is organized as follows. Chapter 2 presents the design of the Scout I robot and all of its subsystems. This was robot was used for most of the experimental work of this thesis. The robot is then modelled in Chapter 3, expanding on the work of Cocosco [8]. A simple walking controller, originally proposed by Cocosco is then presented and analyzed in both simulation and experiment. The discrepancies between theory and experiment are examined in detail. Chapter 4 presents a variety of other behaviors for Scout I or Scout II. These include a different type of walking controller plus controllers for turning, side stepping, sitting down, laying down, and step and stair climbing. Finally, in Chapter 5 future work is proposed.

Chapter 2

The Scout I Robot

2.1 Introduction

Scout I (Figure 2.1) was the first robot developed at the Ambulatory Robotics Laboratory to demonstrate the feasibility of a robot walking on stiff legs based on the momentum transfer principle. It was also used as a testbed for a variety of new sensors and other systems.

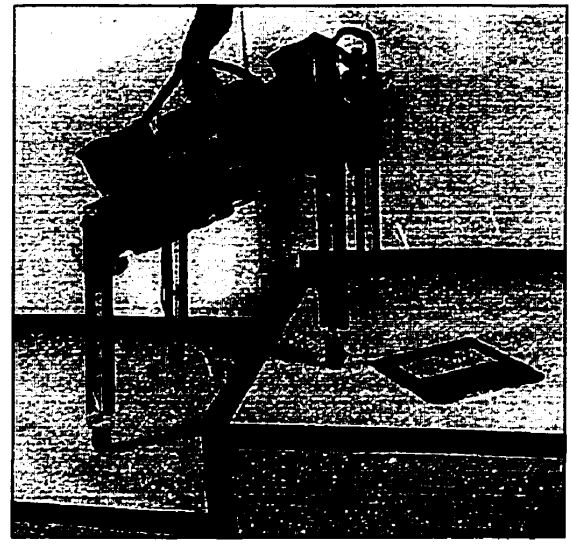

Figure 2.1: The Scout I Robot

This chapter describes the Scout I robot, which was used in the majority of experiments in this thesis. It is divided into a number of sections corresponding to the various subsystems on the robot. Each section is intended to provide a basic knowledge of the subsystem while attempting to give some insight into the reasoning behind its design.

To begin with, a number of definitions are required. Figure 2.2 shows a top view of Scout I. It defines the convention for naming the legs and as well as the directionality of the robot. As can be seen from the figure, the rear legs are spaced farther apart than the front legs. This was intended to allow the front and back legs to cross without interfering. The decision to place the back legs on the outside was motivated by observations of nature. When a dog runs at high speed, its front legs cross its back legs by passing in between the back legs. This was documented by Muybridge [34] using photographic techniques in the 1800's.

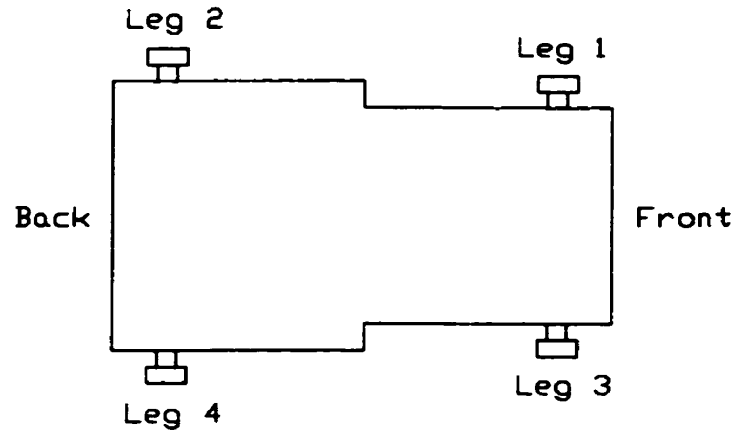

Figure 2.2: Top View of Scout I

Figure 2.3 shows a side view of Scout I. It defines the leg angle conventions. Angles ϕ_1, ϕ_2, ϕ_3, and ϕ_4 correspond to legs 1, 2, 3, and 4 respectively.

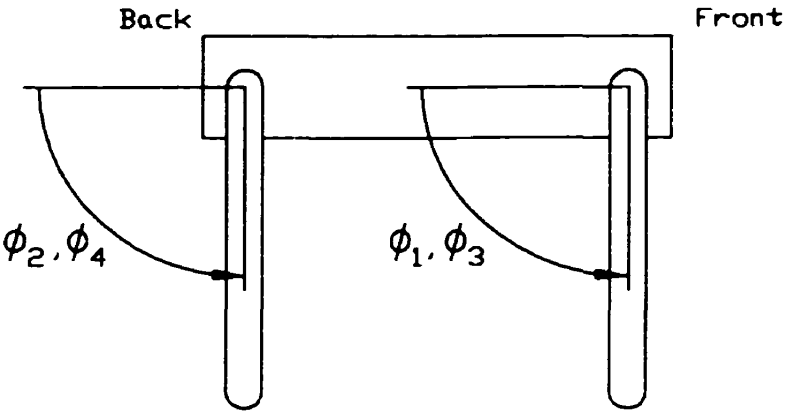

Figure 2.3: Side View of Scout I

2.2 R/C Servo Actuators

R/C servos were selected as Scout I's actuators. These systems, normally used in radio controlled aircraft were very attractive for a number of reasons, detailed below.

- They came as a complete unit, with motor, position sensor, control electronics, and gearhead all in one package. See Figure 2.4.
- Low cost, due to their wide use in R/C modelling. The typical price varied from $20 to $140 CAN depending on the quality of the servo and they were available from a variety of distributers, Sunset Radio Control [42] and Tower Hobbies [44] being examples.
- Easy interfacing. There were only three input signals, consisting of:
  1. Ground.
  2. Power. This was typically in the range of 5 to 6 volts.
  3. Control signal. This consisted of a pulse whose duration (typically 1 to 2 ms) was translated into a commanded position. The pulse was repeated every 8 to 12 ms. See Figure 2.5.

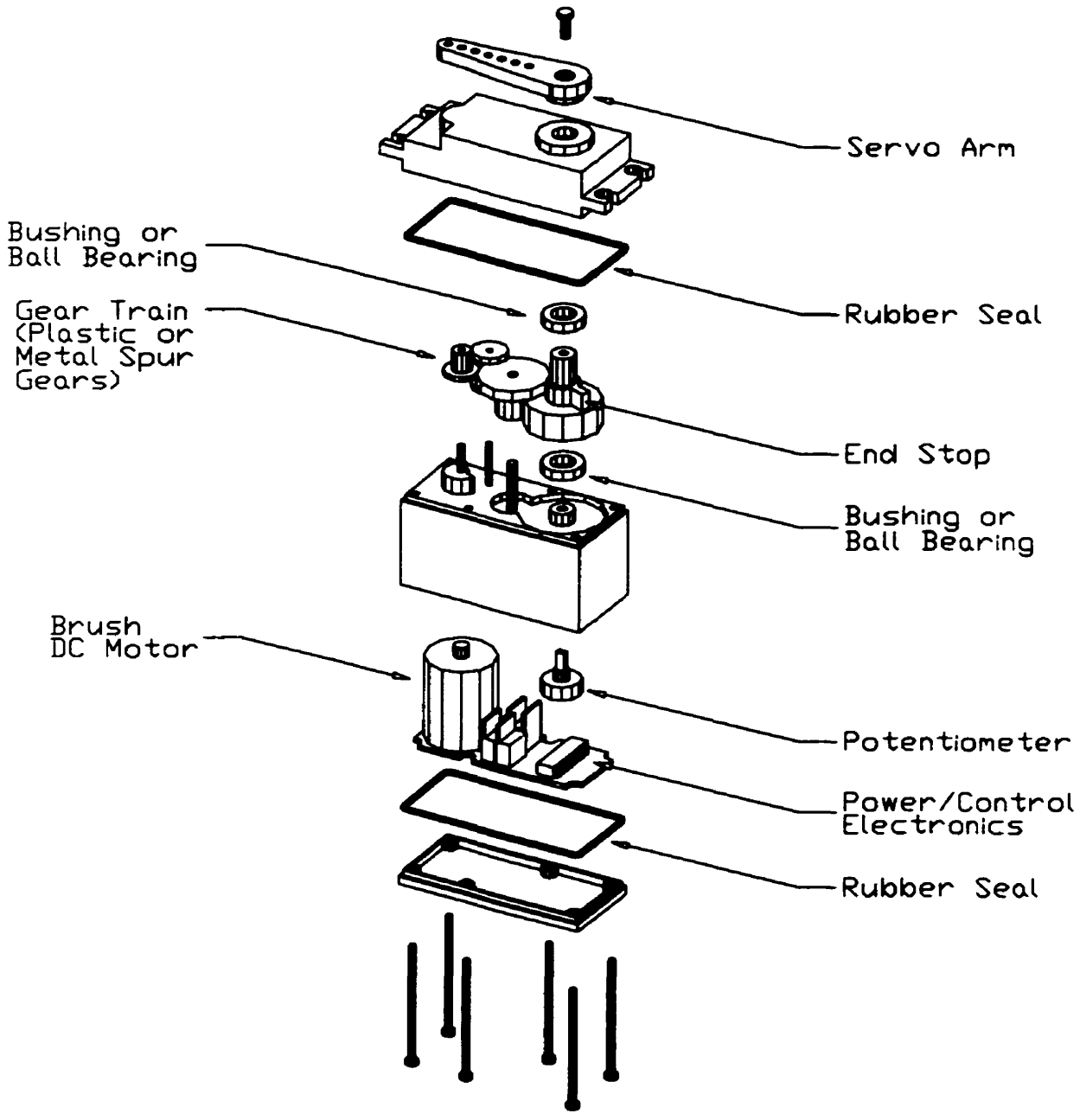

Figure 2.4: An R/C Servo (Exploded View)

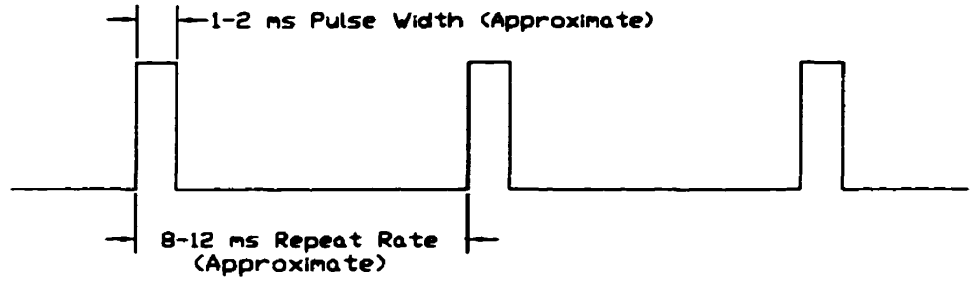

Figure 2.5: Control Waveform for an R/C Servo

Two different types of R/C servo motors were tested on Scout I. These two servos were selected for their high quality and performance characteristics. In its original configuration, two Airtronics (Model 94158) were used at the front and two Hitec (Model HS-805BBJ) were used at the back of Scout I. Later, to increase available torque and symmetry, Hitec servos were used in all four locations. The characteristics of each are summarized in Table 2.1 below.

MANUFACTURER (MODEL NUMBER)	RATED TORQUE	RATED SPEED	RANGE OF TRAVEL	MASS	COST (CAN)
Airtronics (94158)	0.91 Nm	1.9 rps	240 deg	60 g	$133.00
Hitec (HS-805BBJ)	1.96 Nm	1.0 rps	200 deg	140 g	$67.00

Table 2.1: The R/C Servos On Scout I

While the R/C servos had a number of appealing characteristics, the reliance on the built-in controller resulted in limitations. The slow command rate and inability to directly control the torque applied by the motor resulted in delays and tracking errors. However, these problems were reduced by the application of a leg controller in software, described by

$$\phi_{commanded} = \phi_{desired} + K_p(\phi_{desired} - \phi_{actual}) + K_{offset}. \quad (2.1)$$

The effectiveness of this controller is demonstrated in Figure 2.6 which shows the response of leg 4 to two step inputs under a number of different conditions. Under no load and with no leg controller the response was generally good with a small steady-state error. However, when a 0.56 kg mass was applied at a distance of 0.18 m from the leg joint (corresponding to 0.99 Nm or approximately half of the rated stall torque of the servo), the result was a significant steady-state error of 5 degrees. The effectiveness of the leg controller (2.1) was demonstrated when it was applied with K_p=1.0 and K_{offset}=-4.5 degrees under the same half load conditions. The result was a significant reduction in the steady-state error. K_p and K_{offset} were selected experimentally, as was the case for the ramp walking tests in Chapter 3.

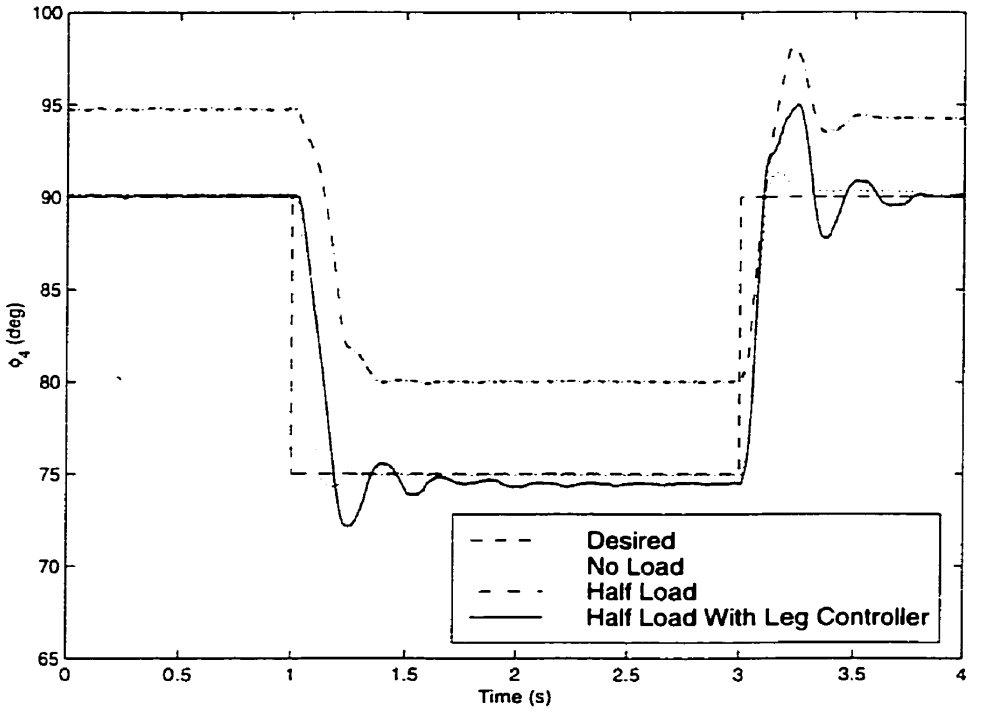

Figure 2.6: Leg Response to Step Inputs

2.3 Sensors

A variety of sensors were mounted and tested on Scout I. A listing is included below.

- Joint angle measurements were made possible by tapping into the R/C servo motor potentiometers (Figure 2.4). This allowed the tracking of the legs to be evaluated and some additional feedback control to be applied (2.1).

- Two roller lever switches (Radio Shack InterTAN [18] Model 275-017) were mounted, one near a front toe and one near a back toe. These detected contact with the ground. Figure 2.7 details one of these sensors. The roller had a diameter of approximately 5 mm.

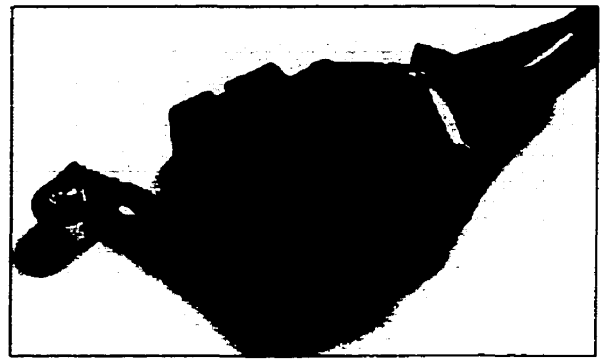

Figure 2.7: Contact Sensor

- Two infrared proximity sensors manufactured by STM [41] (Amplifier Model V6BNS47 with Reflective Sensor Model RL50) were mounted, one near a front toe and one near a back toe. Figure 2.8 displays a sensor head and amplifier. The sensor head, measuring approximately 5 mm in diameter is the cylinder in the foreground and the amplifier is the box in the background. By using the analog output from these sensors, a rough distance to the ground could be determined. This provided an alternate method other than the contact sensors for detecting touchdown. However, the sensor output's dependence on both the surface reflectance and angle of incidence complicated the distance measurement.

This relationship has been studied in more detail by Petryk [37] and Petryk and Buehler [36].

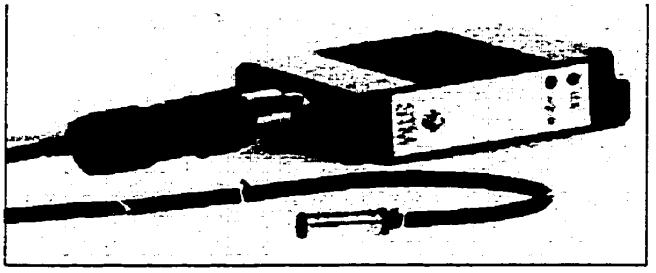

Figure 2.8: STM Infrared Sensor Head and Amplifier

- Two accelerometers (Analog Devices Model ADXL05 [3]) were mounted, one near a front toe and one near a back toe. By assuming that gravity was the only acceleration affecting the sensor currently in touchdown, the leg angle with respect to the ground could be measured. Since the angle of the legs with respect to the body could also be measured (see first item), the body angle with respect to the ground could be calculated. Vibrations generated from the R/C servos introduced a large amount of noise to the measurement, however. Figure 2.9 details one accelerometer. The sensor measured approximately 9 mm in diameter.

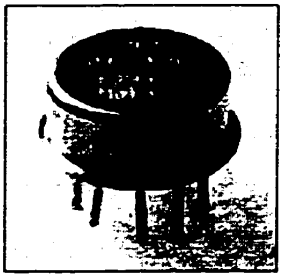

Figure 2.9: Analog Devices Accelerometer

- A small black and white camera (Marshall Electronics [22] Model Number V-X007-PCB) with UHF transmitter (TV Genie TR-200) was mounted on Scout

I to evaluate picture stability in the presence of body rocking and impacts with the ground. With a wide angle lens, the picture was stable enough to monitor the progress of the robot. Figure 2.10 shows the transmitter on the left and the camera on the right. The transmitter base measured approximately 72 mm by 88 mm.

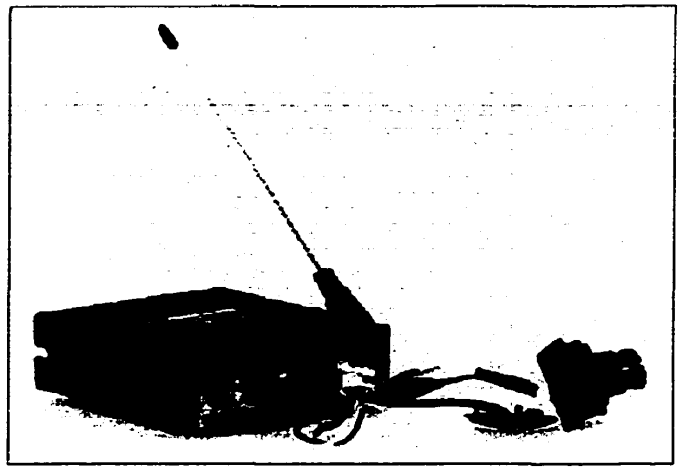

Figure 2.10: Camera with Transmitter

- A low cost solid state gyroscope manufactured by Murata [33] (Model Number ENC-05EA) was mounted on Scout I's body to measure angular velocity. Body angle was determined by integrating the signal and periodically resetting when all legs were on the ground (when body angle could be determined from kinematics only). Since this resetting occurred more than once per second, drift was not a problem. In addition, the range of the sensor was found to be considerably better than specified by the manufacturer. Where as the gyroscope was rated to $\pm 80 \frac{deg}{s}$ ($1.40 \frac{rad}{s}$), it was found to be accurate up to and including $\pm 450 \frac{deg}{s}$ ($7.85 \frac{rad}{s}$) with an absolute error of less than $9 \frac{deg}{s}$ ($0.157 \frac{rad}{s}$) at maximum angular velocity. Most of the testing of this sensor was performed by Sami Obaid at ARL. Figure 2.11 details the gyroscope. The sensor had a footprint of approximately 9 mm by 22 mm.

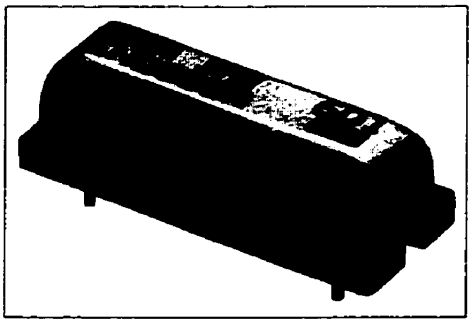

Figure 2.11: Murata Gyroscope

- A fluid-based inclinometer manufactured by Applied Geomechanics [4] (Model Number 900-45T) was mounted on the body of Scout I to measure its angle with respect to the horizontal. Figure 2.12 details this sensor. It had a footprint of approximately 51 mm by 51 mm. The inclinometer was generally not

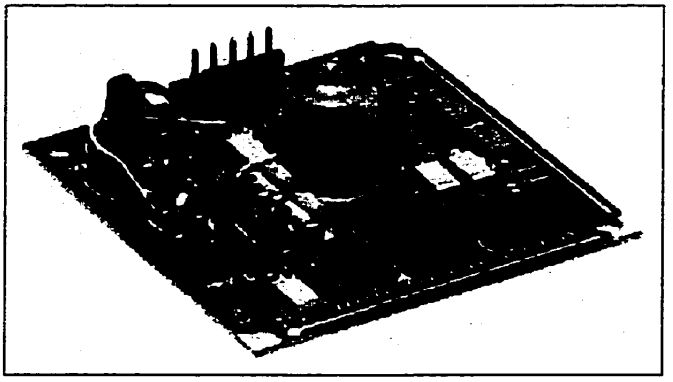

Figure 2.12: Applied Geomechanics Inclinometer

successful in this application for two primary reasons. Firstly, the sensor measured angle based on the inclination of the fluid in the central bubble assuming that gravity was the only acceleration affecting that inclination. However, the sensor was also affected by the accelerations of the robot. These were far from negligible. Secondly, the bandwidth of the sensor was considerably less than the manufacturer had specified. Figure 2.13 shows the experimentally determined frequency response plots of the sensor. Two different excitation amplitudes with two different viscosity fluids were examined. One fluid was designed to provide

a critically damped response to a step input while the second was designed to provide a faster response. The top plot clearly indicates that the magnitude of the sensor output fell off as the input increased beyond 0.5 Hz. The bottom plot indicates that the sensor output lagged significantly behind the input even at that frequency. The data provided by Applied Geomechanics is also shown in Figure 2.13 for reference.

Nine sensors eventually became the core sensors on Scout I. The wiring of these sensors is located in Appendix A.

- 4 joint angle sensors.
- 2 contact sensors.
- 2 infrared proximity sensors.
- 1 gyroscope.

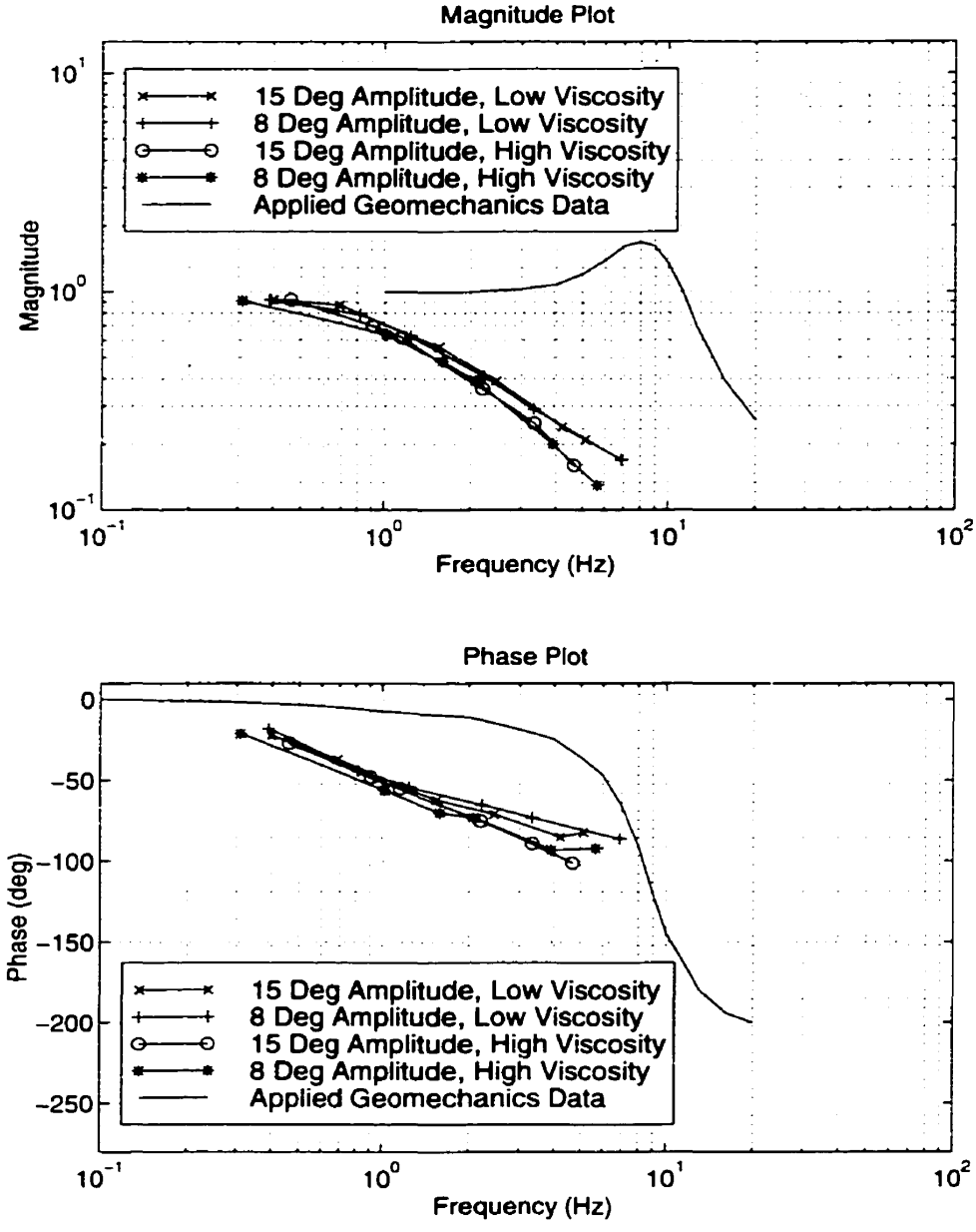

Figure 2.13: The frequency response of the Applied Geomechanics inclinometer, based on experimental data.

2.4 Electronics and Power

2.4.1 The SPP/SPI System

Scout I's various sensors, actuators, and LED outputs were interfaced to its controlling computer using an SPP/SPI (Standard Parallel Port/Serial Peripheral Interface) system. The system was designed by Nadim El-fata for ARL and developed by Dave McMordie and the author. Its design enabled up to 8 outputs and 8 inputs to be driven and read through a single standard PC parallel port with a total communication time of 120 μsec. The system consisted of a multiplexer board which interfaced the parallel port to a variety of I/O modules compatible with the SPI standard [25],[26]. Scout I utilized the following I/O modules:

- ADIO (Analog to Digital Input Output Module). This module was designed to read one analog voltage input with 12-bits of resolution. On Scout I, it was used to read the majority of its sensors. The module could be configured for use in an electrically isolated or an electrically nonisolated mode, both of which were used on the robot.

- DIN (Digital Input Module). This module was designed to read in up to ten high/low inputs. It was utilized on Scout I to read the two contact sensors.

- RCIO/DOUT (R/C Servo Input Output Module/Digital Output Module). This module was developed with dual functionality. As an RCIO, it was designed to drive up to two R/C servos and as a DOUT, it was designed to drive up to eight high/low outputs. Scout I used the module in both configurations to drive the leg actuators and a set of eight LEDs. The module was designed to ignore a communication if it was sent a zero.

Figure 2.14 provides a general overview of the SPP/SPI system on Scout I. Fully detailed circuit diagrams are located in Appendix A.

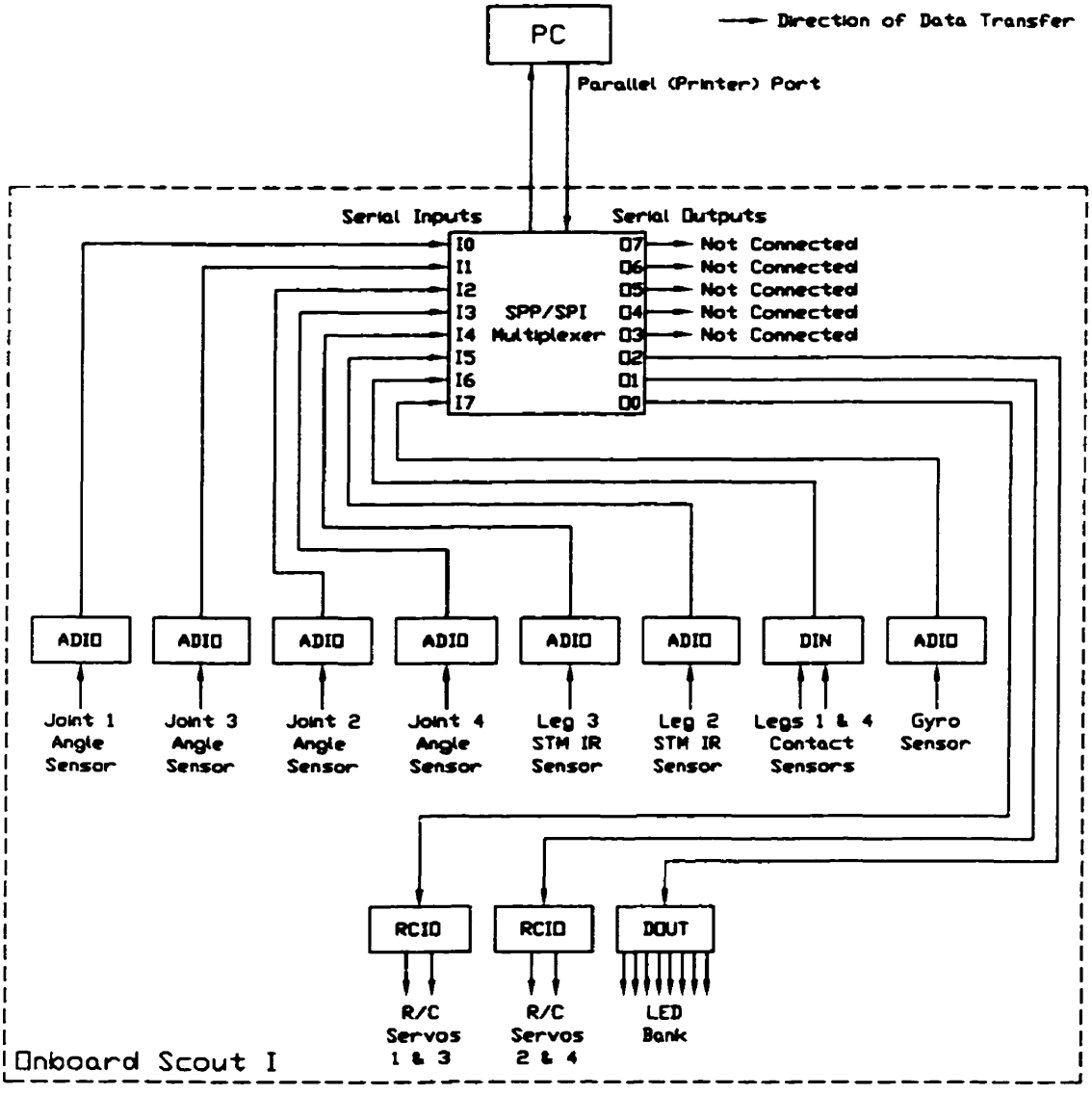

Figure 2.14: SPP/SPI System On Scout I

2.4.2 Power

The decision to mount batteries on Scout I was motivated by the desire to increase autonomy. In addition, the reduced amount of wiring running into the robot provided less disturbances to the robot's dynamics.

Two nickel-cadmium battery packs, normally used in R/C applications were mounted on Scout I. Each pack consisted of five 1.3 Ahr cells in series and produced a nominal 6V for the robot's systems. Power was distributed so that one battery pack powered the left actuators and one pack powered the right actuators. This was done because the motion of Scout I generally required the use of both front or both back actuators in parallel. With this distribution, power was being provided by both battery packs when this occured. One of the battery packs was also used to power a DC-DC converter (Lambda [21] Model Number AS10-5-5), which provided regulated +5V to the SPP/SPI system. This resulted in an additional 0.85 A load on that pack. In an attempt to even out the loading, all other systems requiring power, such as contact sensors and LEDs were powered by the other pack. Figure 2.15 details the power distribution and Table 2.2 details the robot's endurance with this power system.

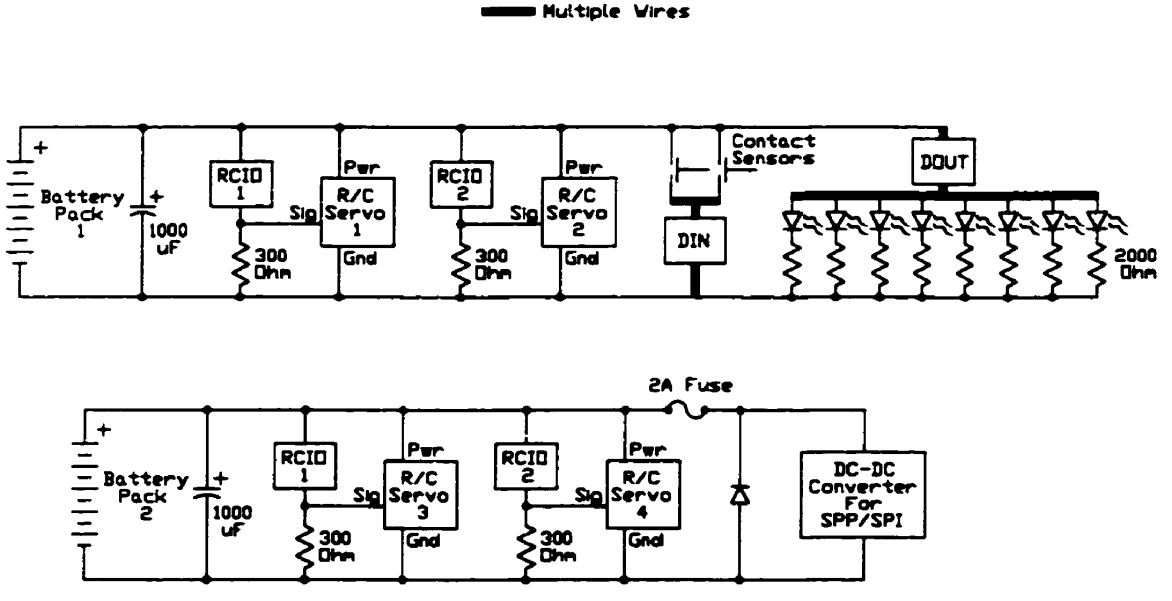

Figure 2.15: Power Distribution On Scout I

BEHAVIOR	RUN TIME
Continuous Walking	10 minutes
Standby (Electronics Powered)	90 minutes

Table 2.2: Endurance of Scout I

These values, while not exceptional provided enough freedom to carry out experiments and demonstrations without difficulty.

2.5 Structural Design

Figure 2.16 shows an assembled view of Scout I. Structurally, the backbone of the robot was the reinforced bottom platform. Directly attached to this were the R/C servos and all of the SPP/SPI input modules. A second platform was attached to the top of the servos, forming a sandwich structure. This platform mounted the two battery packs and the SPP/SPI multiplexer and output modules. The multiplexer also supported a third platform which mounted the LED bank and the DC-DC converter for supplying regulated +5V to the SPP/SPI system. This configuration provided easy access to Scout I's 18 fuses.

The legs of the robot were bolted directly to the servo arms of the R/C servo motors. At the base of each leg, a housing was provided for mounting sensors. To facilitate rapid prototyping, hot glue was typically used to secure these sensors in place. Hot glue also found application in securing the SPP/SPI modules and the top platform.

Scout I's small size (leg length approximately 0.20 m) somewhat limited the load carrying capacity of the robot. However, this sacrifice also resulted in many distinct advantages, listed below.

- Cost. The size of Scout I allowed commercial R/C systems to be used in a

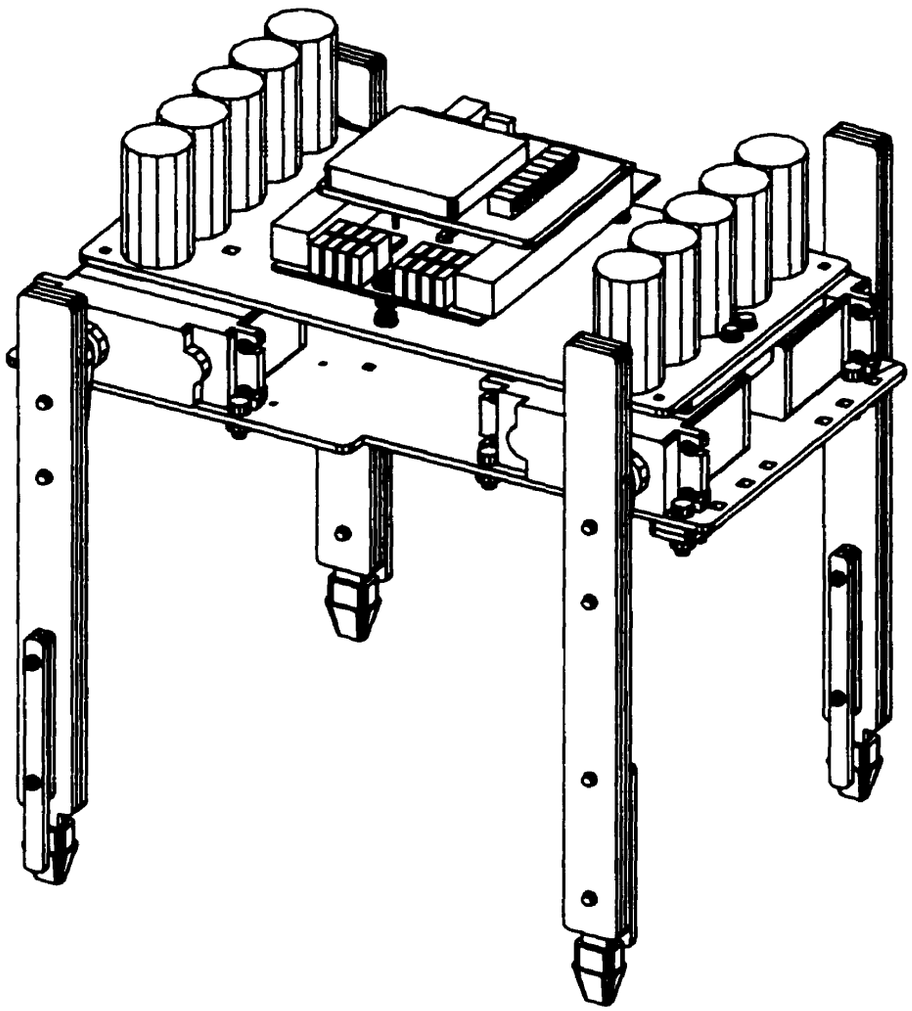

Figure 2.16: Scout I Robot Assembly

variety of areas. This eliminated some of the need for custom components to be developed for the robot, significantly reducing its price tag.

- Ease of Manufacture. Scout I's small size and light weight allowed Plexiglas to be used as the major structural component. This simplified manufacturing, as components could be built without the need for a fully equipped machine shop.

- Ease of Transport. This was appealing because the robot could easily be demonstrated outside of its native lab environment. To date, Scout I has been demonstrated at Carnegie Mellon University (December 5th, 1997) and the University of Sherbrooke (October 2nd, 1998).

- Safety. An operator could easily try out new control algorithms without the risk of injury if some unexpected behavior occurred.

For a more detailed description on the design of the various mechanical components and the assembly of the robot, refer to Appendix B.

2.6 Control Hardware and Software

2.6.1 Hardware

Scout I's "brain," a Pentium 100 based desktop PC was the only component not mounted directly on the robot. This setup was easier to implement and kept the computer safe from damage. Communication with the SPP/SPI system was provided by a light-weight ribbon-type parallel cable to minimize the cable's effect on the dynamics of the robot.

2.6.2 Software

All experimental software was written in "C" and run on the QNX realtime operating system [38]. The maximum data collection rate was 1000 Hz. Figure 2.17 shows a

flowchart of the experimental code used on Scout I. A basic description of each block is provided below. The nature of the SPP/SPI software module was that the outputs were driven and the inputs were read in the same routine. This was undesirable for the experimental code which required that the sensors be read, control algorithms applied, and then outputs driven upon the completion of those calculations. This was the reason for two calls to the SPP/SPI system during each iteration.

- Initialize. In this block, a number of start-up routines were performed. The major items are listed below.
  - The parallel port was configured for communication with the robot.
  - The values from a data file (named S0) were loaded and assigned to the appropriate variables. By modifying this file, items such as experiment duration, iteration rates, and control algorithm type could be quickly changed without requiring recompilation of the code.
- Set Thresholds. Here, thresholds for the IR sensors and the offset for the gyro (the voltage at zero angular velocity) were determined. These values tended to be environment dependent, prompting the need for a calibration at the beginning of the experiment.
- Control Timing. This block was responsible for maintaining a constant iteration rate for the experimental code.
- Get Data. Here the SPP/SPI system was called, reading the inputs and commanding the outputs on the robot. Conversions were then performed on the input data (mapping voltage to leg angle, for example) and filtering was performed on some signals. Although commands were sent, they had no effect on the outputs. This was accomplished by sending the same command to the LEDs that was sent during the last iteration and by sending zeroes to the RCIO's controlling the actuators.

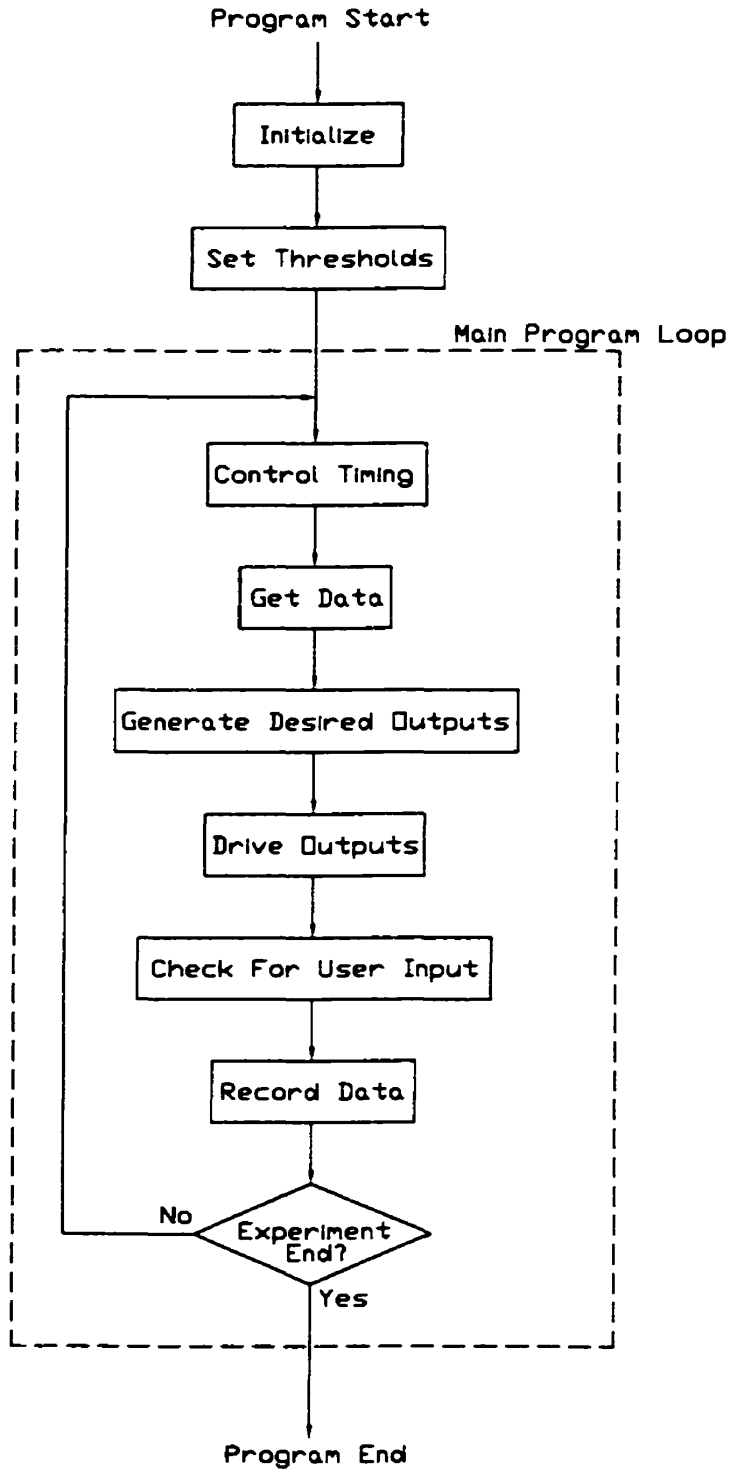

Figure 2.17: Experimental Software Flowchart

- Generate Desired Outputs. At this point, the high-level control was applied. The sensor readings and time were used to generate desired actuator angles and led values.

- Drive Outputs. Here, the SPP/SPI system was called for a second time. The command sent to the LEDs was the updated value generated from the block above. A valid command was sent to the RCIO's if enough time had elapsed since the last command. If this was not the case, zeroes were once again sent to the RCIO's. Some low level control was also applied at times to improve actuator tracking. The data collected from the sensors was simply discarded.

- Check for User Input. This block provided a user interface with the experimental software. Its purpose was to allow for occasional changes to the controller being applied and for an elegant bail out of the program, if required.

- Record Data. At this point, the relevant data was recorded to memory for downloading to a file at experiment end. A setting in the S0 file allowed this recording to occur at less frequent intervals than once per iteration.

- Experiment End? At the end of every iteration, a flag was checked to see if another iteration was to occur. If the flag indicated not, the program loop would terminate and the collected data would then be written to a file. The flag used in this check was set by either Check For User Input in the case of program bail out or by Record Data if the program end time had been reached.

2.7 Mechanical Properties

For modelling purposes, both the mass and inertia of Scout I were required. The overall mass of the robot was 2.3 kg. This included everything onboard the robot plus a small portion of the parallel cable connecting it to its computer. A mass breakdown was also calculated by summing the major components of the robot. Table 2.3 details

this breakdown. The mass of the robot was split approximately evenly amongst the four major subsystems, actuators, batteries, structure, and electronics. The robot's total calculated mass was 0.11 kg short of the actual value. This could be accounted for by various cables, glue, etc. which were not included in the calculations.

ITEM	MASS (PERCENTAGE)
Actuators	0.58 kg (26.5%)
Batteries	0.50 kg (23.0%)
Structure	0.58 kg (26.5%)
Electronics	0.53 kg (24.0%)
Total	2.19 kg (100%)

Table 2.3: Mass Distribution of Scout I

The inertia of the body was determined using both a basic calculation and from experiment. The two methods resulted in an inertia of 0.014 to 0.015 kgm^2. Descriptions of the methods are located in Appendix C. The center of mass of the robot was experimentally found to be offset 0.02 m above the plane formed by the four actuator joints.

2.8 Summary

This chapter presented Scout I, a mechanically simple legged robot that was used to test a variety of systems and control algorithms. It was actuated by four low-cost R/C servo motors whose tracking was improved by the addition of position feedback and a proportional plus offset controller. A number of sensors were evaluated on the robot as was a new hardware interface, the SPP/SPI system. The control software used with the robot was also presented. Finally, for modelling purposes the mass and inertia of the robot were found, both theoretically and experimentally. A summary

of Scout I's major characteristics (in its final configuration) is shown in Table 2.4.

DIMENSIONS	Length	0.26 m
	Width	0.23 m
	Height	0.27 m
	Leg Length	0.20 m
	Hip Separation (Between the front and back hips)	0.20 m
MASS	Overall	2.3 kg
POWER	Source	2 NiCd Battery Packs
	Total Capacity	2.6 Ahr @ 6.0 V
	Robot Endurance	10 min Continuous Walking
CONTROL	Source	External Pentium 100
	Iteration Rate	1000 Hz
ACTUATION	Source	4 R/C Servo Motors
	Rated Output (Stall)	1.96 Nm at Each Hip Joint
SENSING	Angular Rate Gyro	Body Angular Velocity
	R/C Servo Potentiometers	Leg Angles Relative to Body
	Roller Lever Switches	Foot Contact With Ground
	IR Sensors	Foot Contact With Ground

Table 2.4: Scout I's Major Characteristics

Using the experience gained with the development of Scout I, a new robot has been developed at the Ambulatory Robotics Laboratory. This robot, named Scout II (Figure 1.9) was designed by Robert Battaglia and is a larger, more robust version of Scout I. It has improved sensing and the capability to test behaviors using more sophisticated legs.

Chapter 3

An Analysis of Walking With Scout I

3.1 Introduction

In [8], Cocosco developed a mathematical model for the Scout-type of robots and three different controllers for walking. Two of these controllers were implemented on Scout II, a larger (more industrial) version of Scout I. This chapter examines more thoroughly the most promising of these three walking controllers and bridges the gap between mathematical predictions and experimental results from Scout I. Sections 3.2, 3.3, and 3.4 present the work of Cocosco [8] that is relevant to this chapter, but most of the equations and figures have been modified and expanded from their original form. This was done in order to incorporate a model parameter not previously considered and to match a notation standard implemented for the robots at the Ambulatory Robotics Laboratory.

Sections 3.2 and 3.3 present the development of a model for the Scout I robot. This is followed by Section 3.4, which details a simple controller for walking that utilizes a minimum of feedback, in essence being open loop. Section 3.5 next examines this walking controller in simulation using two different packages and experimentally using

the robot itself. The sensitivity of the system to both model and control parameters is also presented. Finally, Section 3.6 examines the stability of the system using all three of the above techniques.

3.2 The Scout I Model

A mathematical model for Scout I was developed based on a number of simplifying assumptions, detailed below.

1. The motion of Scout I was to be a walk (in which the robot never entirely left the ground) in a bounding motion (involving rocking of the body). This particular gait was chosen because of the limitations of the simple stiff legs on the robot. In order to advance along the ground by walking, a legged robot must swing its free legs forward while its remaining legs support the body. If Scout I attempted a gait such as a trot (in which diagonally opposing legs moved together), then toe stubbing would have occurred due to the fixed leg length (Figure 3.1a). However with a bounding-type motion, the rocking of the body would allow the free legs to swing forwards without stubbing on the ground (Figure 3.1b).

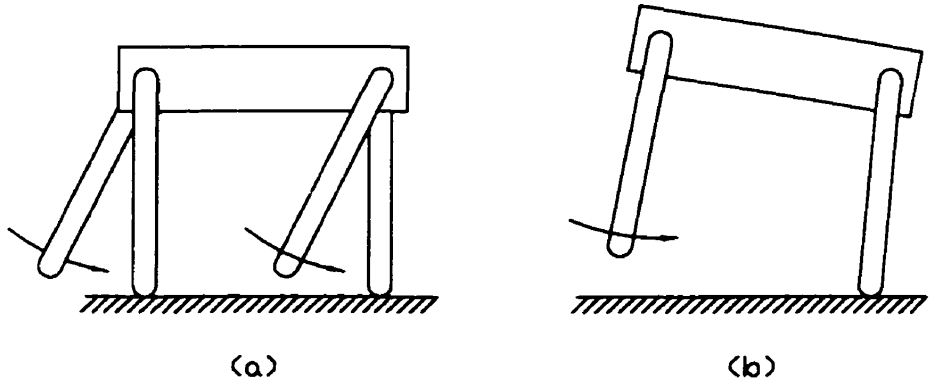

Figure 3.1: Toe stubbing when trotting (a) could be prevented when bounding (b).

This assumption of a bounding gait, in which both front legs moved together and both back legs moved together enabled the quadruped to be collapsed down

to a planar biped with one leg at the front (leg 1) and one leg at the back (leg 2). Therefore, with the exception of the experimental results, throughout the remainder of this chapter reference will only be made to leg 1 and leg 2.

2. The compliance of the body and legs was small, allowing them to be treated as rigid bodies.

3. The mass and inertia of the legs were small in comparison with the body, allowing their effects on the dynamics of the system to be neglected.

4. When a toe was in contact with the ground, it could be treated as a frictionless pin joint. This implied that no slipping occurred between the toe and the ground and that the toe made a point contact with the ground.

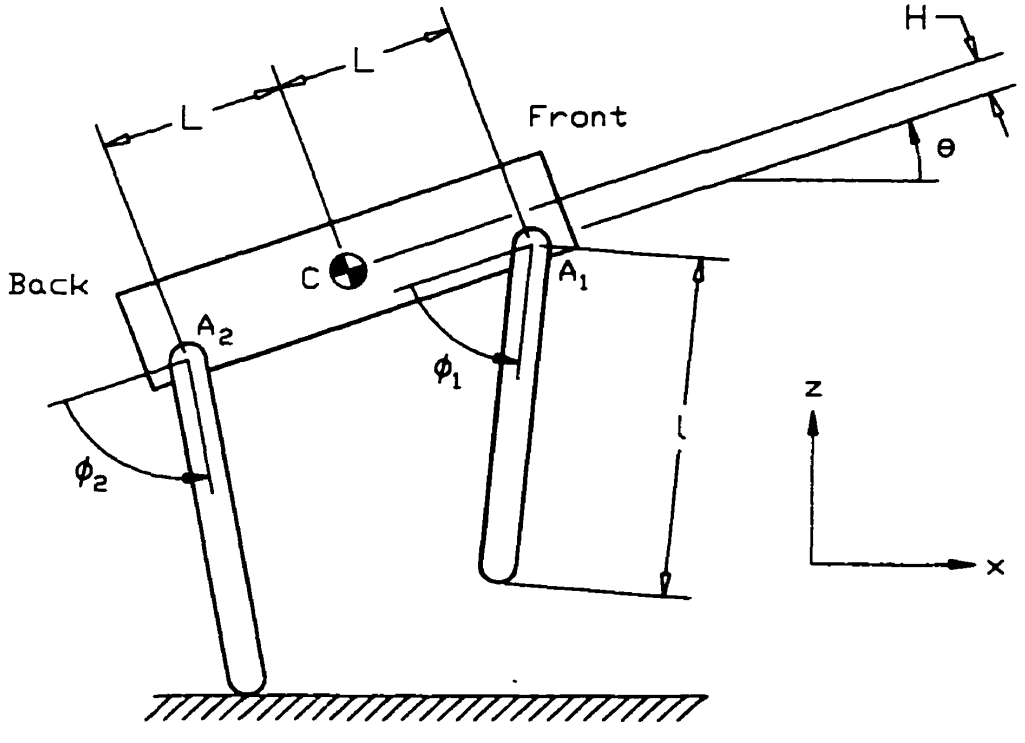

Figure 3.2: The Scout I Model

Figure 3.2 details the Scout I model. The body was connected to the legs at the hips, A_1 and A_2 which were capable of rotational motion only. The actuators were

located at the hips and provided torques to control ϕ_1 and ϕ_2. The body center of mass was located at C. Table 3.1 describes the variables used in the modelling of Scout I.

VARIABLE	DESCRIPTION
l	Leg length.
L	Half the distance between the hip joints.
H	Offset of the body center of mass from a line passing through both hip joints.
θ	Body angle with respect to the horizontal.
ϕ_1	Angle between the body and leg 1.
ϕ_2	Angle between the body and leg 2.
τ_1	Torque applied by the actuator at hip 1.
τ_2	Torque applied by the actuator at hip 2.
m	Body mass.
I	Body inertia about the center of mass.
r	Body radius of gyration ($I = mr^2$).

Table 3.1: Scout I Variables

3.3 Modelling the Phases of a Step

Each step of the bounding motion of Scout I was divided into a four distinct phases. A mathematical model was developed for each of these phases and a complete step was created by splicing the models together in the appropriate order. The condition when both front and back legs were on the ground was modelled as instantaneous; therefore for all practical purposes, Scout I was always supported by only one leg. This meant that the robot was always falling and hence the walking motion was dynamic. Figure

3.3 details a complete step. The equations associated with each phase are presented in Sections 3.3.1 and 3.3.2.

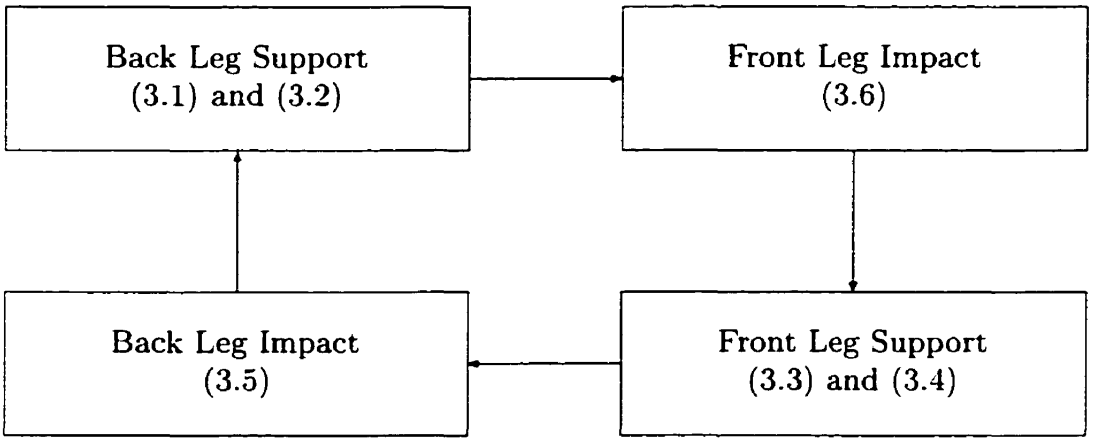

Figure 3.3: The Modelling of a Complete Step

3.3.1 Modelling Single Leg Support

When the robot was supported either on its back leg or its front leg, it was modelled as a double inverted pendulum with a torque input applied between the two links and a pin joint between the first link and the ground. This was possible due to the assumption of negligible leg mass and inertia. Thus, the leg currently in flight and the actuator associated with it had no effect on the dynamics of the system and could be ignored. Using the Lagrange method, the equations of motion were derived for the back leg support phase,

$$\begin{aligned} &[l^2 + L^2 + H^2 + r^2 + 2Ll\cos(\phi_2) + 2Hl\sin(\phi_2)]\ddot{\theta} \\ &+l[l + L\cos(\phi_2) + H\sin(\phi_2)]\ddot{\phi_2} - 2l[L\sin(\phi_2) - H\cos(\phi_2)]\dot{\theta}\dot{\phi_2} \\ &+l[-L\sin(\phi_2) + H\cos(\phi_2)]\dot{\phi_2}^2 \\ &+g[l\cos(\theta + \phi_2) + L\cos(\theta) - Hsin(\theta)] = 0 \end{aligned} \quad (3.1)$$

$$\begin{aligned} l^2\ddot{\phi}_2 + l[l + L\cos(\phi_2) + H\sin(\phi_2)]\ddot{\theta} & \\ +l[L\sin(\phi_2) - H\cos(\phi_2)]\dot{\theta}^2 + gl\cos(\theta + \phi_2) &= \frac{\tau_2}{m}. \end{aligned} \quad (3.2)$$

The same method was used to derive the equations of motion for the front leg support phase,

$$\begin{aligned} [l^2 + L^2 + H^2 + r^2 - 2Ll\cos(\phi_1) + 2Hl\sin(\phi_1)]\ddot{\theta} & \\ +l[l - L\cos(\phi_1) + H\sin(\phi_1)]\ddot{\phi}_1 + 2l[L\sin(\phi_1) + H\cos(\phi_1)]\dot{\theta}\dot{\phi}_1 & \\ +l[L\sin(\phi_1) + H\cos(\phi_1)]\dot{\phi}_1^2 & \\ +g[l\cos(\theta + \phi_1) - L\cos(\theta) - H\sin(\theta)] &= 0 \end{aligned} \quad (3.3)$$

$$\begin{aligned} l^2\ddot{\phi}_1 + l[l - L\cos(\phi_1) + H\sin(\phi_1)]\ddot{\theta} & \\ -l[L\sin(\phi_1) + H\cos(\phi_1)]\dot{\theta}^2 + gl\cos(\theta + \phi_1) &= \frac{\tau_1}{m}. \end{aligned} \quad (3.4)$$

Detailed derivations of the equations of motion are presented in Appendix D. An inspection of (3.1), (3.2), (3.3), and (3.4) indicates that these models for single leg support utilize a torque input. However, some models have assumed that the hip angles (ϕ_1, ϕ_2) and the hip angular velocities ($\dot{\phi}_1$, $\dot{\phi}_2$) could be controlled explicitly, ignoring any torque limitations. In fact, this was done for double leg support in Section 3.3.2. If the hip angles and angular velocities were desired as inputs for single leg support, then the equations of motion were completely described by (3.1) and (3.3).

The two models for single leg support were highly nonlinear (even if the hip angles and angular velocities were assumed to be explicitly controllable) and underactuated with the body angle θ being uncontrollable in the classical control sense. Exact integration of these models to find something as simple as stance durations and the

states at impact as a function of hip trajectories, $\phi_1(t)$ and $\phi_2(t)$ has to date proven intractable.

3.3.2 Modelling Double Leg Support

The transition from back to front and front to back legs occurred during an impact with the ground. The hip angles and angular velocities were assumed to be perfectly controllable. Thus the system could be considered to be perfectly rigid and the impact was modelled as instantaneous where the angular momentum about the impacting toe was conserved. This resulted in an instantaneous step change in the angular velocities of Scout I's rigid bodies while their positions remained unchanged. Using these assumptions the momentum transfer equation for back leg impact was derived,

$$\begin{aligned}\left[r^2 - L^2 + H^2 + l^2\cos(\phi_1^B - \phi_2^B) + Ll[\cos(\phi_1^B) - \cos(\phi_2^B)] + Hl[\sin(\phi_1^B) + \sin(\phi_2^B)]\right]\dot{\theta}^{B-} \\ +l[l\cos(\phi_1^B - \phi_2^B) + L\cos(\phi_1^B) + H\sin(\phi_1^B)]\dot{\phi}_1^B = \\ \left[r^2 + L^2 + H^2 + l^2 + 2l[L\cos(\phi_2^B) + H\sin(\phi_2^B)]\right]\dot{\theta}^{B+} \\ +l[l + L\cos(\phi_2^B) + H\sin(\phi_2^B)]\dot{\phi}_2^B.\end{aligned} \tag{3.5}$$

The identical method was applied to the momentum transfer equation for front leg impact and resulted in

$$\begin{aligned}\left[r^2 - L^2 + H^2 + l^2\cos(\phi_1^F - \phi_2^F) + Ll[\cos(\phi_1^F) - \cos(\phi_2^F)] + Hl[\sin(\phi_1^F) + \sin(\phi_2^F)]\right]\dot{\theta}^{F-} \\ +l[l\cos(\phi_1^F - \phi_2^F) - L\cos(\phi_2^F) + H\sin(\phi_2^F)]\dot{\phi}_2^F = \\ \left[r^2 + L^2 + H^2 + l^2 - 2l[L\cos(\phi_1^F) - H\sin(\phi_1^F)]\right]\dot{\theta}^{F+} \\ +l[l - L\cos(\phi_1^F) + H\sin(\phi_1^F)]\dot{\phi}_1^F.\end{aligned} \tag{3.6}$$

Table 3.2 details the notation used for the impact equations above. Detailed derivations are presented in Appendix E.

VARIABLE	DESCRIPTION
X^B	Value at back leg impact.
X^F	Value at front leg impact.
X^{B-}	Value just before back leg impact.
X^{F-}	Value just before front leg impact.
X^{B+}	Value just after back leg impact.
X^{F+}	Value just after front leg impact.

Table 3.2: Superscript Notation for Impact Models

3.4 The Ramp Controller

Of the three different control strategies developed by Cocosco [8], the most promising for implementation on Scout I was the ramp controller. This was due to the fact that the controller required a minimum of sensing (leg angles and toe contact with the ground) as well as requiring easily achievable leg trajectories. In fact, the controller utilized essentially no feedback and was open loop for all practical purposes.

With this controller, the front leg was commanded to a fixed angle ($\phi_1 = constant$) throughout the walking motion. This decision was chosen as a compromise between increasing speed and decreasing the chances of back toe stubbing. Intuitively, it made sense to sweep the front leg backwards while it was providing support, much like a dog does when running [34]. However, this motion would have had the tendency to lower the back of the body and since the length of the legs could not be changed, the chances of toe stubbing during the retracting of the back leg would have been very high. Alternately, the front leg could have been swept forwards while it was providing

support. This would have greatly reduced the changes of toe stubbing but would have required Scout I to take a step backwards during each complete step! Therefore, a fixed front leg angle was chosen as a reasonable compromise.

The motion of the back leg was more interesting. At back leg impact, the back leg was always commanded to a fixed angle (ϕ_2^B). During back leg support, the leg was commanded to sweep at a constant angular velocity backwards ($\dot{\phi}_2 = constant$) until the front leg impacted. This caused Scout I to take a step forwards. At front leg impact, the back leg was commanded to hold at whatever angle it had reached (ϕ_2^F). After a fixed length of time t_{start}, the back leg was retracted to ϕ_2^B over a time of $t_{retract}$. This process is detailed in Figure 3.4.

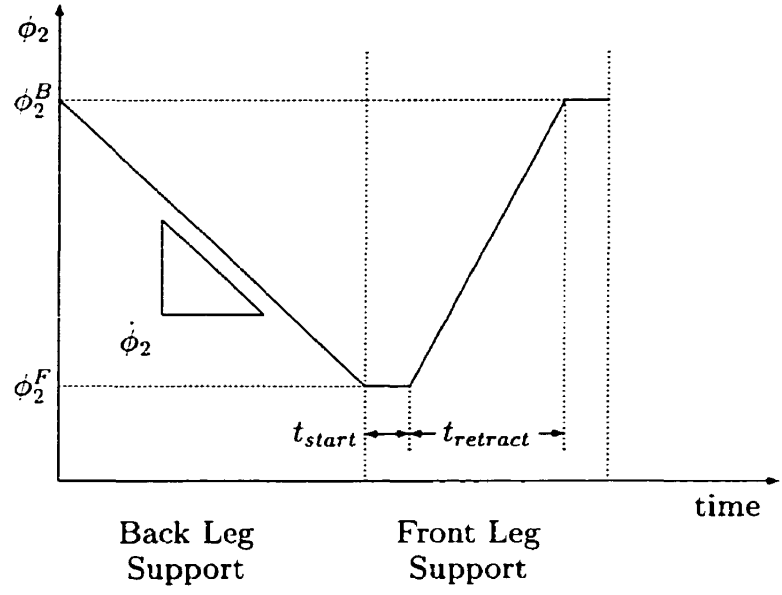

Figure 3.4: Ramp Controller Input For ϕ_2 For One Complete Step

To summarize, the controller was open loop in the sense that the back legs were commanded a fixed angular velocity, starting from a fixed angle. The minor closed loop element was that the back leg motion started when the back legs impacted (touched down) and ended when the front legs impacted.

Thus, there were five parameters which needed to be specified for the ramp controller, of which three were the most critical. These three were the fixed front leg angle

(ϕ_1), the back leg angle at back leg impact (ϕ_2^B), and the ramp slope during back leg support ($\dot{\phi}_2$). The remaining two parameters, t_{start} and $t_{retract}$ were selected to avoid toe stubbing during back leg retract and to ensure that ϕ_2^B was reached before back leg impact.

Since the mathematical models in Section 3.3 required a torque input and the ramp controller generated desired leg angles, a high gain PD-controller was used to map between the two.

3.5 Setpoint Generation and Sensitivity Analysis

In order to evaluate the ramp controller as well as the mathematical model of Scout I, a setpoint was found and analyzed using two simulation methods. The setpoint was then examined experimentally. These methods and the results are detailed in Sections 3.5.1, 3.5.2, and 3.5.3. For each investigation method, an identical set of ramp controller parameters were used. Table 3.3 details these parameters. For back leg retract, t_{start} was set to 0.04 seconds and $t_{retract}$ was set to 0.09 seconds. Figure 3.5 presents the steady state $\theta(t)$'s for one step for the major simulations and experiments that were studied. Reference will be made to this figure throughout this section.

ITEM	VALUE
ϕ_1	90.0 deg (1.571 rad)
ϕ_2^B	96.0 deg (1.676 rad)
$\dot{\phi}_2$	-42.0 $\frac{deg}{s}$ (-0.7330 $\frac{rad}{s}$)

Table 3.3: Ramp Controller Parameters

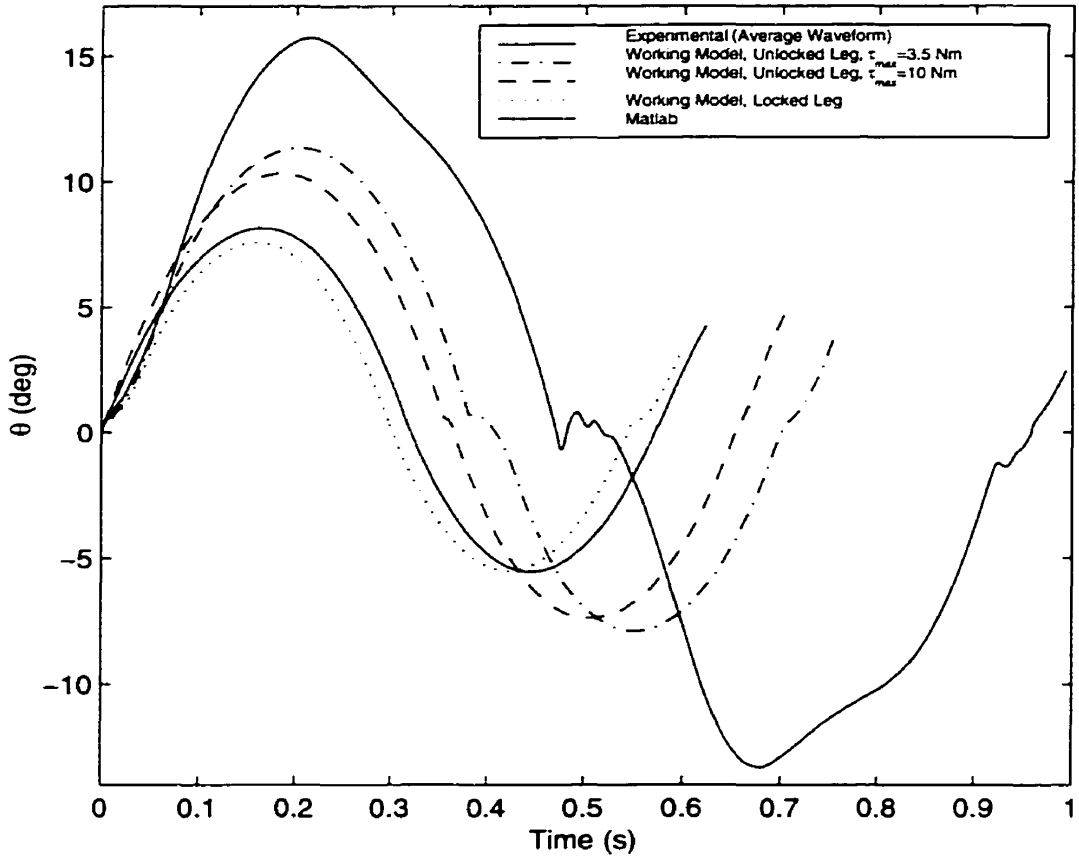

Figure 3.5: A steady state comparison of $\theta(t)$ for the major simulations and experiments. The Matlab and experimental results may be distinguished by the apex body angle during during back leg stance, θ_{max}. The experimental is the larger of the two.

3.5.1 Matlab Analysis

A setpoint was generated by performing a numerical simulation in Matlab [23] using the models developed in Sections 3.2 and 3.3 and iterating through several steps (Figure 3.3) until steady state was reached. Tables 3.3 and 3.4 details the values used in finding the setpoint. The kinematic parameters, mass, inertia, and maximum torque were selected from Sections 2.7 and 2.8 in order to match the Scout I robot as closely as possible. For the inertia, an average of the calculated and experimental results

was used. The simulated torques were conservatively limited to slightly less than the rated stall torque of the R/C servo motors. The initial point of the simulation was taken to be the condition just before back leg impact with $\dot{\theta}^{B-} = 70.0\frac{deg}{s}(1.222\frac{rad}{s})$. Figures 3.6 and 3.7 detail the results of this simulation.

ITEM	VALUE
m	2.3 kg
I	0.0145 kgm^2
r	0.078 m
l	0.20 m
L	0.10 m
H	0.02 m
K_p (PD controller)	20.0 $\frac{Nm}{deg}$ (1146 $\frac{Nm}{rad}$)
K_d (PD controller)	1.25 $\frac{Nms}{deg}$ (71.62 $\frac{Nms}{rad}$)
τ_{max} (PD controller)	3.5 Nm
Simulation time step	0.001 s
Integrator type	4th and 5th order Runge-Kutta

Table 3.4: Matlab Setpoint Parameters

As can be seen from the θ and $\dot{\theta}$ plots in Figure 3.6, the Matlab simulation of Scout I converged to steady periodic motion after a few steps, suggesting the existence of a fixed point with at least local stability. Figure 3.5 details $\theta(t)$ at steady state for one step. The ground clearance of each toe in Figure 3.6 indicated that toe stubbing was not a problem for this setpoint, supporting the use of a fixed front leg angle for the ramp controller. The speed of Scout I in this simulation was approximately 0.079 $\frac{m}{s}$.

For comparison purposes, it was desirable to select a single point of one of the state variables. The apex body angle θ_{max} was chosen as this point for a number of reasons. Firstly, the body states were of more interest than the leg states. Secondly, an angle

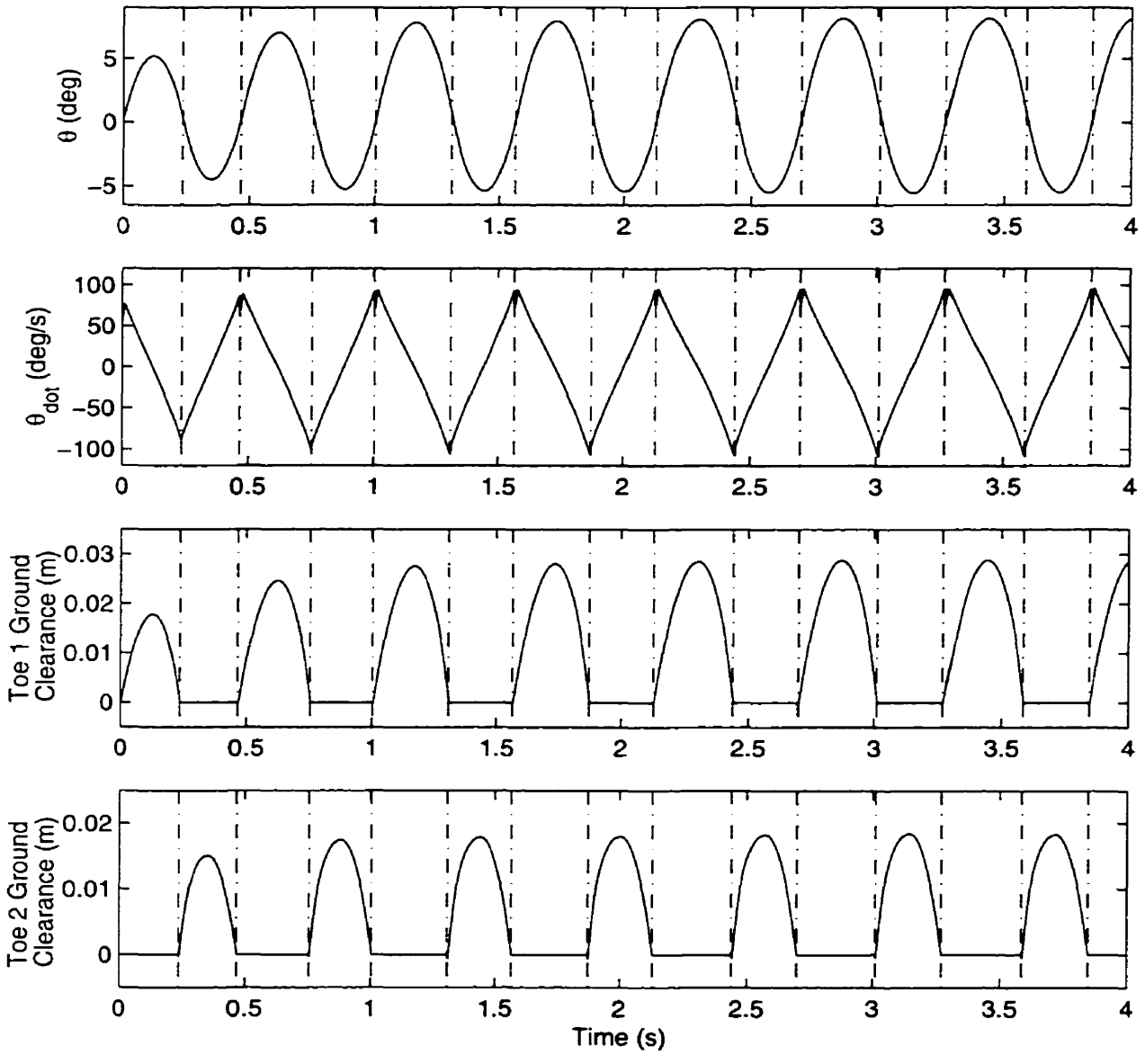

Figure 3.6: Matlab simulation of the ramp controller, showing θ, $\dot{\theta}$, and toe distances from the ground. The transitions of leg support are indicated by the dot dashed lines.

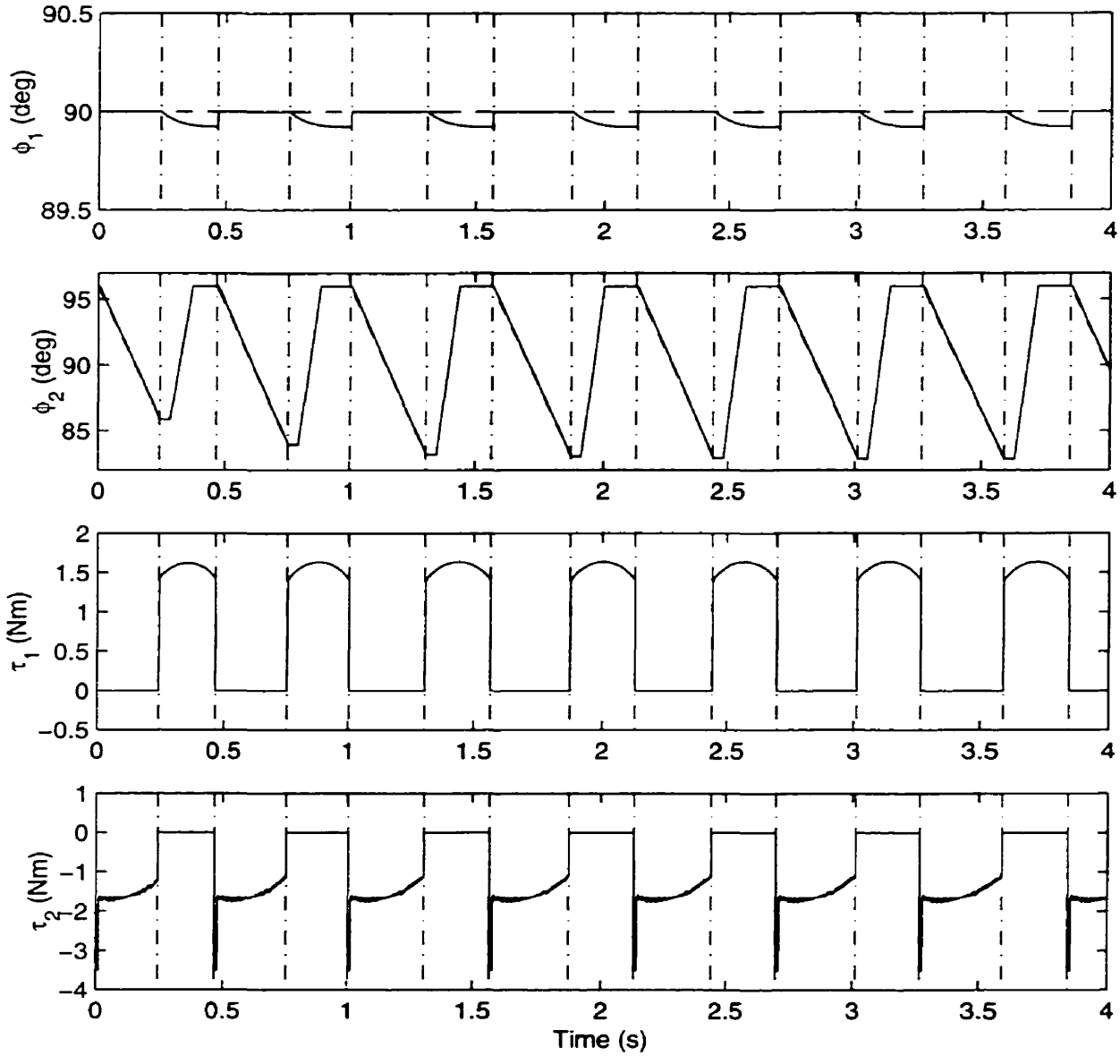

Figure 3.7: Matlab simulation of the ramp controller, showing ϕ_1, ϕ_2, τ_1, and τ_2. Desired leg angles are shown by dashed lines while actual angles are shown solid. The transitions of leg support are indicated by the dot dashed lines.

was easier to visualize than an angular velocity. Thirdly, for this setpoint at least the maximum body angle had a greater magnitude than the minimum body angle. The Matlab simulation resulted in a θ_{max} of 8.15 deg (0.142 rad) with little variation from step to step at steady state.

In Figure 3.7, the top two plots show the desired and actual leg angles for both the front (ϕ_1) and back (ϕ_2) legs. The tracking was good for both cases with an error of less than 0.1 deg (0.0017 rad) for ϕ_1 and 0.15 deg (0.0026 rad) for ϕ_2. The error in tracking for ϕ_2 is not visible on the plot due to the scale. This suggested that good tracking should be possible with the Scout I robot, even given the torque limitations of the machine. This was further supported by the bottom two plots in Figure 3.7 which show the torque applied by each actuator. In most cases, a torque of less than 2 Nm sufficed, except for the beginning the ramp just after back leg impact. This was due at least in part to the step change in $\dot{\phi}_2$ required by the ramp controller at the beginning of the back leg sweep. In any case, even this large spike in the required torque was well within the capabilities of the actuator which could provide near full stall torque at low actuator velocities. It should be noted that the PD controller for each leg was only active when that leg was in contact with the ground. When a leg was in the air, it was assumed to track the desired trajectory perfectly.

The sensitivity of this setpoint was investigated by re-running the above Matlab simulation a number of times, varying a single parameter each time. The results of the simulations were compared by examining the apex body angle θ_{max} of each simulation and are shown in Figure 3.8. The results were difficult to compare quantitatively because of the widely varying nature of the parameters being examined. However, to simplify inspection, the vertical axes were all plotted to the same scale (with the exception of the bottom right plot) and the nominal value for each parameter was placed at the midpoint of each of the horizontal axes. Furthermore, each parameter was examined over what was judged as a "reasonable" range of possible variation. For the length variables, a value of ± 0.01 m was selected (in the case of hip separation,

variation in 2L was used). Angles were varied by ±4.0 deg (0.070 rad). For the remaining parameters, a range of approximately ±10% was selected. Thus, with these assumptions a somewhat quantitative comparison could be made by examining the slopes of each plot (again with the exception of the bottom right case).

The top left plot in Figure 3.8 indicated that the system was not sensititive to small variations in the mass of the system. This was expected from the mathematical model. An inspection of (3.5) and (3.6) revealed that mass was not a factor in the momentum transfer. Furthermore, for the single leg support phases, mass only become a factor in (3.2) and (3.4). As was discussed in Section 3.3.1, these equations did not apply if it was assumed that the hip angles and angular velocities were controlled while torque limitations were ignored. Since the tracking of the legs was found to be very good (Figure 3.7), this situation applied and mass could be eliminated as a parameter for the system.

The top right plot in Figure 3.8 indicated a very small sensitivity to body inertia. However, the remaining plots suggested that the setpoint had a relatively large sensitivity (at least 10% variation in θ_{max} over the range examined) to the remaining parameters. The largest sensitivity was found to be to the back leg angle at back leg impact, ϕ_2^B which amounted to as much as 85% when the angle was increased from 96.0 deg (1.676 rad) to 100.0 deg (1.75 rad). If it was decided that feedback control needed to be applied to the ramp controller, this would be the obvious parameter to vary.

These large sensitivities indicated a possible problem with the open loop nature of the ramp controller. Any small variations from the nominal model were very likely to cause significant variation from the predicted setpoint.

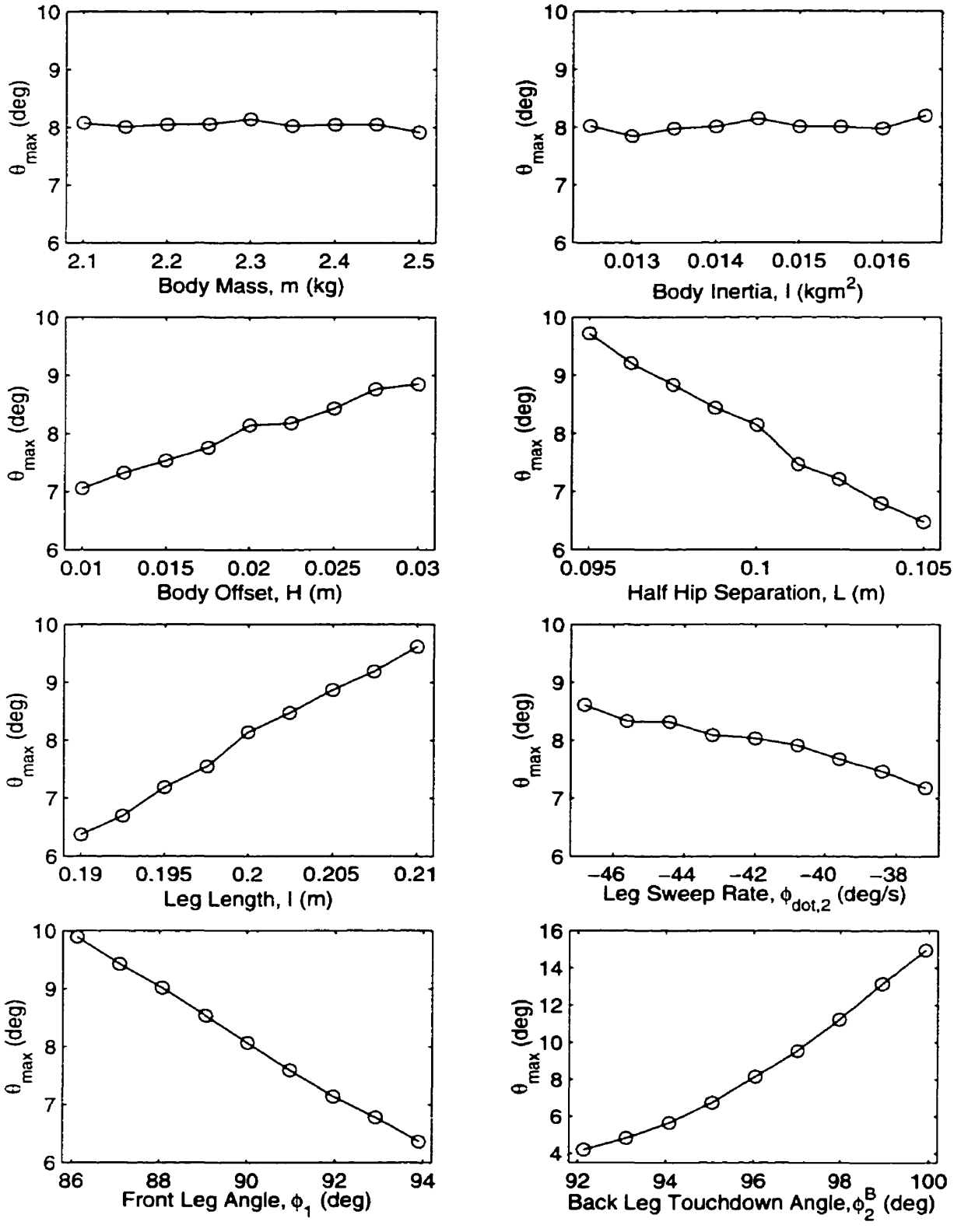

Figure 3.8: Setpoint sensitivity to model and ramp controller parameters.

3.5.2 Working Model Analysis

In order to justify the simplifying assumptions made in modelling Scout I (Sections 3.2 and 3.3), the robot with ramp controller was simulated in Working Model 2D [19]. This software package did not rely on direct knowledge of the equations developed in section 3.3. Instead, Working Model 2D integrated the forces and moments acting on a rigid body over a finite period of time to get the resulting accelerations, velocities and positions. The package also allowed a more realistic model of Scout I to be used.

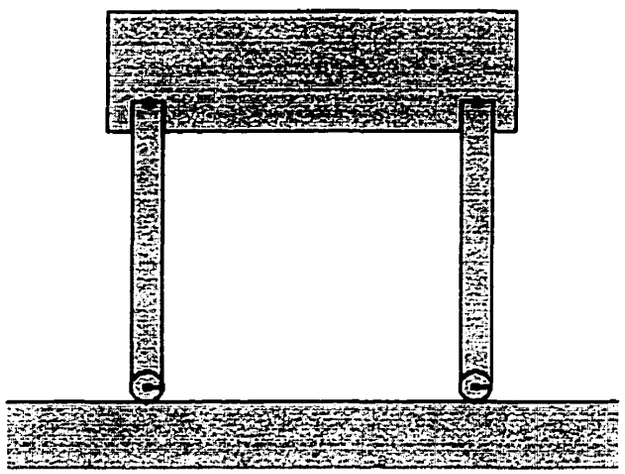

Figure 3.9: Working Model Version of Scout I

Figure 3.9 shows the Working Model version of Scout I. It was modelled as five rigid bodies which consisted of the main body, a front and back leg, and a front and back toe. Each rigid body was given a mass and inertia which closer modelled the actual distribution on the robot. In the simulation, the toes were not treated as pin joints. As can be seen from Figure 3.9, they were circles of radius 0.01 m. To prevent slipping and bouncing during impacts with the ground, the coefficients of friction where set very high and the elasticities of the bodies were set to zero. The back actuator was a simple torque input provided by a PD controller. However, since the front actuator never moved it was selected to act as a rigid joint. Tables 3.3 and 3.5 detail the values used in simulating the robot and ramp controller. The animation

time step represented the rate at which the animation of the robot, the various meters, and the desired leg angles were updated. It also represented the maximum time step for integration. The accuracy of the simulation was set by the integrator error. An integration was first performed at the animation time step and the error estimated. This was then compared with the integrator error. If the error was too large, then the time step was halved and the procedure repeated. This was done until an acceptable error was achieved. High simulation accuracy was achieved by running the same simulation a number of times, reducing the integrator accuracy each time until the results converged asymptotically. This was done and an integrator error of 0.000001 m was found to suffice.

The simulation was begun with the robot in the configuration of Figure 3.9 with an angular velocity of 120 $\frac{deg}{s}(2.094\frac{rad}{s})$ about the back toe. Throughout the first rocking motion, the back leg was commanded to ϕ_2 =90.0 deg (1.571 rad). The ramp controller was only started after the front leg impact with the ground. Figures 3.10 and 3.11 detail the results of this simulation.

The plots in Figure 3.10 were very similar to the results generated by Matlab (Figure 3.6). The θ and $\dot{\theta}$ plots showed that the Working Model simulation of Scout I converged to steady periodic motion after a few steps and the toe clearance plots indicated that toe stubbing was not a problem. At steady state, θ_{max} varied approximately 0.015 deg (0.00026 rad) about an average of 7.56 deg (0.132 rad). This amounted to approximately 8% less than the values achieved in Matlab. Figure 3.5 details this relationship. However, considering the setpoint sensitivities found in the Matlab analysis (Figure 3.8), this was an acceptably small error most likely caused by the redistribution of some mass to the legs and toes. This change effectively lowered the overall center of mass, decreasing θ_{max} with it. The speed of Scout I for this simulation was approximately 0.079 $\frac{m}{s}$.

The top plot in Figure 3.11 shows the desired and actual back leg angles. When compared with the second plot of Figure 3.7 it is obvious that there was a larger

ITEM	VALUE
m_{body}	2.1 kg
m_{leg}	0.096 kg each
m_{toe}	0.006 kg each
I_{body}	0.014 kgm^2
I_{leg}	0.00046 kgm^2 each
I_{toe}	0.0000003 kgm^2 each
l (Distance from the hip joint to the ground in the Figure (3.9) configuration)	0.20 m
L	0.10 m
H	0.02 m
K_p (PD controller, back leg)	20.0 $\frac{Nm}{deg}$ (1146 $\frac{Nm}{rad}$)
K_d (PD controller, back leg)	1.25 $\frac{Nms}{deg}$ (71.62 $\frac{Nms}{rad}$)
τ_{max} (PD controller, back leg)	3.5 Nm
Animation time step	0.001 s
Integrator type	5th order Runge-Kutta
Integrator error	0.000001 m

Table 3.5: Working Model Setpoint Parameters

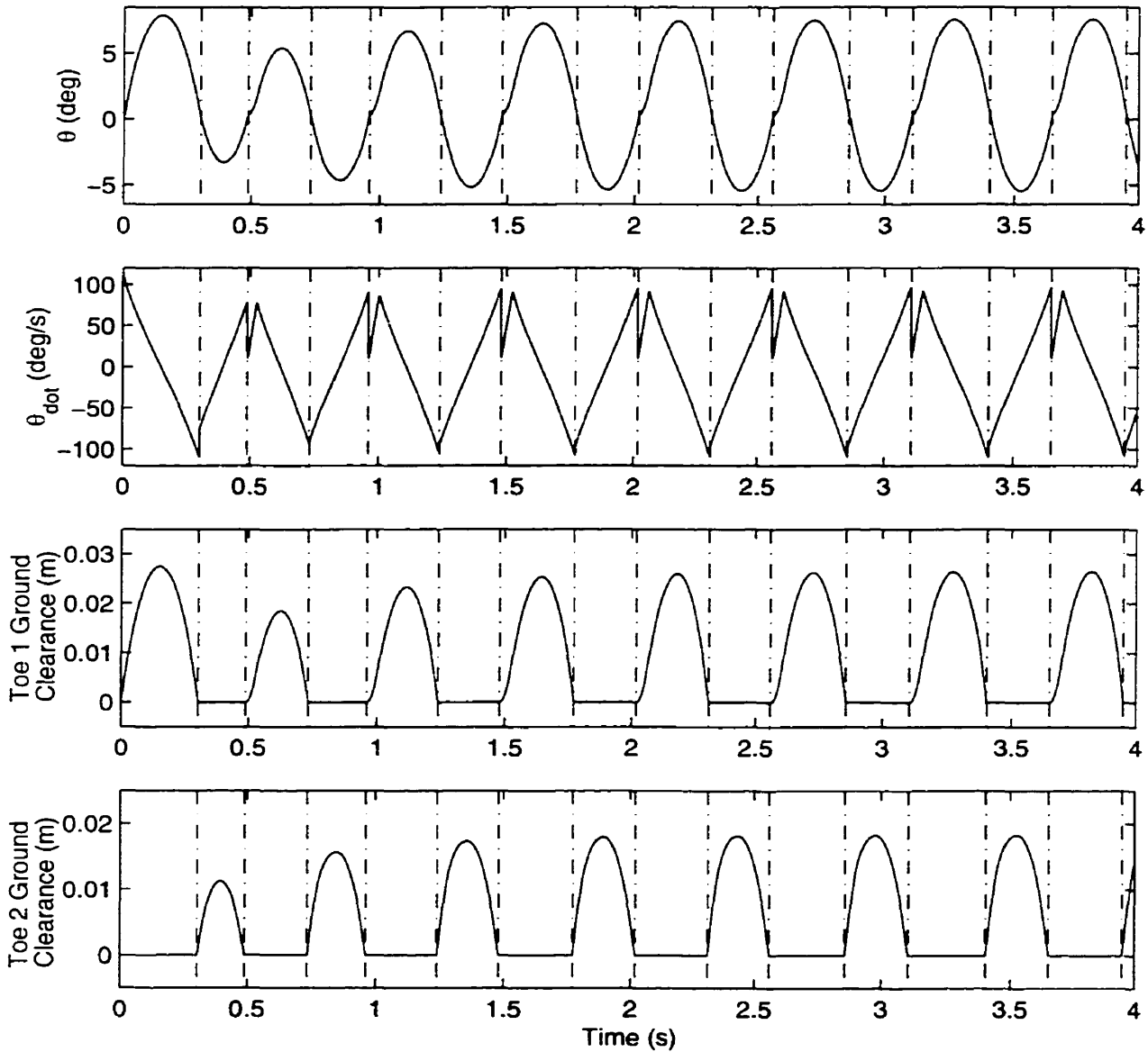

Figure 3.10: Working Model simulation of the ramp controller (front leg locked), showing θ, $\dot{\theta}$, and toe distances from the ground. The transitions of leg support are indicated by the dot dashed lines.

tracking error in the Working Model simulation. In fact, the maximum tracking error was 2.3 deg (0.040 rad). This difference was caused by the fact that the impact model used in Matlab, (3.5) assumed that ϕ_2 could be controlled without error. In the case of the Working Model simulation, the torque controlled back leg actuator was not quite capable of this. However, this tracking error appears to have had little effect on the setpoint. When a second Working Model simulation was run with $\tau_{max} = 10.0Nm$, the maximum tracking error was reduced to 0.45 deg (0.0079 rad), but this resulted in a negligible change in θ_{max}.

The bottom plot in Figure 3.11 shows the torque input to the back actuator. This result compared very well with the Matlab results (Figure 3.7). However, there is one thing worth noting. A number of torque spikes appeared in the Working Model plot that did not appear in the Matlab plot. These peaks were all accounted for by the step changes in desired $\dot{\phi}_2$ at the end of the back leg sweep and at the beginning and end of the back leg retract (Figure 3.4 and Table 3.3). These cases could not be examined in Matlab with the models developed.

From the above analysis, there appeared to be a good correspondence between the two simulation methods. However, there was one further point of realism that could be examined in Working Model. Recall that the previous Working Model simulation was run with a rigid joint between the front leg and body. This was now replaced with a torque actuator under an identical PD control as the back hip actuator. All values used for this simulation corresponded to Tables 3.3 and 3.5. Figures 3.12 and 3.13 detail the results.

Figure 3.12 indicated that this simulation of Scout I had the same trends as the previous Matlab and Working Model simulations. It once again converged to steady state after a few steps with no toe stubbing problems. However, the setpoint reached θ_{max} =11.35 deg (0.198 rad) with a steady state fluxuation of $\pm$0.015 deg (0.00026 rad) represented at 51% difference from the previous Working Model setpoint of 7.56 deg (0.132 rad)! This relationship is detailed in Figure 3.5. The speed of Scout I for

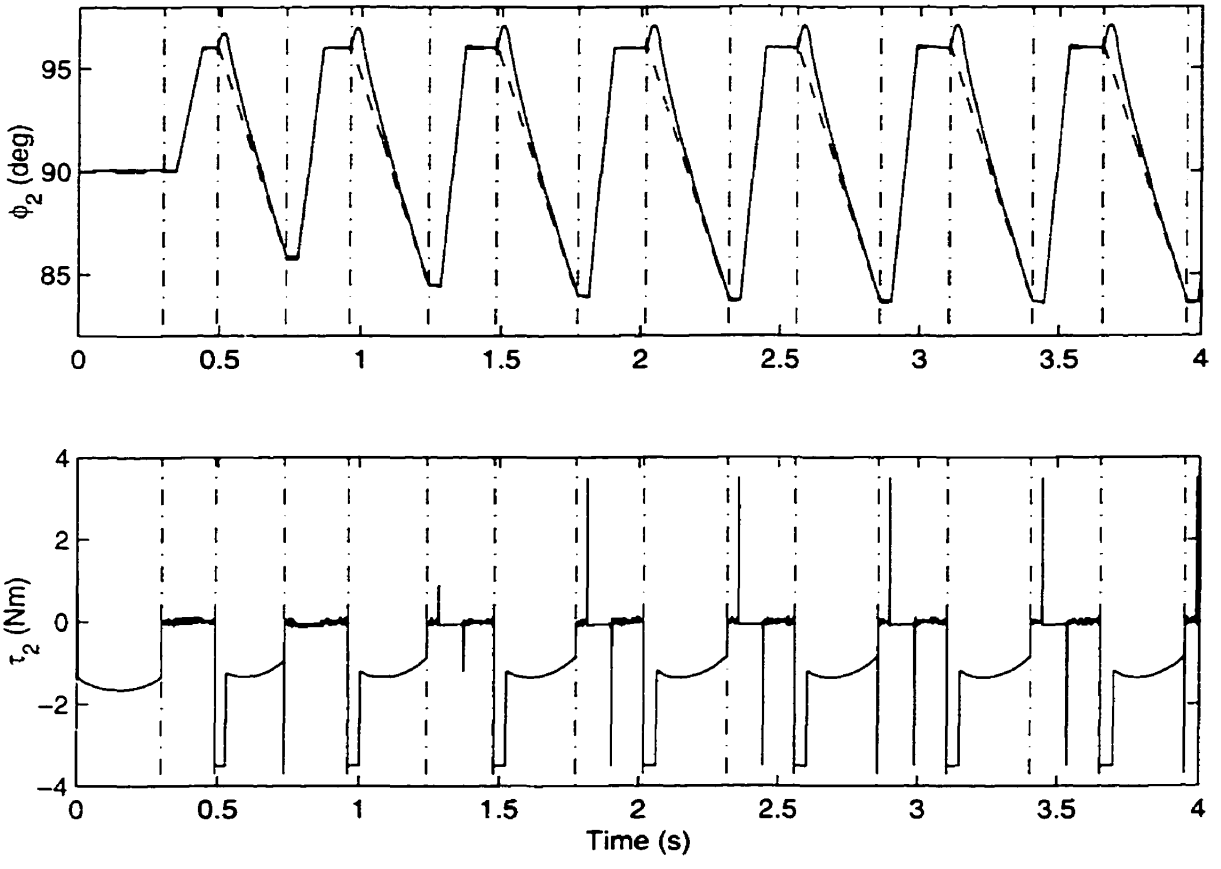

Figure 3.11: Working Model simulation of the ramp controller (front leg locked), showing ϕ_2 and τ_2. Desired leg angles are shown by dashed lines while actual angles are shown solid. The transitions of leg support are indicated by the dot dashed lines.

this simulation averaged 0.079 $\frac{m}{s}$.

The only item that had been changed between the Working Model simulations was the unlocking of the front hip, so the source of the error had to be related to that. The major difference between a locked and unlocked hip was that the angle was no longer explicitly controlled and the joint no longer perfectly rigid. It was hypothesized that this decrease in rigidity was the source of the setpoint error. This was examined below.

An inspection of the tracking of the front and back legs (Figure 3.13) revealed a fairly large tracking error in ϕ_1 and ϕ_2 just after impacts with the ground. A number of simulations were run with higher torque limits and PD gains to examine the effect on the setpoint value θ_{max}. Table 3.6 details the results. The steady state values for $\theta(t)$ for most of these results can be found in Figure 3.5.

K_p $\frac{Nm}{deg}(\frac{Nm}{rad})$	K_d $\frac{Nms}{deg}(\frac{Nms}{rad})$	τ_{max} Nm	Maximum Tracking Error		θ_{max} deg (rad)	Error %
			ϕ_1 deg (rad)	ϕ_2 deg (rad)		
20.0 (1146)	1.25 (71.62)	3.5	3.8 (0.066)	2.8 (0.049)	11.35 (0.198)	51
20.0 (1146)	1.25 (71.62)	10.0	0.91 (0.016)	0.32 (0.0059)	10.3 (0.180)	36
20.0 (1146)	1.25 (71.62)	50.0	0.17 (0.0030)	0.05 (0.00087)	10.1 (0.176)	34
50.0 (2865)	3.125 (179.0)	50.0	0.17 (0.0030)	0.05 (0.00087)	10.2 (0.178)	35
Leg Rigidly Locked			0.0 (0.0)	0.0 (0.0)	7.56 (0.132)	0

Table 3.6: The Effects of Torque Limit and PD Gains On θ_{max}

An increase in τ_{max} from 3.5 to 10.0 Nm did significantly reduce the error in θ_{max} from 51% to 36%, indicating that the torque limit was a contributing factor to the error. However, a further increase in the torque and gains produced little change in the resulting θ_{max}. Thus, the torque limit didn't explain everything.

Next the front leg impact was studied in more detail by modifying the simulation so that the impact could be examined under identical initial conditions with a variety of

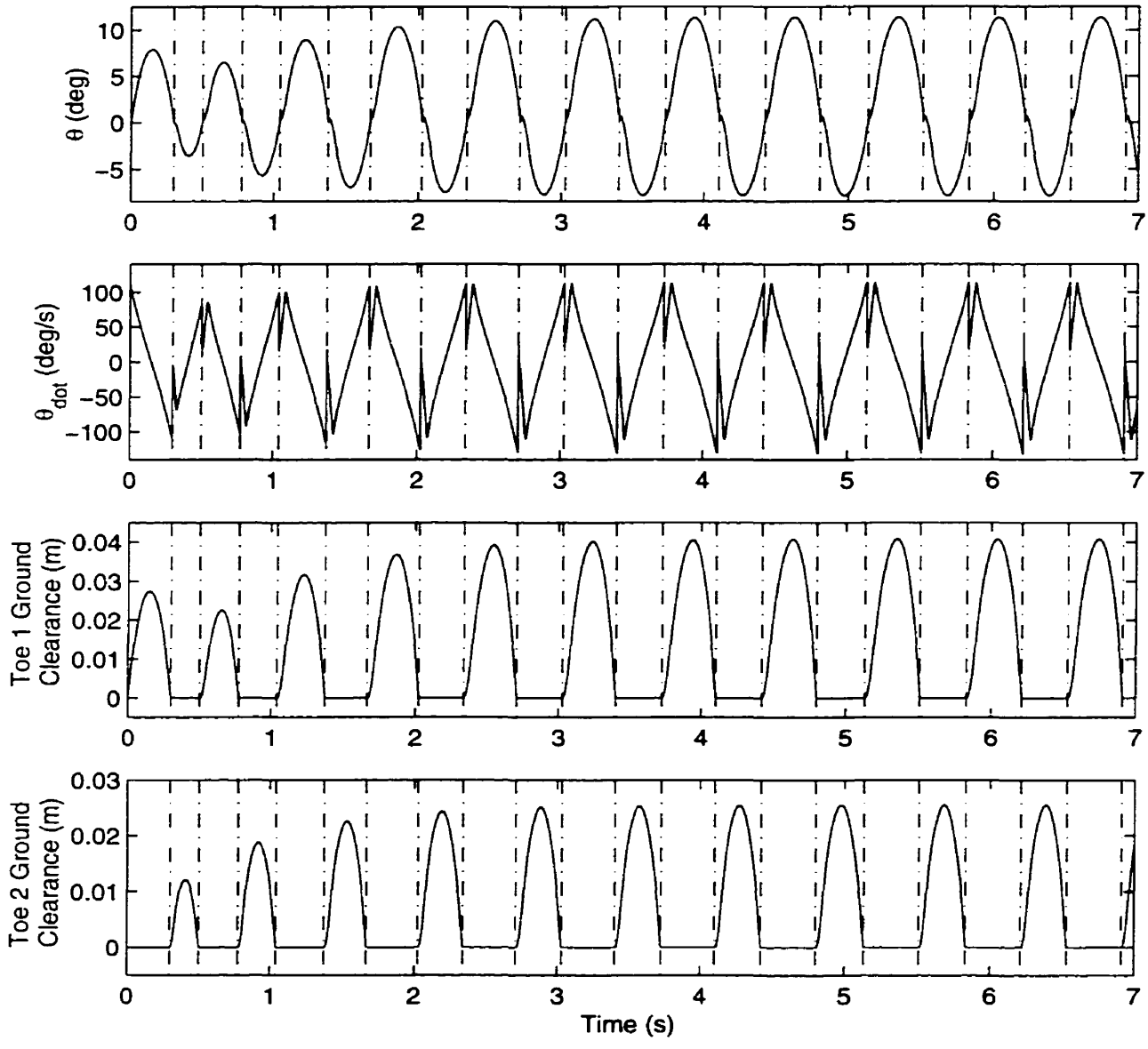

Figure 3.12: Working Model simulation of the ramp controller (front leg unlocked), showing θ, $\dot{\theta}$, and toe clearances from the ground. The transitions of leg support are indicated by the dot dashed lines.

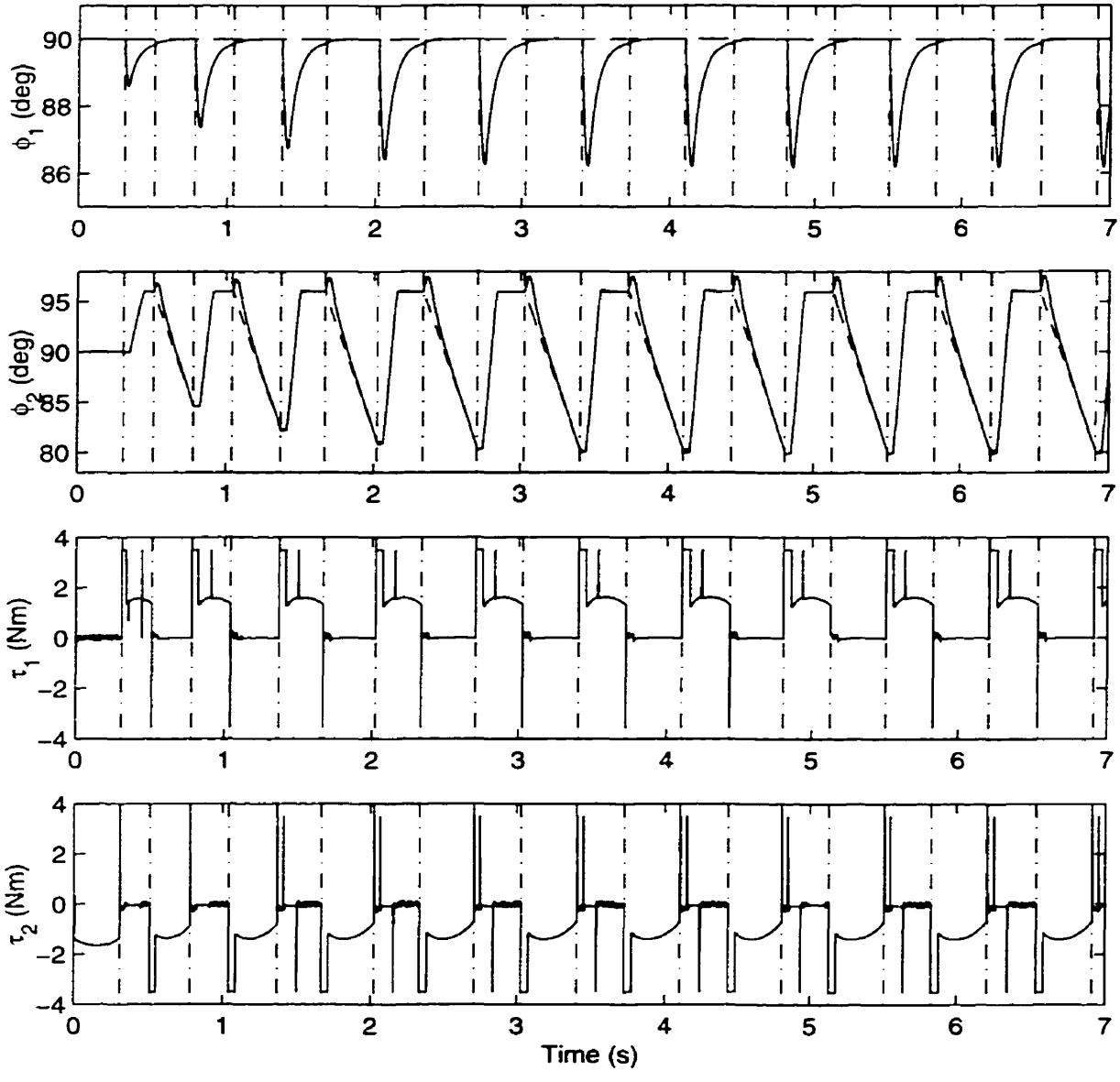

Figure 3.13: Working Model simulation of the ramp controller (front leg unlocked), showing ϕ_1, ϕ_2, τ_1, and τ_2. Desired leg angles are shown by dashed lines while actual angles are shown solid. The transitions of leg support are indicated by the dot dashed lines.

different front leg actuators. The same five sets of gains and torque limits as in Table 3.6 were then examined. Table 3.7 details the initial conditions just before impact.

ITEM	VALUE
ϕ_1^F	90.0 deg (1.57 rad)
ϕ_2^F	79.4 deg (1.39 rad)
θ^F	0.79 deg (0.014 rad)
$\dot{\phi}_2^{F-}$	-42 $\frac{deg}{s}$ (-0.73 $\frac{rad}{s}$)
$\dot{\theta}^{F-}$	-124 $\frac{deg}{s}$ (-2.16 $\frac{rad}{s}$)

Table 3.7: Initial Conditions Just Before Impact

Figure 3.14 shows the body angular velocities, $\dot{\theta}$ around one impact. Before the impact, which occurred between 0.353 and 0.354 seconds, it can be seen that the angular velocities for the five simulations were virtually identical, as was desired. Four of the simulations then show a large spike in the angular velocity at the point of impact. These were the unlocked cases and the change was due to the slight 'folding up' of the front leg with the body before the PD controller could properly react. This effect can also been seen at back leg impact in the simulation with the locked front leg (Figure 3.10) and in both impacts when the front leg was unlocked (Figure 3.12). The smaller spikes in angular velocity just before 0.4 and 0.5 sec were attributed to the back leg retract start and end (Figure 3.4). However, the most important result of Figure 3.14 can be seen after the impact. The five simulations resulted in three general trends, shown by the three lines towards the right of the plot. This in itself did not mean much, but the three lines also matched the general trend of the five setpoints in Table 3.6 (one setpoint at 0%, three at ≈35%, and one at 51%)! It was concluded that these differences were at the root of the error in the setpoint. The difference between the bottom and middle lines was previously found to be due to τ_{max}. The difference between the top and middle lines was more difficult to explain. One possibility was the

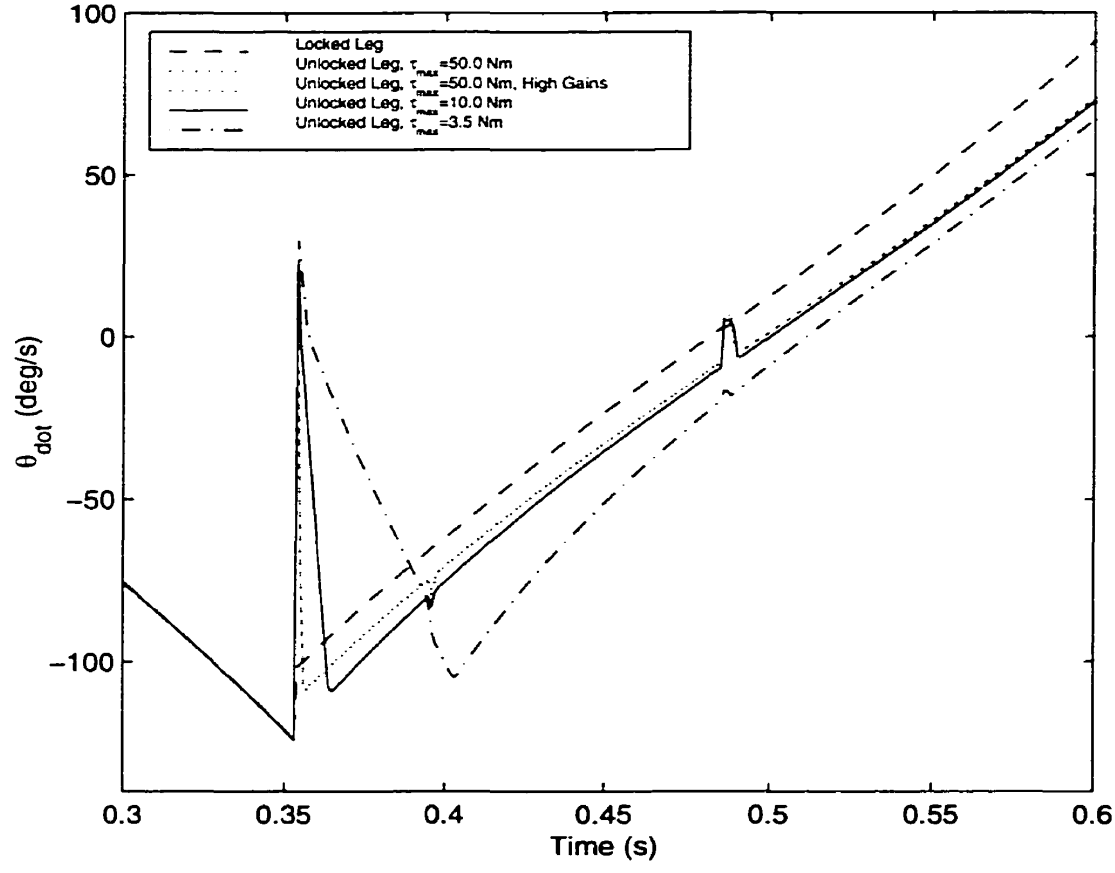

Figure 3.14: Working Model simulations of front leg impacts. The two 50 Nm cases virtually overlap with each other.

fact that a PD controller must by necessity react (with associated delay) to an error in the position or velocity where as a rigid joint can react instantaneously. However, high gains and torque limits should have minimized this effect. This may have been a limitation in the Working Model simulation package. It may not have been able to properly model this decrease in reaction time. In any case, this effect appeared to be due to the decrease in the rigidity of the system at impact. This resulted in a slight change in the impact results which coupled with the high sensitivity of the system resulted in the radical change in setpoint and θ_{max}. This problem was only apparent when both the front and back legs where unlocked. This was because if one leg was locked, then the system at impact was rigid, since slipping with the ground was not possible due to the high friction.

One final item of interest was a comparison between the Working Model impact with the fixed front leg and the predicted results of (3.6). Using the initial conditions from Table 3.7, the Equation predicted $\dot{\theta}^{F+} = -103\frac{deg}{s}(-1.79\frac{rad}{s})$. The Working Model simulation resulted in $\dot{\theta}^{F=} = -102\frac{deg}{s}(-1.78\frac{rad}{s})$, less than a 1% error. This was a remarkable accuracy, since Working Model 2D did not use an accurate algebraic relation (such as with (3.5) and (3.6)) to calculate the changes in angular velocities, but only the continuous integration of the rigid body dynamics interacting with the ground.

3.5.3 Experimental Analysis

As the final step in examining the setpoint generation, the ramp controller was applied to the actual Scout I robot discussed in Chapter 2. Tables 3.3 and 3.8 detail the values used for the experimental run. The gains and offsets for the R/C servo controller (2.1) were determined experimentally. The robot was started by first leaning back from $\phi_1 = \phi_2 = \phi_3 = \phi_4 = 90.0$ deg (1.571 rad) to 101.0 deg (1.763 rad). The back legs were then given a step input to $\phi_2 = \phi_4 = 79.0$ deg (1.379 rad). This gave Scout I an initial jump. When the front legs were in the air, ϕ_1 and ϕ_3 were set to 90.0 deg

(1.571 rad). The ramp controller only became active after the first impact with the ground. To minimize slipping, the robot was run on a high friction surface, the belt of a treadmill. Despite this, videos taken of Scout I during experimental runs indicated that there was some slipping during front leg impact. However, this was limited to approximately 0.015 m. The treadmill was not moving during the experiment.

ITEM	VALUE
$K_{p,1}$ ((2.1), front legs)	1.0
$K_{p,2}$ ((2.1), back legs)	2.0
$K_{offset,1}$ ((2.1), front legs)	3.5 deg (0.061 rad)
$K_{offset,2}$ ((2.1), back legs)	-9.0 deg (0.16 rad)
Actuator update rate	83.3 Hz
Control and sensing rate	1000 Hz

Table 3.8: Experimental Setpoint Parameters

Figures 3.15 and 3.16, show the results of this experiment. Transitions from front to back and back to front legs were shown by a dot dashed line. Unlike the simulations, which had an impact time of 0.001 seconds or less, the Scout I robot had a distinct phase when all legs were on the ground. This amounted to approximately 0.050 seconds for each impact or slightly over 10% of the entire step time. Since no control inputs were developed for the ramp controller during double stance, for the purposes of control the robot was assumed to transfer leg support at the instant of leg touchdown. The transition lines on the plot, however have been placed at the midpoint of the double support phase. The first three seconds of the experiment involved Scout I leaning back and thus were not shown. However, the initial jump, at just after 3.5 seconds was displayed.

The plots of θ and $\dot{\theta}$ in Figure 3.15 indicate the same trend as both the Matlab and Working Model simulations; the robot rapidly converged to steady state. Figure 3.5

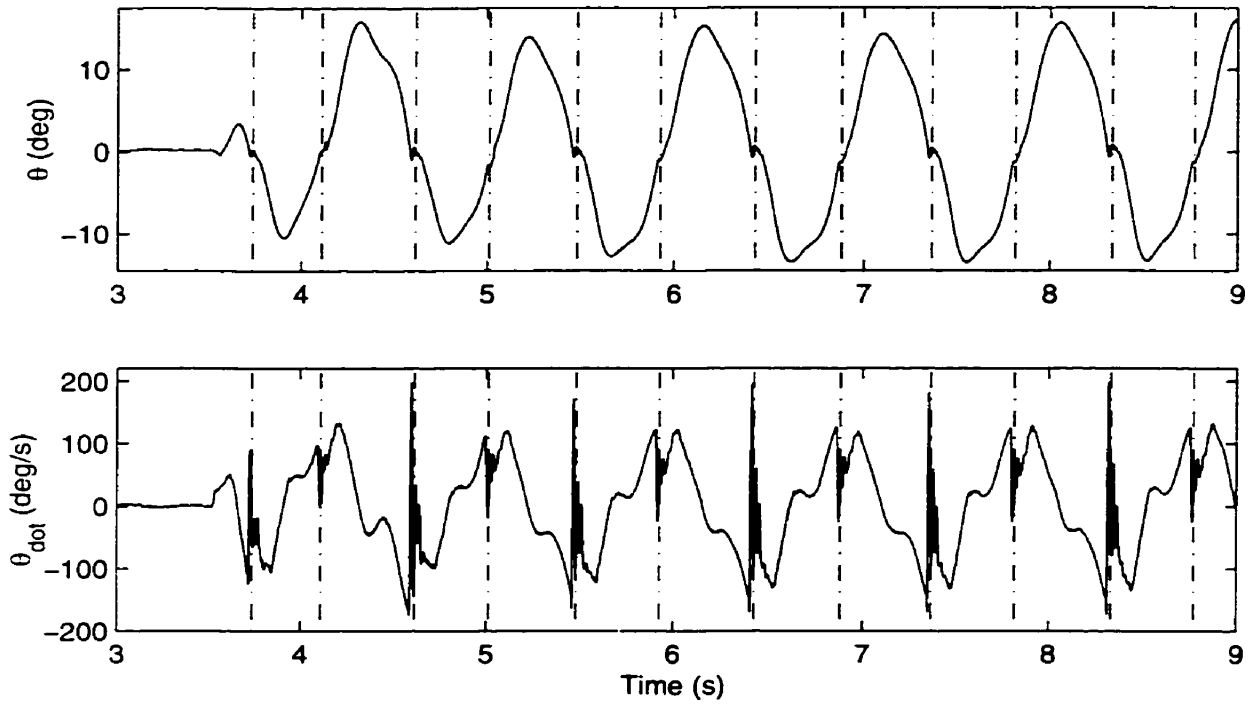

Figure 3.15: Experimental results of the ramp controller, showing θ and $\dot{\theta}$. The transitions of leg support are indicated by the dot dashed lines.

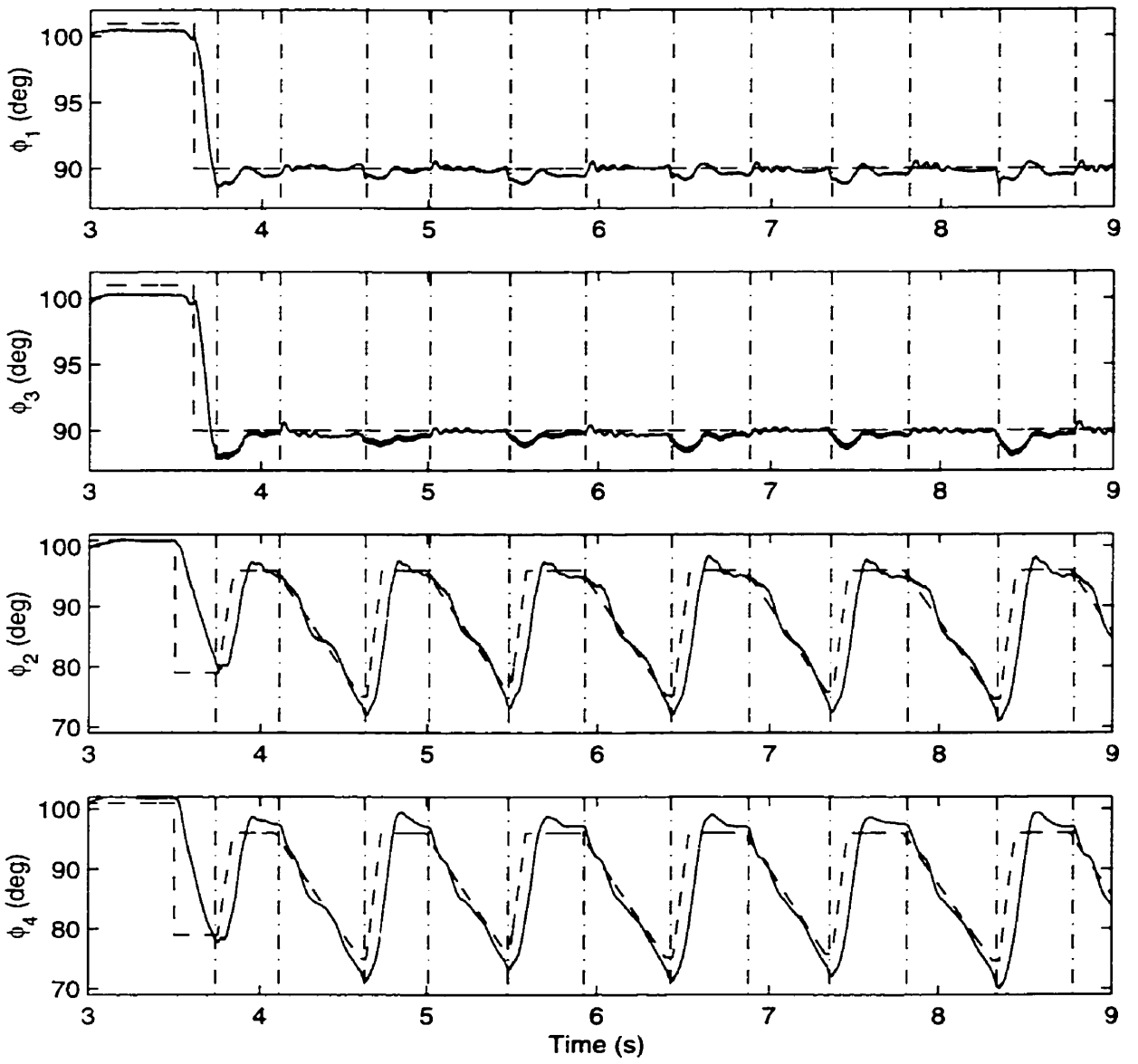

Figure 3.16: Experimental results of the ramp controller, showing ϕ_1, ϕ_2, ϕ_3, and ϕ_4. Desired leg angles are shown by dashed lines while actual angles are shown solid. The transitions of leg support are indicated by the dot dashed lines.

details this relationship. An inspection of $\dot{\theta}$ also revealed a very similar pattern to the $\dot{\theta}$ plot in Figure 3.12, the most realistic of the simulations (Working Model, with front leg unlocked and a torque limit of τ_{max}= 3.5 Nm). Figure 3.16, showing the desired and actual leg angles, ϕ_1, ϕ_2, ϕ_3, and ϕ_4 indicated that tracking was generally good for the run. There were, however a number of significant differences. The setpoint reached, θ_{max}=15.8 deg (0.276 rad) represented a 39% error from the setpoint reached in Figure 3.12. In addition, there was also a much larger fluctuation in the setpoint value θ_{max} than in the simulations. It varied by +2.8 deg (+0.049 rad) and -1.8 deg (-0.031 rad). Scout I averaged approximately 0.085 $\frac{m}{s}$ for this experiment.

The large fluctuations in setpoint value could be explained by the Matlab sensitivity analysis (Figure 3.8). Any small fluxuation from step to step, which is inevitable in an experiment would result in larger fluxuations in θ_{max}. This was indeed the case.

The 39% error in setpoint value, θ_{max} was most likely due to an extension of the phenomenon discovered in the Working Model analysis. The low update rate of the R/C servo motors (Table 3.8) as well of the use of Plexiglas as the main structural component in Scout I resulted in an even less rigid structure during impact than the Working Model simulation (Figure 3.12). This resulted in an even greater discrepancy from the Matlab and locked front leg Working Model results. This observation is supported by the experimental results of $\dot{\theta}$ just at impact. The body angular velocity spikes to almost 200 $\frac{deg}{s}$ (3.49 $\frac{rad}{s}$) compared to the spike of less than 50 $\frac{deg}{s}$ (0.873 $\frac{rad}{s}$) for the Working Model results with the unlocked front leg. In the ideal case of a rigidly locked front leg, there would be no spike at all. Nevertheless, despite these differences stable walking was achieved.

3.6 Stability Analysis

As the final item in the analysis of the ramp walking controller with Scout I, the stability of several simulations and experiments were examined. Recall from section 3.5, that all simulations and experiments were found to converge to a steady cyclic

motion. This convergence was examined over a wider range of θ_{max} using the same ramp controller parameters as in all previous cases (Table 3.3). The cases studied are detailed below.

- The Matlab simulation described in Table 3.4.
- The Working Model simulation described in Table 3.5 with a rigidly locked front leg.
- The Working Model simulation described in Table 3.5 with a torque controlled front leg.
- The Working Model simulation with $\tau_{max} = 10.0$ Nm with a torque controlled front leg (All other parameters as Table 3.5).
- Experiments on the actual Scout I robot (Table 3.8).

The results of these investigations were plotted on a discrete step-to-step return map. θ_{max} was chosen as the variable of interest. Thus, the step-to-step return map displayed θ_{max} at step n+1 given the θ_{max} at step n. If the magnitude of the slope of the resultant curve was less than 1 at the point where $\theta_{max,n} = \theta_{max,n+1}$, then local convergence would result. An ideal step-to-step return map would have had a slope of 0, indicating that the setpoint could be achieved after only one step.

Figure 3.17 details the results of this investigation. Both the simulations and experimental results show that the ramp controller converged to steady state over a surprisingly wide range of $\theta_{max,n}$. In fact, the Matlab simulation converged over the entire practical range of $\theta_{max,n}$. At the extreme left of the Matlab results, there was no angular velocity after back leg impact. Beyond the curve to the extreme right, there was a narrow area where the Scout I simulation did not rock high enough after front leg impact to retract its legs. Beyond that, the simulation predicted that Scout I would simply roll over backwards. The Working Model simulations were not pushed to this extent but still show the same trend as the Matlab simulation. Each Working

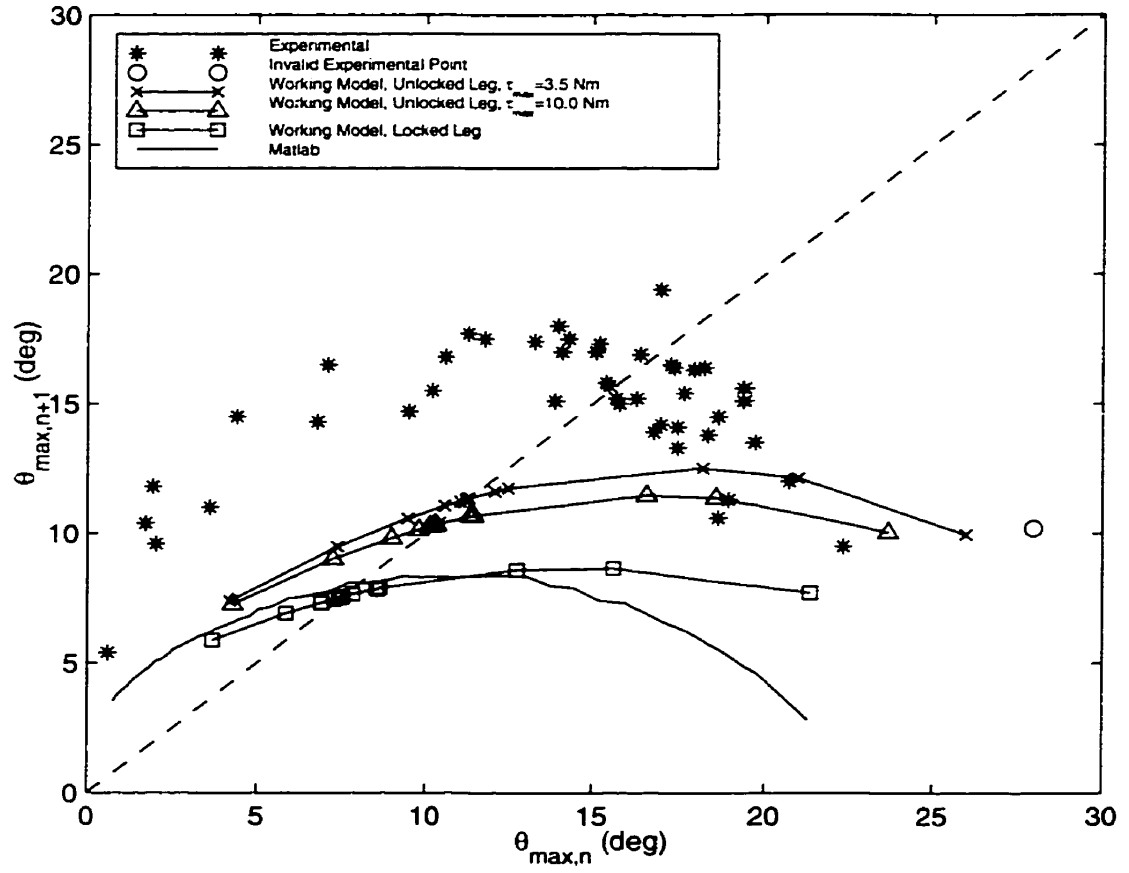

Figure 3.17: Step-to-step return map for the Matlab and Working Model simulations and experimental results. The condition $\theta_{max,n} = \theta_{max,n+1}$ is indicated by the diagonal dashed line.

Model curve consists of four separate simulations. The experimental results (asterisks with no connecting lines), which were derived from 10 experiments also show this general trend. As expected, there was a fair degree of scatter in the results, due to the sensitivity of the system. The invalid point marked by an "o" was an extreme case when Scout I rocked to θ_{max}=28.0 deg (0.489 rad). Due to the high θ_{max}, the back stance time was also unusually large and the back legs swept over a large arc. The resulting front impact with the ground was very severe and and Scout I did not rock high enough on its front legs to properly retract its back legs. Instead, they retracted by dragging along the ground for a part of the sweep. Despite this disturbance to the system, Scout I still recovered.

3.7 Summary and Conclusions

In this chapter, a planar mathematical model of Scout I was developed. This model treated the robot as a double inverted pendulum when it was supported by its front or its back legs. Impacts were assumed to be instantaneous, with angular momentum about the impacting toes being conserved. A walking controller for Scout I was then presented which utilized a bounding gait and a minimum of sensing, in essence being open loop. The mathematical model and ramp controller were then analyzed in Matlab and the results verified using a second simulation package, Working Model. The system was found to be very sensitive to most of the model and ramp controller parameters, suggesting a potential problem with the open loop nature of the ramp controller. Good correspondence was found between Matlab and Working Model if the robot in Working Model was made as rigid as possible by locking the front leg in place. However, as the robot was made less rigid by unlocking the front leg and imposing realistic torque limitations, a large error resulted. This error was also apparent and significantly larger in the experiments on Scout I itself. Here, further reduction in rigidity by the low bandwidth of the R/C actuators and the compliance of the structure, resulted in an even larger error. Despite the differences in the setpoints,

they were all found to result in stable walking, even from very large disturbances to the system.

Chapter 4

Additional Behaviors

4.1 Introduction

For a legged robot to be practical, it must be capable of performing a wide range of behaviors. These behaviors should either enhance mobility or for entertainment applications make the robot look more interesting. This chapter presents a variety of other behaviors that were investigated with Scout I (or in one case, Scout II). The behaviors presented here have not been examined in great detail; rather they are presented as proof that the Scout class of robots are capable of much more than just a simple walking motion.

With the exception of Section 4.3 Scout I can be considered planar and Figure 3.2 applies. Thus, unless otherwise specified leg 1 can be taken to refer to both legs 1 and 3, while leg 2 can be taken to refer to both legs 2 and 4. The reverse also applies.

For all of the experimental results in this chapter, the leg controller variables K_p and K_{offset} in (2.1) were set to zero. Like the ramp controller experiments in Sections 3.5.3 and 3.6 all of the experiments in this chapter (with the exception of Section 4.5.1) were run on a stationary treadmill belt to minimize slipping.

4.2 The Step Controller

The first walking controller that was implemented on Scout I was the step controller. Like the ramp controller (Section 3.4), the robot moved in a bounding motion and kept its front leg fixed at all times (at a value of ϕ_1). The difference was in the motion of the back leg. Instead of a ramp input, a step input was applied to ϕ_2. At back leg impact, the back leg was commanded to a fixed angle, ϕ_2^B. During back leg support, after a length of time t_{step}, the back leg was commanded to a new angle, ϕ_2^F. This caused the robot to take a step forwards. After front leg impact, a second delay was imposed, t_{return} before the back leg was retracted to ϕ_2^B using another step input. This second delay was to prevent toe stubbing. The parameters t_{step} and t_{return} were selected based on the stance times during the last step. For t_{step}, a fraction of the previous back leg stance time was used and for t_{return}, a fraction of the previous front leg stance time was used. Figure 4.1 details this process.

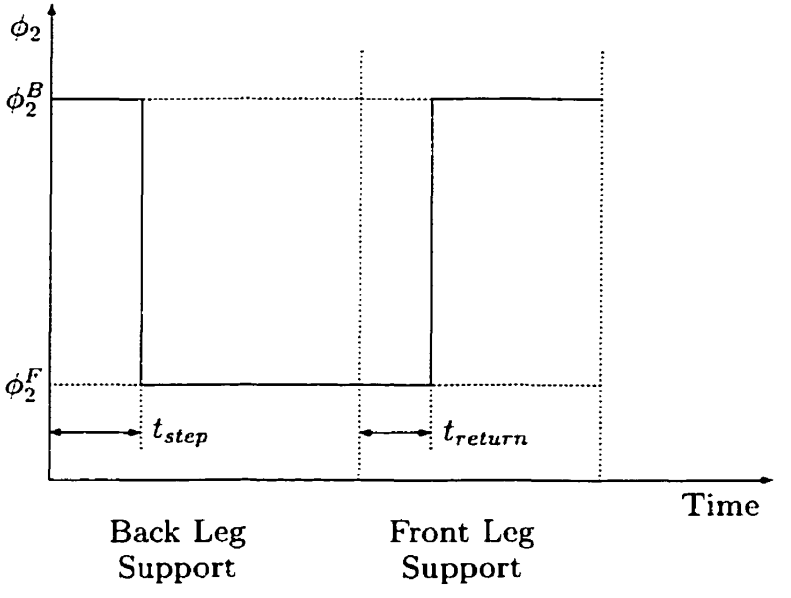

Figure 4.1: Step Controller Input For ϕ_2 For One Complete Step

This walking controller was examined experimentally using the parameters in Table 4.1. As with the ramp controller experiment (Section 3.5.3) the experiment was

started with $\phi_1 = \phi_2 = \phi_3 = \phi_4$ =90.0 deg (1.571 rad). The robot then leaned back to $\phi_1 = \phi_2 = \phi_3 = \phi_4 = 101.0$ deg (1.763 rad) and after a brief pause, ϕ_2 and ϕ_4 were given a step input to 79.0 deg (1.379 rad). This gave the robot an initial jump. The front legs ϕ_1 and ϕ_3 were then set to 90.0 deg (1.571 rad) before the first impact with the ground. The step controller only started after the first front impact.

ITEM	VALUE
ϕ_1	90.0 deg (1.571 rad).
ϕ_2^B	96.0 deg (1.676 rad).
ϕ_2^F	82.0 deg (1.431 rad).
t_{step}	30% of the previous back stance time
	(Set to 0.1 s for the first step).
t_{return}	30% of the previous front stance time
	(Set to 0.1 s for the first step).

Table 4.1: Step Controller Parameters

The results of this experiment are detailed in Figures 4.2 and 4.3. The initial lean back sequence was not displayed on the plots. However, the step input to the back legs was. This is why Figures 4.2 and 4.3 start at a time of 3 seconds. The transitions of support from front to back and back to front legs are indicated by the vertical dot dashed lines. In reality, the transitions of support were not instantaneous. During back impact, all four legs were on the ground for a period that averaged 0.102 seconds. During front impact, the duration averaged 0.042 seconds. Both of these impacts together amounted to approximately 19% of the total step time. Since the step controller was not developed with this support phase in mind, for the purposes of control, the robot was assumed to transfer leg support at the instant of leg touchdown. However, in Figures 4.2 and 4.3 the transitions of support indicate the midpoint of the double support phase.

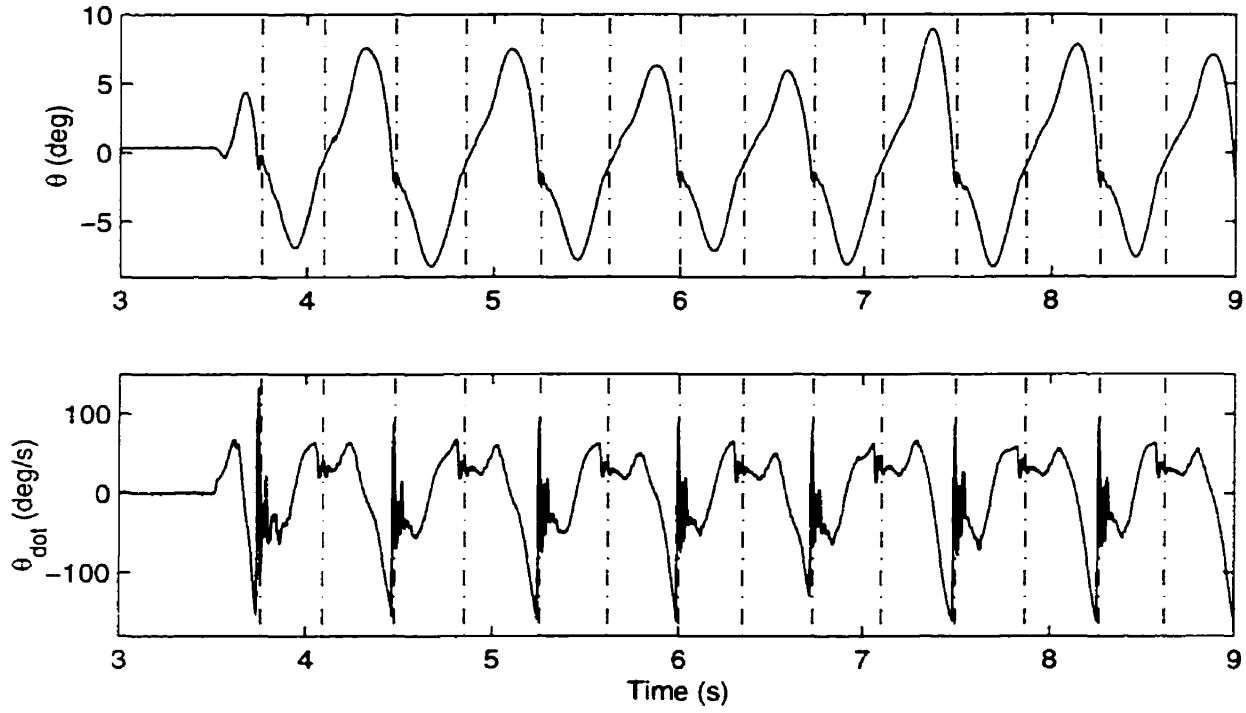

Figure 4.2: Experimental results of the step controller, showing θ and $\dot{\theta}$. The transitions of leg support are indicated by the dot dashed lines.

An inspection of Figure 4.2 indicates that Scout I converged to steady periodic motion after only a few steps, indicating that this controller like the ramp controller was at least locally stable. The apex body angle, θ_{max} averaged 7.1 deg (0.124 rad) with a variation of +1.8 deg (0.0314 rad) and -1.2 deg (0.0209 rad). The robot averaged approximately 0.075 $\frac{m}{s}$.

Figure 4.3 shows the desired and actual leg angles, ϕ_1, ϕ_2, ϕ_3, and ϕ_4. For the front legs, ϕ_1 and ϕ_3 tracking was quite poor with a maximum tracking error of around 5.1 deg (0.089 rad). However, this did not seem to affect the stability of the walking motion. The large tracking error in back leg angles, ϕ_2 and ϕ_4 mostly due to the step inputs also didn't seem to cause a problem.

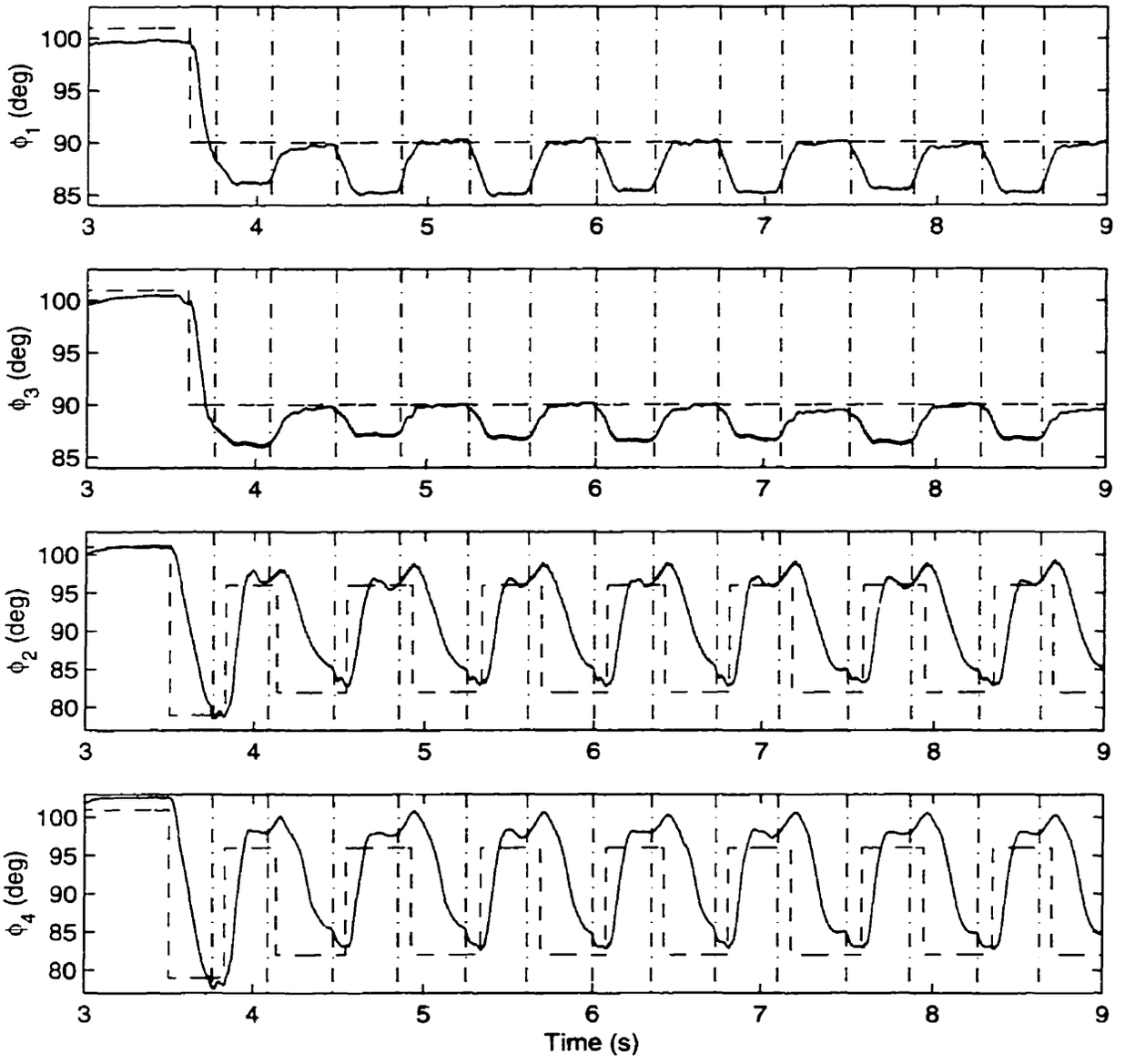

Figure 4.3: Experimental results of the step controller, showing ϕ_1, ϕ_2, ϕ_3, and ϕ_4. Desired leg angles are shown by dashed lines while actual angles are shown solid. The transitions of leg support are indicated by the dot dashed lines.

4.3 Non-planar Motion

Up to this point, it has always been assumed that Scout I's motion was planar. However, the real world is three dimensional and for a robot to function within it, the machine must be able to break out of the plane.

This section presents two behaviors that fit this category. Each behavior broke out of the plane by applying a differential angle to the left and right legs of both the front and back leg pairs, thus giving Scout I a twisting motion. Before each behavior is presented, a modified step controller must be defined. Figure 4.4 details the motion of the back legs for one complete step. At back leg impact, the back legs were commanded to a fixed angle, ϕ_2^B. During back leg support, after a time t_{back} each back leg was then given a slightly different step input to ϕ_2^F and ϕ_4^F. This gave Scout I a twisting motion. After front leg impact a second delay was incorporated, t_{front} before both legs were once again commanded to ϕ_2^B. This gave time to prevent toe stubbing.

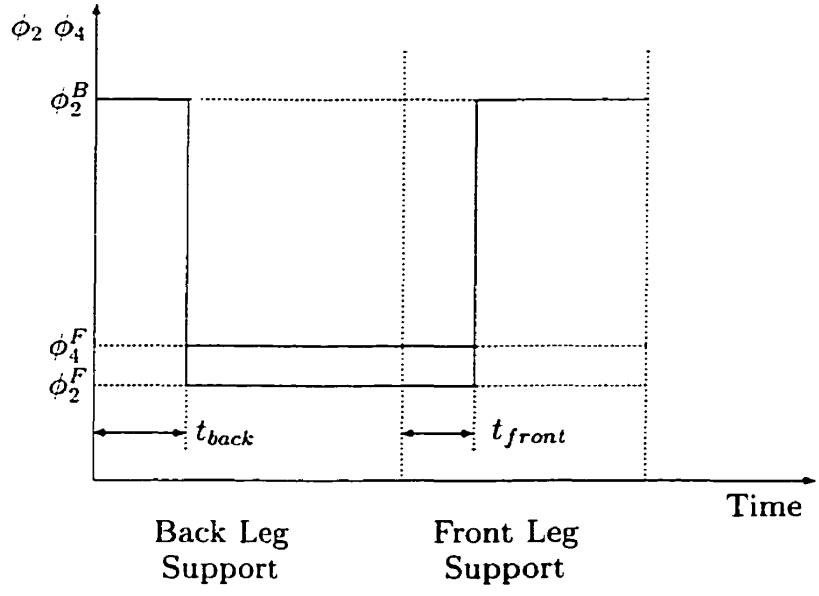

Figure 4.4: Back Leg Inputs For Non-planar Motion

Unlike all of the previous controllers examined, this controller also allowed for the

possibility of moving the front legs. Figure 4.5 details the motion of the front legs for one complete step. At back leg impact, the front legs were commanded to slightly different angles, ϕ_1^B and ϕ_3^B. After a time t_{back}, they were both given a step input to ϕ_1^F. The delay t_{back} was intended to prevent toe stubbing. A second delay t_{front} was applied after front impact before the legs were once again commanded to the slightly different angles ϕ_1^B and ϕ_3^B.

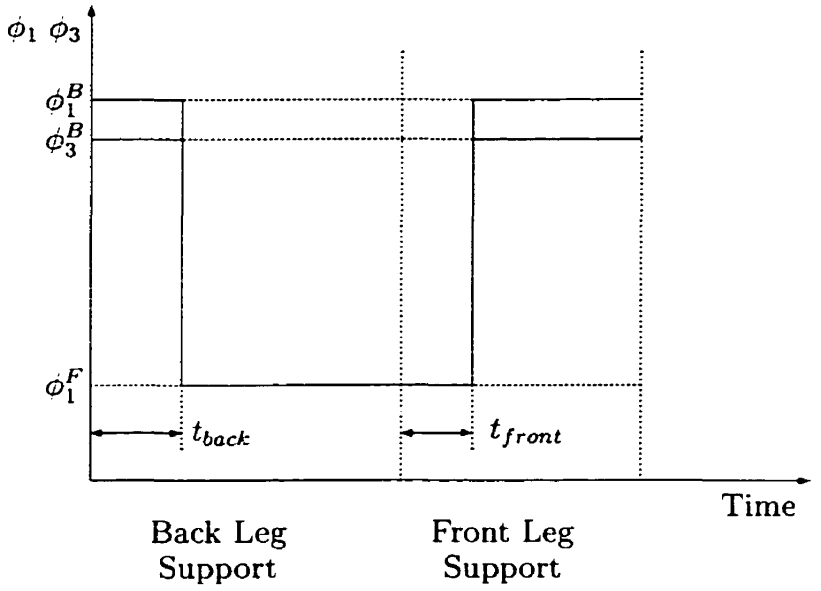

Figure 4.5: Front Leg Inputs For Non-planar Motion

Like the step controller, the delays t_{back} and t_{front} were selected based on the stance times during the last step. For t_{back} a fraction of the previous back leg stance was used and for t_{front} a fraction of the previous front leg stance was used.

4.3.1 Turning

In order to enable turning, the leg differentials for both the front and back legs were set to twist Scout I in the same direction. Referring to Figure 4.4 the back leg angles were defined according to

$$\phi_2^F = \phi_{2,nominal}^F - \phi_{turn} \quad (4.1)$$

$$\phi_4^F = \phi_{2,nominal}^F + \phi_{turn}. \quad (4.2)$$

Similarly, referring to Figure 4.5 the front leg angles were defined as

$$\phi_1^B = \phi_{1,nominal}^B - \phi_{turn} \quad (4.3)$$

$$\phi_3^B = \phi_{1,nominal}^B + \phi_{turn} \quad (4.4)$$

$$\phi_1^F = \phi_{1,nominal}^B. \quad (4.5)$$

With this arrangement, the amount and direction of turning could be specified by one variable ϕ_{turn}. A positive value resulted in turning to the right while a negative value resulted in turning to the left. Setting ϕ_{turn} to zero resulted in the turning controller collapsing down to the step controller (Section 4.2).

The effectiveness of this controller was examined experimentally using the parameters in Table 4.2 and the results are displayed in Figures 4.6, 4.7, and 4.8. The experiment was identical to the one in Section 4.2 for the first 6.5 seconds ($\phi_{turn} = 0$). At that point, ϕ_{turn} was changed to 3.6 deg (0.063 rad) and the turn begun. As with all previous experiments, the transitions of support indicated on Figures 4.6 and 4.7 are the midpoints of the impact phases (when all four legs were on the ground) and for control purposes, the transition of support was assumed to occur at the start of the impact. There was very little difference in these stance times between straight walking and turning.

Figure 4.6 indicated that during both straight walking and turning, Scout I achieved steady periodic motion. However, during turning there was an apparent increase in θ_{max}. This effect tended to grow as ϕ_{turn} was increased, limiting the radius of turn that could be achieved.

Figure 4.7 shows the desired and actual leg angles. As with straight walking (Figure 4.3) the tracking was poor. However, this did not seem to affect the results shown in

ITEM	VALUE
$\phi^B_{1,nominal}$	90.0 deg (1.571 rad).
ϕ^B_2	96.0 deg (1.676 rad).
$\phi^F_{2,nominal}$	82.0 deg (1.431 rad).
ϕ_{turn}	3.6 deg (0.063 rad).
t_{step}	30% of the previous back stance time (Set to 0.1 s for the first step).
t_{return}	30% of the previous front stance time (Set to 0.1 s for the first step).

Table 4.2: Turning Controller Parameters

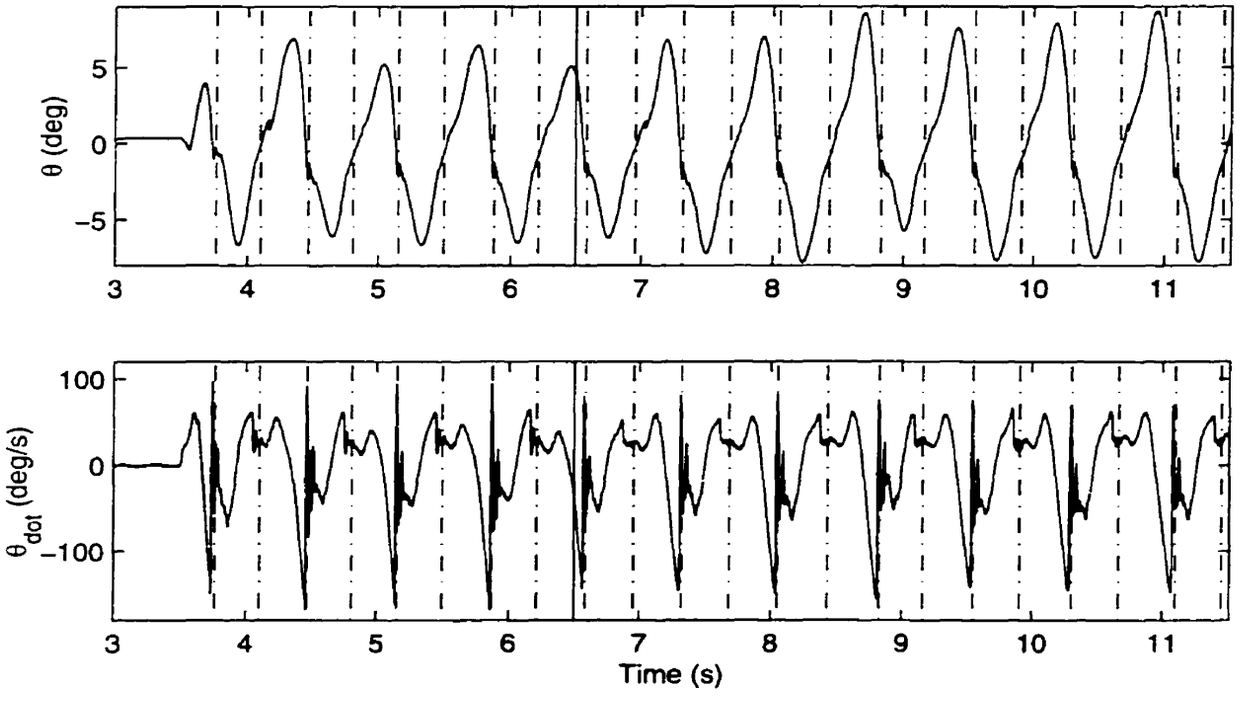

Figure 4.6: Experimental results of the turning controller, showing θ and $\dot{\theta}$. The transitions of leg support are indicated by the dot dashed lines. The command to turn is indicated by the solid vertical line.

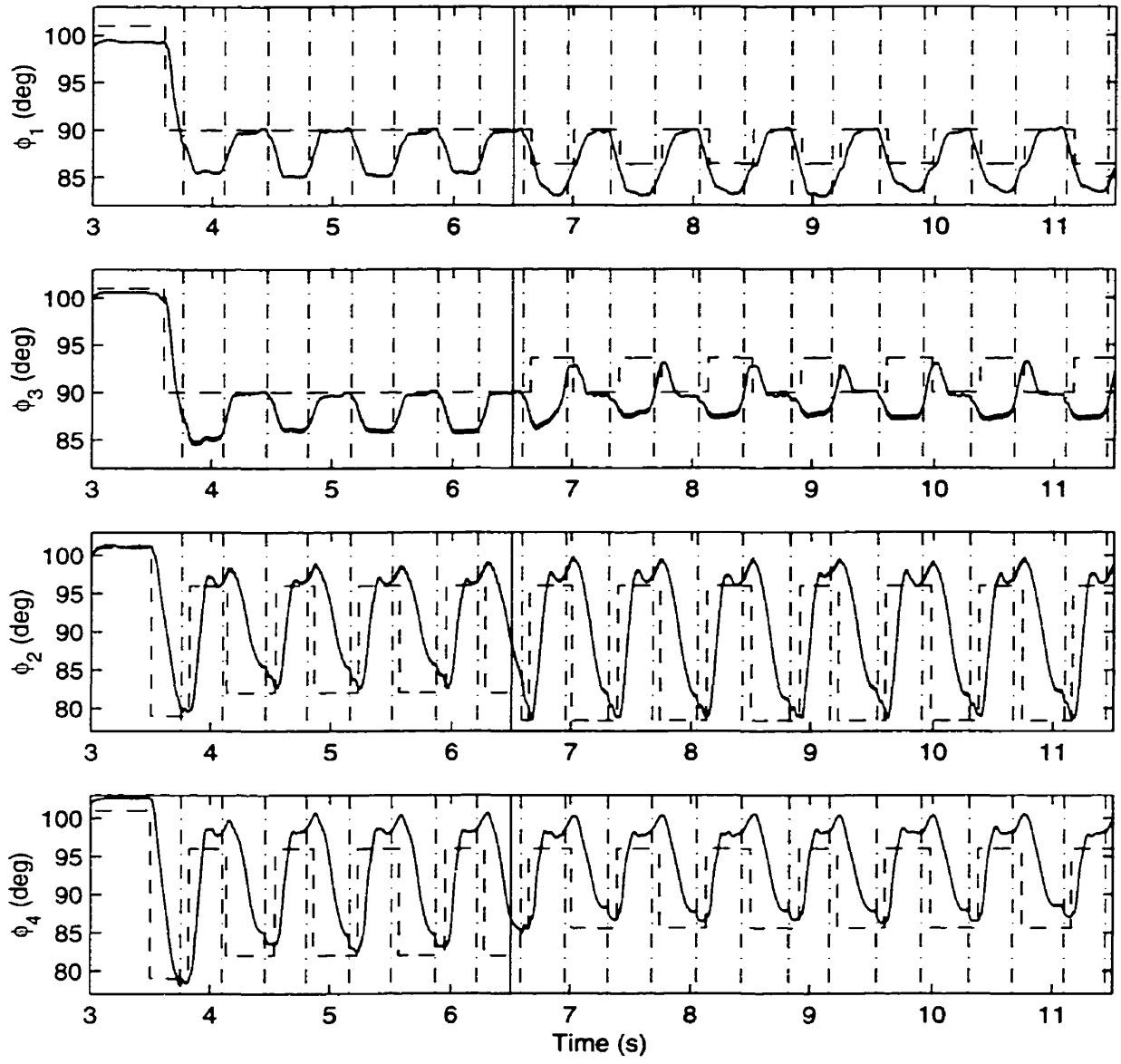

Figure 4.7: Experimental results of the turning controller, showing ϕ_1, ϕ_2, ϕ_3, and ϕ_4. Desired leg angles are shown by dashed lines while actual angles are shown solid. The transitions of leg support are indicated by the dot dashed lines. The command to turn is indicated by the solid vertical line.

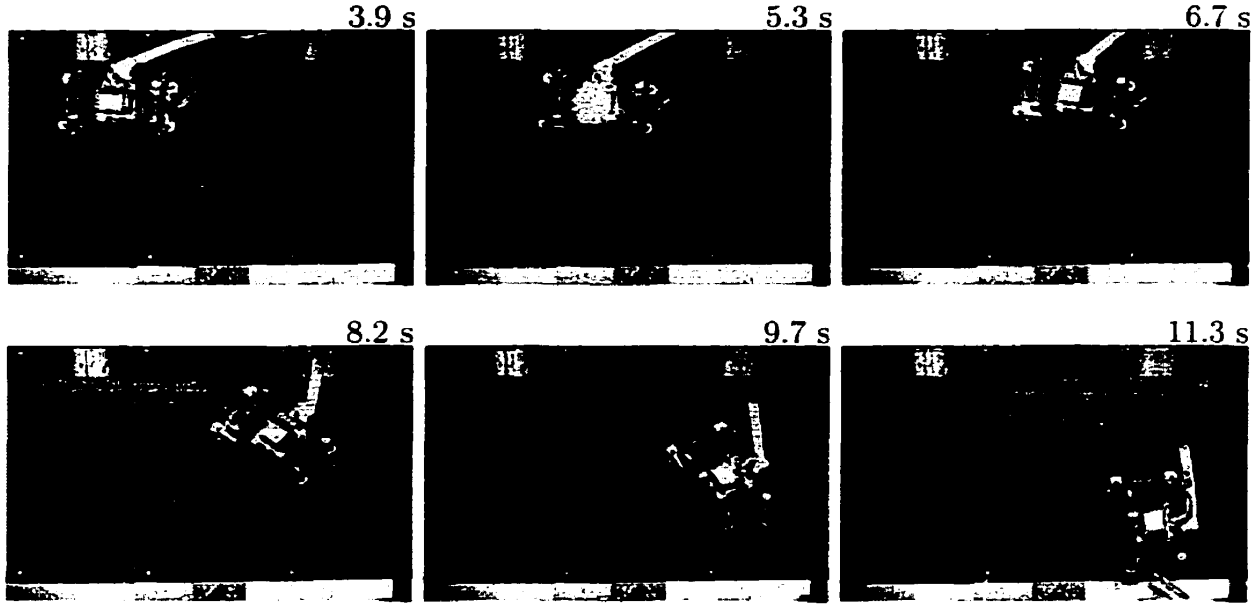

Figure 4.8: Top view of Scout I turning 80.0 deg (1.40 rad). The time index is accurate to approximately ±0.1 s.

Figure 4.8 which indicate Scout I making an approximately 80.0 deg (1.40 rad) turn. This was accomplished in 7 steps.

4.3.2 Side Stepping

The twisting motion created by the controller of Figures 4.4 and 4.5 had not only a rotational component, but also one to the side. If all other components but the side motion could be cancelled out, then side stepping would result. To accomplish this, five parameters were used, ϕ_{impact}, ϕ_{sweep}, $\phi_{sidestep}$, t_{back}, and t_{front}. Referring to Figure 4.4 the back leg angles were defined as

$$\phi_2^B = \phi_{impact} \tag{4.6}$$

$$\phi_2^F = \phi_{sweep} - \phi_{sidestep} \tag{4.7}$$

$$\phi_4^F = \phi_{sweep} + \phi_{sidestep}. \tag{4.8}$$

Similarly, referring to Figure 4.5 the front leg angles were defined as

$$\phi_1^B = 180.0(deg) - \phi_{sweep} + \phi_{sidestep} \quad (4.9)$$

$$\phi_3^B = 180.0(deg) - \phi_{sweep} - \phi_{sidestep} \quad (4.10)$$

$$\phi_1^F = 180.0(deg) - \phi_{impact}. \quad (4.11)$$

The front leg sweep was the opposite of the back leg sweep in order to eliminate forwards motion. Similarly, the differentials were defined to cancel the turning motion caused by the twisting of Scout I. With this arrangement, the amount and direction of side stepping could be specified with the one variable $\phi_{sidestep}$. A positive value resulted in side stepping to the right while a negative value resulted in side stepping to the left. Setting $\phi_{sidestep}$ to zero resulted in no sideways motion and the robot would simply walk in place.

This controller was examined experimentally using the parameters in Table 4.3 and the results are displayed in Figures 4.9, 4.10, and 4.11. The start-up sequence was identical to the experiment with the step controller (Section 4.2) up to the first front impact (around 3.7 s) except that ϕ_1 and ϕ_3 were set to 89.0 deg (1.553 rad) before front impact. At that point, the side stepping controller then became active. The transitions of support indicated on Figures 4.9 and 4.10 are the midpoints of the impact phases. Once again, for the purposes of control, transition of support was assumed to occur at the beginning of the impact.

Figure 4.9 indicated that a relatively steady periodic motion was achieved with the side stepping controller. Although the motion was intended to be symmetric, θ_{max} was slightly less than θ_{min} indicating that this was not entirely the case. This was also apparent in the impact durations. The back leg impact averaged approximately 0.03 s while the front leg impact average approximately 0.08 s. This was likely due to some asymmetry in the robot. One possible cause was the differences between the front and back leg separations (Recall from Section 2.1 that the front legs were placed closer together than the back legs). Another possible cause was the asymmetry in Scout I's power supply (Recall from Section 2.4.2 that one battery pack powered the

ITEM	VALUE
ϕ_{impact}	91.0 deg (1.588 rad).
ϕ_{sweep}	82.0 deg (1.431 rad).
$\phi_{sidestep}$	4.5 deg (0.079 rad).
t_{back}	30% of the previous back stance time (Set to 0.1 s for the first step).
t_{front}	30% of the previous front stance time (Set to 0.1 s for the first step).

Table 4.3: Side Stepping Controller Parameters

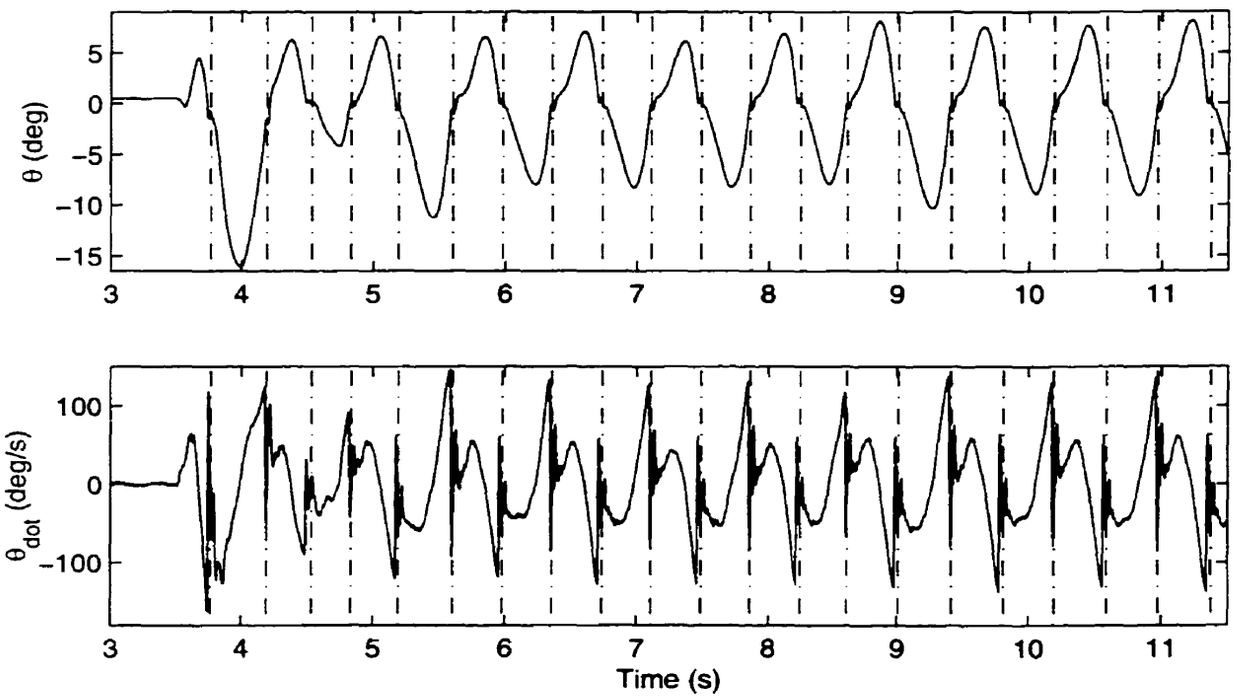

Figure 4.9: Experimental results of the side stepping controller, showing θ and $\dot{\theta}$. The transitions of leg support are indicated by the dot dashed lines.

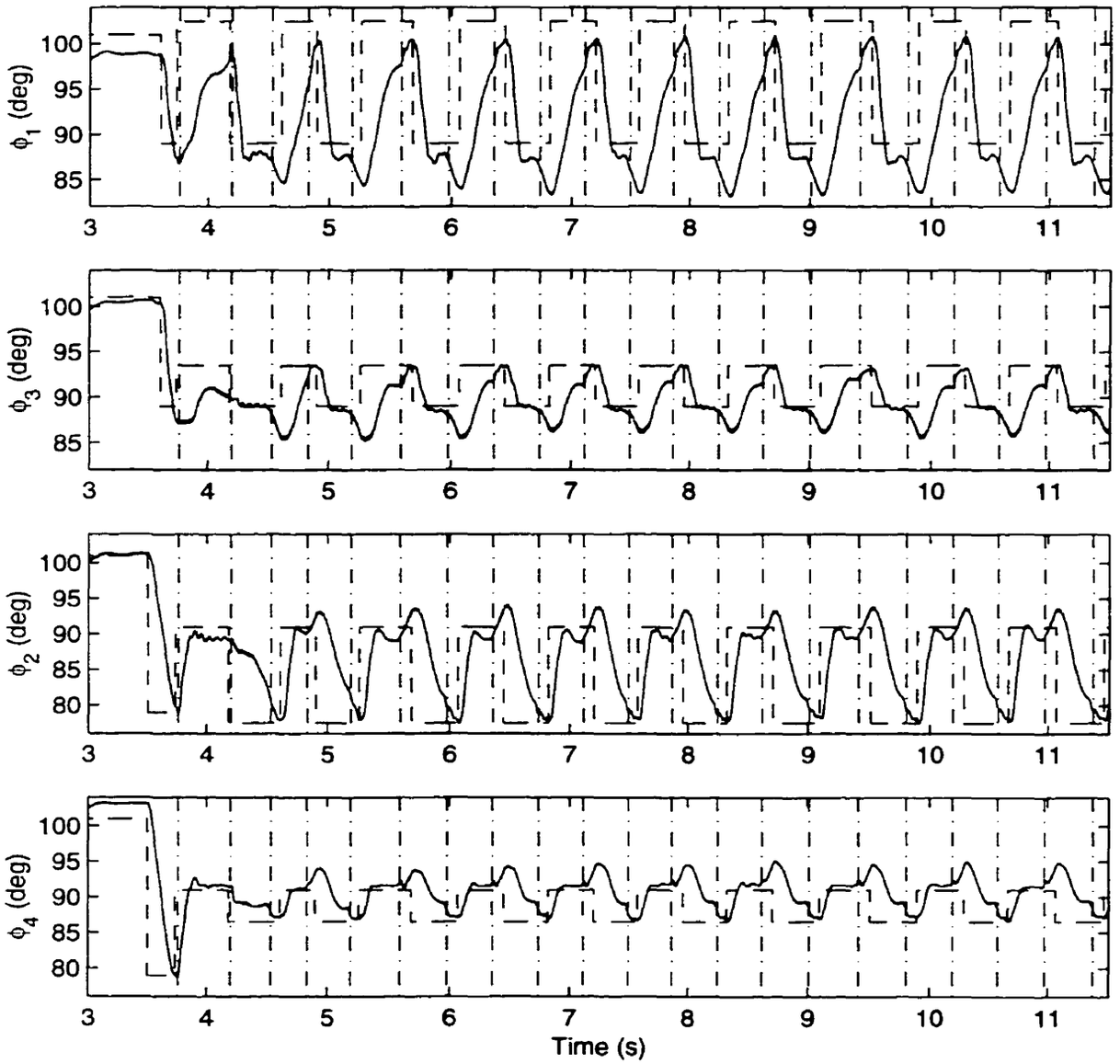

Figure 4.10: Experimental results of the side stepping controller, showing ϕ_1, ϕ_2, ϕ_3, and ϕ_4. Desired leg angles are shown by dashed lines while actual angles are shown solid. The transitions of leg support are indicated by the dot dashed lines.

left actuators while another powered the right but that one battery pack was further loaded by the electronics).

Figure 4.10 shows the desired and actual leg angles. As with all of the step input based controllers, the tracking was poor. However, despite this Figure 4.11 shows that Scout I did generally achieve side stepping, although the robot did drift slowly backwards as well (to the left side of the pictures). The speed was approximately 0.045 $\frac{m}{s}$. This motion was by no means efficient but it demonstrated the possibility of Scout I being able to move in any direction.

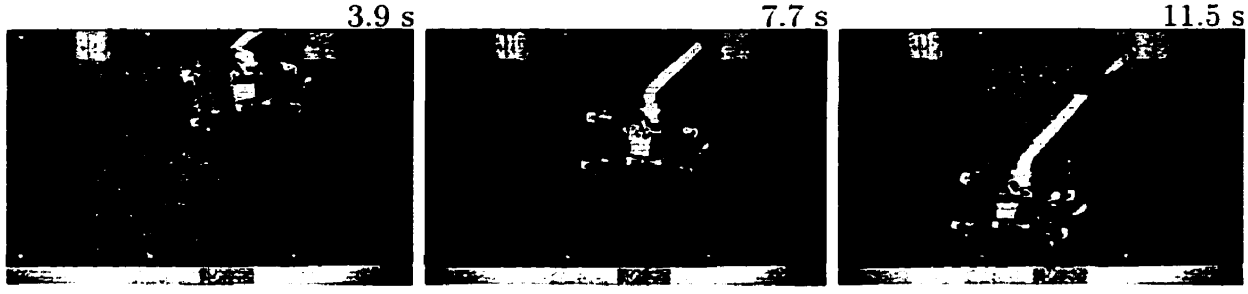

Figure 4.11: Top view of Scout I side stepping. The time index is accurate to approximately ±0.1 s.

4.4 Entertaining Behaviors

For entertainment applications, a robot like Scout I must be able to exhibit interesting behaviors. Two such behaviors are presented in this section.

4.4.1 Sitting Down

Figure 4.12 shows the desired and actual leg angles during a sitting experiment. An inspection of the plots reveals that most of the actual leg angles end between 3 and 4 seconds. This was due to the leg angle sensors going out of range and only the valid data being plotted. The leg commands for this behavior were very simple. From 0.0 to 2.0 s, the legs were commanded to 90.0 deg (1.571 rad). From 2.0 to 3.5 s, the

robot was commanded to lean back to ϕ_1=ϕ_2=ϕ_3=ϕ_4=177.0 deg (3.089 rad). After that, the legs simply remained at 177.0 deg (3.089 rad).

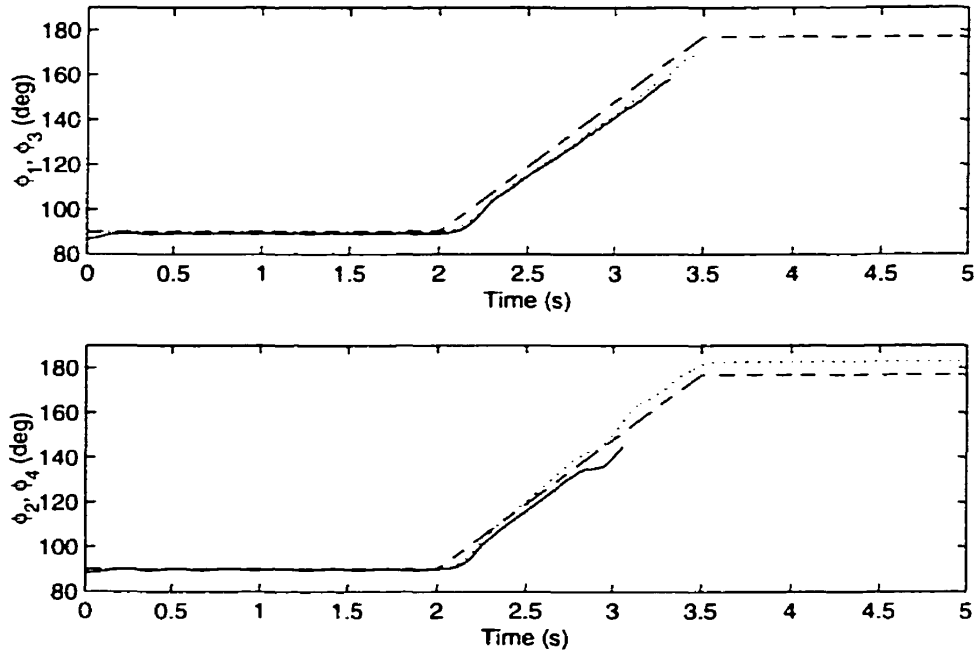

Figure 4.12: Experimental result of the sitting experiment showing ϕ_1, ϕ_2, ϕ_3, and ϕ_4. The desired values are shown by the dashed lines. The left side legs are indicated by solid lines while the right side legs are indicated by the dotted lines.

The effects of this motion are shown in Figure 4.13. As the robot leaned back, it eventually got to the point of toppling (2.6 s) and fell backwards (2.8 s) on to its back body (2.9 s). As the ramp input to the legs was completed, the body was lowered back to horizontal (3.6 s).

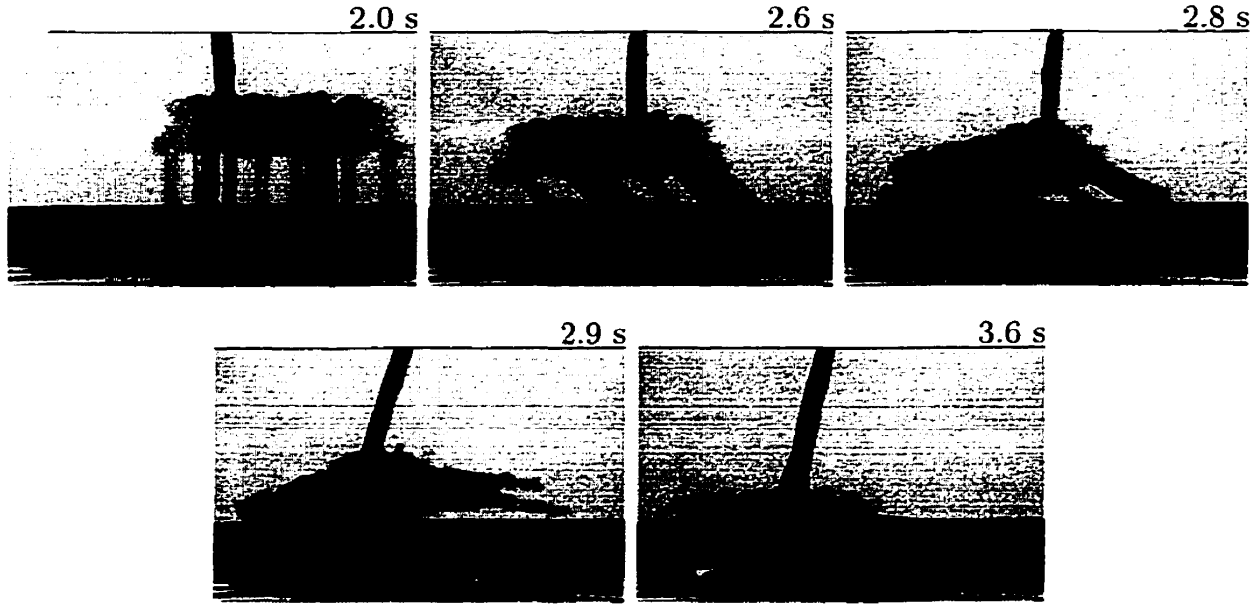

Figure 4.13: Side view of Scout I sitting down. The time index is accurate to approximately ±0.1 s.

4.4.2 Laying Down

Another entertaining behavior was laying down. Figure 4.14 shows the desired and actual leg angles for a laying down experiment. Like the experiment in Section 4.4.1 the leg angle sensors went out of range and only the valid data was plotted in Figure 4.14. This behavior was slightly more complicated than sitting down. From 0.0 to 2.0 s, the legs were commanded to point straight down. Next, from 2.0 to 3.0 s, the robot leaned back to ϕ_1=ϕ_2=ϕ_3=ϕ_4=105.0 deg (1.833 rad) and then waited until 3.5 s. A step input was then applied to the back legs to ϕ_2=ϕ_4=65.0 deg (1.134 rad), causing Scout I to jump forwards. When the front legs were in the air at 3.6 s, they were commanded to ϕ_1=ϕ_3=115.0 deg (2.007 rad). After the robot impacted with the ground it was given until 4.0 s to stabilize before the front legs were commanded to 180.0 deg (3.142 rad) and the back legs to 0.0 deg (0.0 rad) over two seconds. During this motion, the toes were required to slip along the ground. After reaching the fully spread position at 6.0 s, the legs were commanded to hold for the remainder of the

experiment. Figure 4.15 shows a series of frame captures detailing the major motions in the laying down sequence.

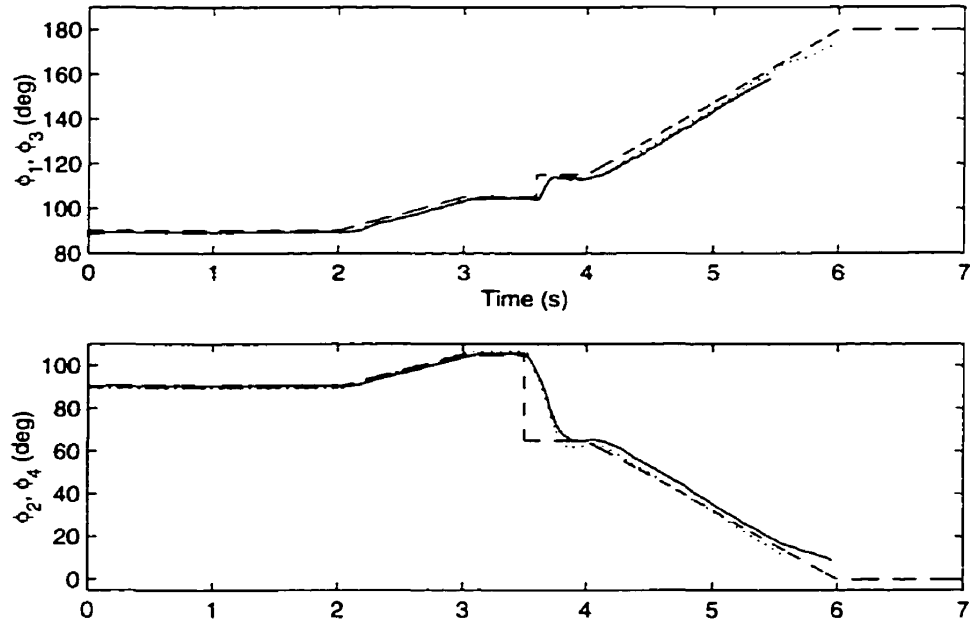

Figure 4.14: Experimental result of the laying down experiment showing ϕ_1, ϕ_2, ϕ_3, and ϕ_4. The desired values are shown by the dashed lines. The left side legs are indicated by solid lines while the right side legs are indicated by the dotted lines.

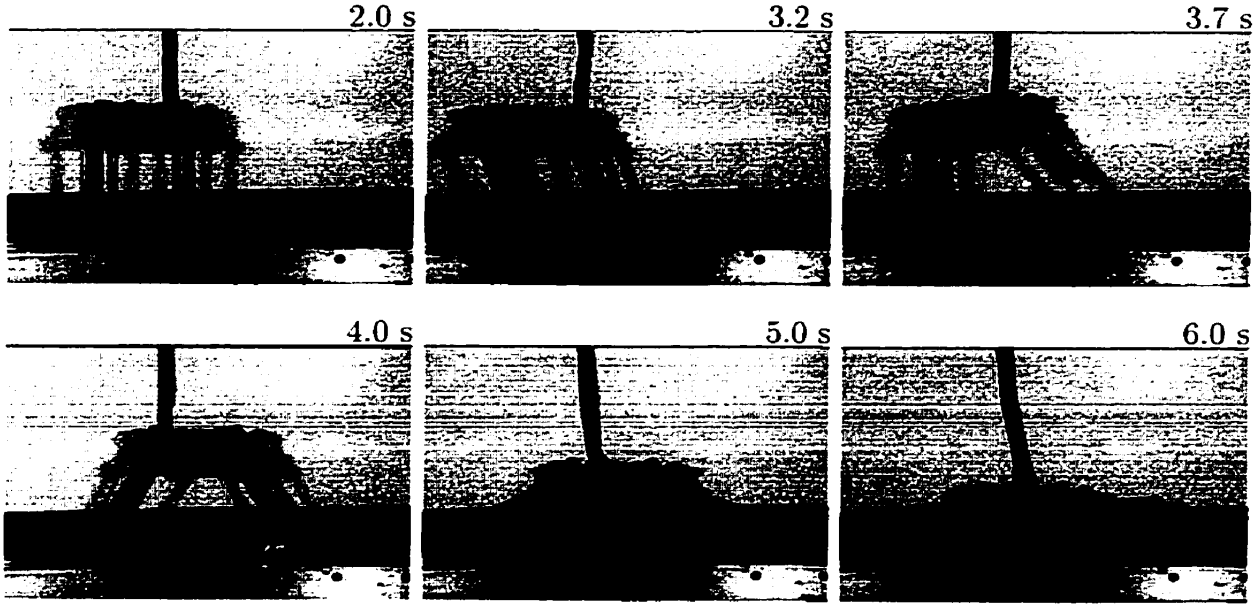

Figure 4.15: Side view of Scout I laying down. The time index is accurate to approximately ±0.1 s.

4.5 Climbing

Wheeled or tracked robots excel in areas where the ground is relatively flat. However, animals are capable of a much wider range of motion due to the use of their arms and legs. This is one of the primary motivations for studying legged locomotion; to go where wheeled or tracked robots can't (Figure 4.16). In this section, a number of behaviors are presented for climbing steps or stairs using either Scout I or Scout II.

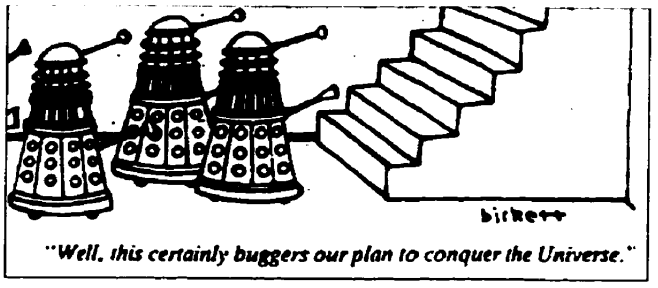

Figure 4.16: Wheeled or tracked robots can be stopped by simple obstacles such as stairs.

4.5.1 Dynamic Step and Stair Climbing

Figure 4.17 details an experiment of Scout I climbing a 0.09 m step (45% of the leg length). This experiment was performed with a much simplified Scout I. Both the batteries (Section 2.4.2) and the SPP/SPI system (Section 2.4.1) were not mounted at this stage and Airtronics R/C servos were still being used in the front positions (Section 2.2). The only sensing was toe contact with the ground and Scout I's mass was 1.2 kg. This experiment was performed with the assistance of Geoff Hawker.

At the experiment start, the legs were commanded to point straight down. The robot then leaned back (0.47 s, 1.90 s) and a step input was applied to the back legs, causing Scout I to jump forwards (2.47 s). The front legs were then set for the first impact. As can be seen at 2.47 s, the robot twisted somewhat during this initial launching but the problem was corrected at front leg impact (2.60 s). Scout I then rocked on its front legs (2.80 s) and swung its back legs in before back touchdown occurred (3.00 s). A second forwards launching was then applied by the back legs (3.27 s) and the front legs set for the second front impact (3.43 s). The front legs were then swept forwards (3.73 s). This raised the body and allowed the back legs to swing in and land on top of the step (3.97 s). A third forwards launch was then commanded (4.10 s) and all the legs set to 90.0 deg (1.571 rad). After front leg impact (4.67 s), Scout I settled on top of the step.

This experiment proved the feasibility of Scout I climbing a step of significant size. Furthermore, using the same type of controller Scout I was simulated climbing a flight of five 0.09 m high by 0.14 m deep stairs in Working Model 2D [19]. However, the motion required to do this involved Scout I rocking very close to its toppling point a number of times. This fact, along with the open loop nature of the controller resulted in a very low success rate in step climbing (approximately 10%). Experimental results with stair climbing would have been appreciably worse. To make the climbing motion reliable, a feedback controller (with appropriate sensors) and higher quality actuators would almost certainly be required.

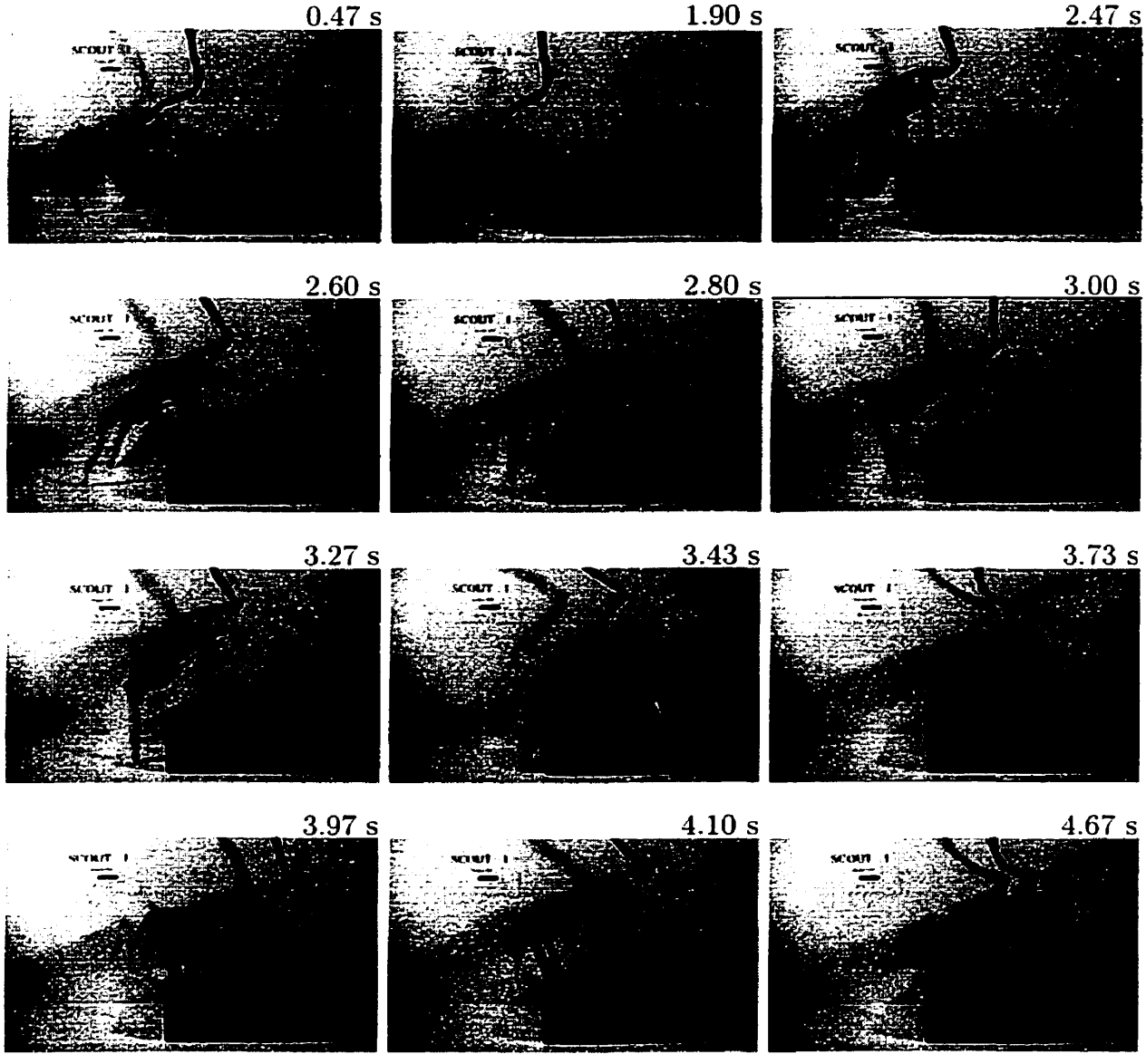

Figure 4.17: Side view of Scout I climbing a 90 mm step. The time index is accurate to approximately ±0.03 s.

4.5.2 Static Stair Climbing

After realizing the difficulty in developing a dynamic climbing algorithm, the possibility of stair climbing using a static gait was investigated. For this analysis, the Scout II robot (Section 2.8) was chosen because of its ability to perform full revolutions with its legs and a generally cleaner body (allowing the body to slide along the stairs without getting caught up). Referring to Figure 3.2, the relevant kinematic parameters are detailed in Table 4.4. The stair dimensions were taken from the stairwell at the Centre for Intelligent Machines.

ITEM	VALUE
l	0.250 m
L	0.275 m
H	0.000 m
Overall body length (Centered about the center of mass)	0.670 m
Overall body height (Centered about the center of mass)	0.120 m
Stair Height	0.170 m
Stair Depth	0.250 m

Table 4.4: Kinematic Parameters For Scout II Stair Climbing

For a robot to balance statically, it must keep its center of mass within the polygon of support made by its supporting feet. If this is done and the robot moves slowly enough to minimize dynamic effects, then toppling can be avoided.

Figure 4.18 details the climbing algorithm that was developed. It was assumed that Scout II's front legs moved together and its back legs move together, resulting in a planar problem. It was further assumed that the robot began in the configuration described in Phase 1 with the back toe 0.150 m from the left edge of a step and the

front toe 0.030 m from the left edge of the step two steps up. During Phase 2, the robot would lean forwards until its body was in contact with the stairs. With the possibility of toppling now eliminated, its would swing its back legs around onto the next step (Phase 3). Sliding backwards would be prevented by the front legs. Next, during Phase 4 the front legs would be swung around onto the next step. Sliding in this case would be prevented by the back legs. With both legs one step higher, Scout II would then stand up (Phase 5). The problem of toppling would be at its worst at this point. However, the center of gravity would be just within the polygon of support due to the fact that the robot has feet of diameter 0.050 m. With the back legs contacting the ground at as shallow an angle as in Phase 4, the effective length of the leg would be slightly less than 0.250 m. At this point, Scout II would be up one stair but in the wrong position to climb another. The problem would be eliminated by leaning forwards and moving the legs to the same angles as in Phase 2. This would cause the robot to slide backwards somewhat, but it would end up in the configuration shown in Phase 2. The procedure could then be repeated from Phase 2 to climb the next step.

This climbing algorithm demonstrates that Scout II can negotiate a flight of stairs using a minimum of sensing. However, for an algorithm such as this to be practical it must be further analyzed and developed to function on a variety of stairs. Furthermore, getting on and off a flight of stairs must be examined.

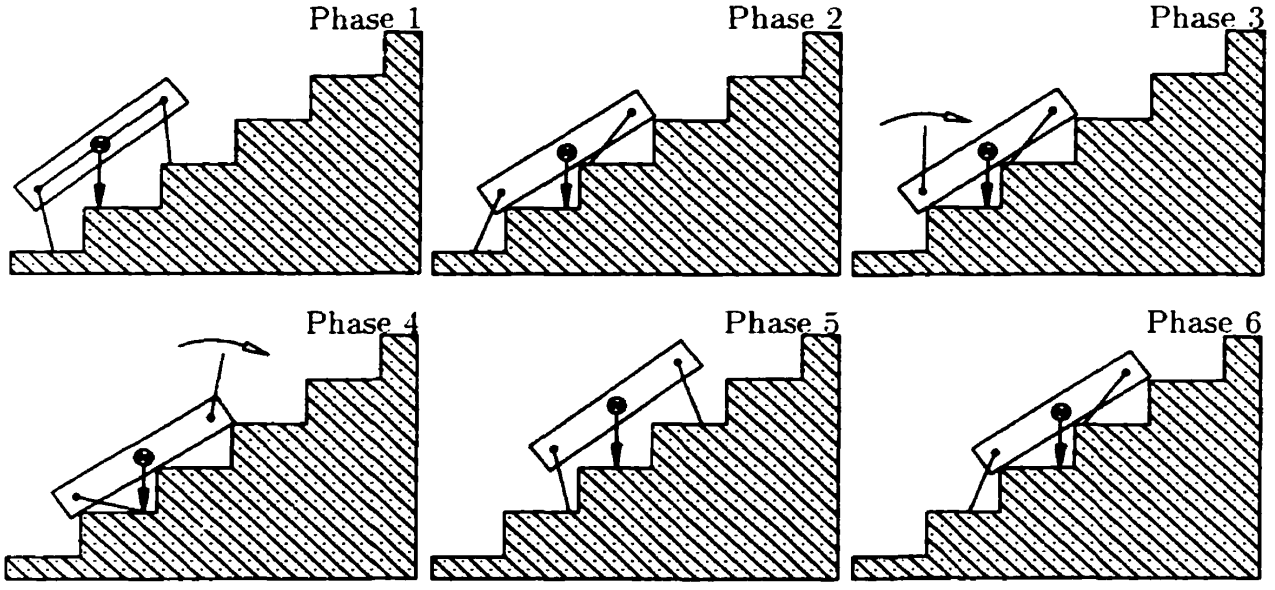

Figure 4.18: Stair climbing algorithm for Scout II. The projection of the center of mass on the ground is indicated by the downward pointing arrows.

4.6 Summary and Conclusions

In this chapter, a number of different behaviors were presented. These included controllers for walking, tuning, side stepping, sitting down, laying down, and climbing steps and stairs. While these behaviors were not rigorously analyzed, they still demonstrated that the Scout class of robots are not confined to simply walking within a plane. The collection of a rich set of behaviors is a step towards a truly practical legged robot.

Chapter 5

Conclusion

5.1 Summary

The design of the first of a new type of quadruped robot was presented. This robot, called Scout I and based on the Scout class utilized a mechanically simple design. Each leg was essentially a stick and had only one actuated degree of freedom, a rotary joint at the hip. This represented a significant reduction from previous designs (typically incorporating three actuated degrees of freedom per leg) and should work to reduce cost and increase reliability. R/C servos were used as the actuators on Scout I. Despite the limited controller built into these servos, good tracking was achieved by instrumenting position feedback and applying a second controller in software.

In modelling the robot, impacts with the ground were assumed to be instantaneous with angular momentum about the impacting toe being conserved. Stance phases were modelled as a double inverted pendulum with a torque input between the two links and a pin joint with the ground. A simple walking controller then was presented that was virtually open loop, requiring only sensing of touchdown with the ground (and leg angles with respect to the body for leg angle control). Scout I with this controller was examined in both simulations and experiments. The simulations indicated that the walking controller was very sensitive to both model and controller parameters. It was

also shown that small errors in the impact model coupled with this high sensitivity lead to significant errors in the setpoint achieved experimentally. The source of the impact model error was traced to the lack of a completely rigid system. This was primarily caused by the fact that the actuators could not lock the legs completely rigidly in place during impacts. However, despite these discrepancies stable open loop walking was achieved for all cases examined.

Chapter 4 presented a variety of other behaviors for both Scout I and its successor, Scout II. These behaviors included a different walking controller, non-planar motion including turning and side stepping, entertaining behaviors such as sitting and laying down, and enhanced mobility in the form of step and stair climbing.

This work has demonstrated that the Scout class of robot, despite the limitations imposed upon it by its simple design and few sensors is still capable of a wide variety of useful behaviors.

5.2 Future Work

The results of this work open a variety of areas for further investigation. The impact modelling error needs to be addressed. This can be done in one of two ways (or both). Either the impact model can be improved to take into account actuator compliance during impact or a more rigid Scout robot can be built. Since the ramp controller requires no motion in the front leg, the actuators can be removed and replaced with a mechanical rigid joint, increasing the rigidity of the system. This should bring the theoretical and experimental results closer together.

By assuming that the front leg is a fixed joint, then the ramp controller inputs can be reduced to two (ϕ_2^B and $\dot{\phi}_2$). A numerical search can then be performed to get both the resultant θ_{max} and velocity for the valid range of ϕ_2^B and $\dot{\phi}_2$. From this, a look-up table can be generated for controlling the velocity of Scout.

A number of the behaviors in Chapter 4 can be examined in more detail. It should be possible to apply turning to the ramp controller with a differential to $\dot{\phi}_2$ and

some sort of differential to the front legs. Further investigation needs to be done on the relationship between the differential applied and how much turning results as well as how stability is affected by the turning. Side stepping can also be further investigated and expanded to provide walking in any direction. Finally, the stair climbing controller for Scout II should also be implemented and the limitations of the algorithm investigated.

With the improvements described in this section plus the new behaviors currently under investigation (described in Section 1.3), it is hoped that the Scout class of robots will lead to a truly practical legged robot.

Bibliography

[1] M. Ahmadi. *Stable Control of a One-Legged Robot Exploiting Passive Dynamics.* PhD thesis, McGill University, Montreal, Quebec, Canada, Mar. 1998.

[2] M. Ahmadi and M. Buehler. Stable control of a simulated one-legged running robot with hip and leg compliance. *IEEE Transactions on Robotics and Automation*, 13(1):96–104, Feb. 1997.

[3] Analog Devices Inc., One Technology Way, P.O. Box 9106, Norwood, MA, 02062-9106, Phone (617) 329-4700. *±1 g to ±5 g Single Chip Accelerometer with Signal Conditioning*, 1995.

[4] Applied Geomechanics Inc., 1336 Brommer Street, Santa Cruz, CA 95062, Phone (408) 462-2801. *Inclinometer Manufacturer.*

[5] T. G. Bartholet. Odetics develops the world's first functionoid. *Nuclear Engineering International*, 30(367):37–38, Apr. 1985.

[6] T. G. Bartholet. Odetics makes great strides. *Nuclear Engineering International*, 31(381):37–38, Apr. 1986.

[7] M. Buehler, R. Battaglia, A. Cocosco, G Hawker, J. Sarkis, and K. Yamazaki. Scout: A simple quadruped that walks, climbs, and runs. In *Proceedings of the IEEE International Conference on Robotics and Automation (ICRA)*, pages 1701–1712, Leuven, Belgium, May 1998.

[8] A. E. Cocosco. Control of walking in a quadruped robot with stiff legs. Master's thesis, McGill University, Montreal, Quebec, Canada, Jul. 1998.

[9] E R. Dunn and R. D. Howe. Towards smooth bipedal walking. In *Proceedings of the IEEE International Conference on Robotics and Automation (ICRA)*, volume 3, pages 2489–2494, May 1994.

[10] E R. Dunn and R. D. Howe. Foot placement and velocity control in smooth bipedal walking. In *Proceedings of the IEEE International Conference on Robotics and Automation (ICRA)*, pages 578–583, Minneapolis, MN, Apr. 1996.

[11] J. Furusho, A Sano, M. Sakaguchi, and E. Koizumi. Realization of bounce gait in a quadruped robot with articular-joint-type legs. In *Proceedings of the IEEE International Conference on Robotics and Automation (ICRA)*, pages 697–702, 1995.

[12] J. A. Golden and Y. F. Zheng. Gait synthesis for the SD-2 biped robot to climb stairs. *International Journal of Robotics and Automation*, 5(4):149–159, Dec. 1990.

[13] P. Gregorio. Design, control and energy minimization strategies for the ARL Monopod. Master's thesis, McGill University, Montreal, Quebec, Canada, Sep. 1994.

[14] P. Gregorio, M. Ahmadi, and M. Buehler. Design, control, and energetics of an electrically actuated legged robot. *IEEE Transactions on Systems, Man, and Cybernetics*, 27B(4):626–634, Aug. 1997.

[15] S. Hirose. A study of design and control of a quadruped walking vehicle. *The International Journal of Robotics Research*, 3(2):113–133, Summer 1984.

[16] S. Hirose, K. Yoneda, and K. Arai adn T. Ibe. Design of a quadruped walking vehicle for dynamic walking and stair climbing. *Advanced Robotics*, 9(2):107–124, 1995.

[17] J. K. Hodgins and M. H. Raibert. Adjusting step length for rough terrain locomotion. *IEEE Transactions on Robotics and Automation*, 7(3):289–298, Jun. 1991.

[18] InterTAN Canada Ltd., Barrie, Canada, L4M 4W5. *Switch Supplier.*

[19] Knowledge Revolution, 66 Bovet Road, Suite 200, San Mateo, California, 94402. *Working Model 2D User's Manual*, 1996.

[20] N. Koyachi, H. Adachi, and E. Nakano. Design and basic control of stair-climbable fixed gait hexapod walking machines. In *Proceedings of the USA Japan Symposium on Flexible Automation Crossing Bridges Advances in Flexible Augtomation and Robotics*, 1986.

[21] Lambda Electronics (Canada) Inc., Kirkland, Quebec, Canada, H9H 3L4, Phone (514) 695-8330. *DC-DC Converter Manufacturer.*

[22] Marshall Electronics, P.O. Box 2027, Culver City, CA 90231, Phone (800) 800-6608. *Camera Manufacturer.*

[23] The MathWorks Inc., Cochituate Place, 24 Prime Park Way, Natick, Mass. 01760. *MATLAB Reference Guide*, Aug. 1992.

[24] K. Matsuoka. A mechanical model of repetative hopping movements. *Biomechanisms*, 5:251–258, 1980.

[25] Maxim Integrated Products, 120 San Gabriel Drive, Sunnyvale, CA 94086, Phone (408) 737-7600. *+5V, Low-Power, 12-Bit Serial ADCs*, 1993.

[26] Maxim Integrated Products, 120 San Gabriel Drive, Sunnyvale, CA 94086, Phone (408) 737-7600. *+5V, Low-Power, Voltage-Output, Serial 12-Bit DACs*, 1997.

[27] G. Mennitto. Compliant articulated robot leg with antagonistic LADD actuation. Master's thesis, McGill University, Montreal, Quebec, Canada, Feb. 1995.

[28] G. Mennitto and M. Buehler. Carl: A compliant articulated robotic leg for dynamic locomotion. *Robotics and Autonomous Systems*, 18:337–344, 1996.

[29] J.L. Meriam and L.G. Kraige. *Engineering Mechanics, Dynamics*, volume 2. John Wiley & Sons Inc., 3rd edition, 1992.

[30] H. Miura and I. Shimoyama. Dynamic walk of a biped. *International Journal of Robotics Research*, 3:60–74, 1984.

[31] R. A. Morrison. Iron mule train. In *Proceedings of Off-Road Mobility Research*, Washington, 1968.

[32] R. S. Mosher. Exploring the potential of a quadruped. In *International Automotive Engineering Congress*, Detroit, Michigan, Jan. 1969. Society of Automotive Engineers Inc.

[33] Murata Electronics North America Inc., 2200 Lake Park Drive, Smyrna, GA 30080. *Gyroscope Manufacturer.*

[34] Eadweard Muybridge. *Animals In Motion.* Dover Publications Inc., 180 Varick Street, New York, N.Y. 10014, 1957.

[35] Y. Ota, Y. Inagaki, K. Yoneda, and S. Hirose. Research on a six-legged walking robot with parallel mechanism. In *Proceedings of the IEEE/RSJ International Conference on Intelligent Robots and Systems (IROS)*, pages 241–248, Victoria, B.C., Canada, Oct. 1998.

[36] G. Petryk and M. Buehler. Robust estimation of pre-contact object trajectories. In *Proceedings of the Fifth Symposium on Robot Control (SYROCO)*, Nantes, France, Sep. 1997.

[37] G. A. Petryk. Dynamic object localization via a proximity sensor network. Master's thesis, McGill University, Montreal, Quebec, Canada, Aug. 1996.

[38] QNX Software Systems Ltd., 175 Terence Matthews Crescent, Kanata, Ontario, K2M 1W8, Phone (613) 591-0931. *Operating System Developer.*

[39] M. H. Raibert. *Legged Robots That Balance.* MIT Press, Cambridge, MA, 1986.

[40] M. E. Rosheim. *Robot Evolution: The Development of Anthrobotics.* John Wiley & Sons Inc., 1994.

[41] Sensor Technologie München GmbH, Postfach 1387, D-8505 Ottobrunn, Phone +90/601 76 37. *Infrared Sensor Manufacturer.*

[42] Sunset Radio Control, Box 716, Millet, Alberta, Canada, T0C 1Z0, Phone (800) 697-8672. *Hobby Supplier.*

[43] A. Takanishi, M. Ishida, Y. Yamazaki, and I. Kato. The realization of dynamic walking by the biped walking robot WL-10RD. In *Proceedings of the International Conference on Advanced Robotics (ICAR)*, 1985.

[44] Tower Hobbies, P.O. Box 9078, Champaign, Illinois, 61826-9078, Phone (800) 637-4989. *Tower Hobbies Catalog*, 1998.

[45] K. J. Waldron and R. B. McGhee. The Adaptive Suspension Vehicle. *IEEE Control Systems Magazine*, 6(6):7–12, Dec. 1986.

[46] K. J. Waldron, V. J. Vohnout, A. Pery, and R. B. McGhee. Configuration design of the Adaptive Suspension Vehicle. *The International Journal of Robotics Research*, 3(2):37–48, Summer 1984.

[47] D. Wettergreen, H. Pangels, and J. Bares. Behavior-based gait execution for the Dante II walking robot. In *Proceedings of the IEEE International Conference on Intelligent Robots and Systems (IROS)*, Pittsburgh, PA, Aug. 1995.

Appendix A

Circuit Diagrams

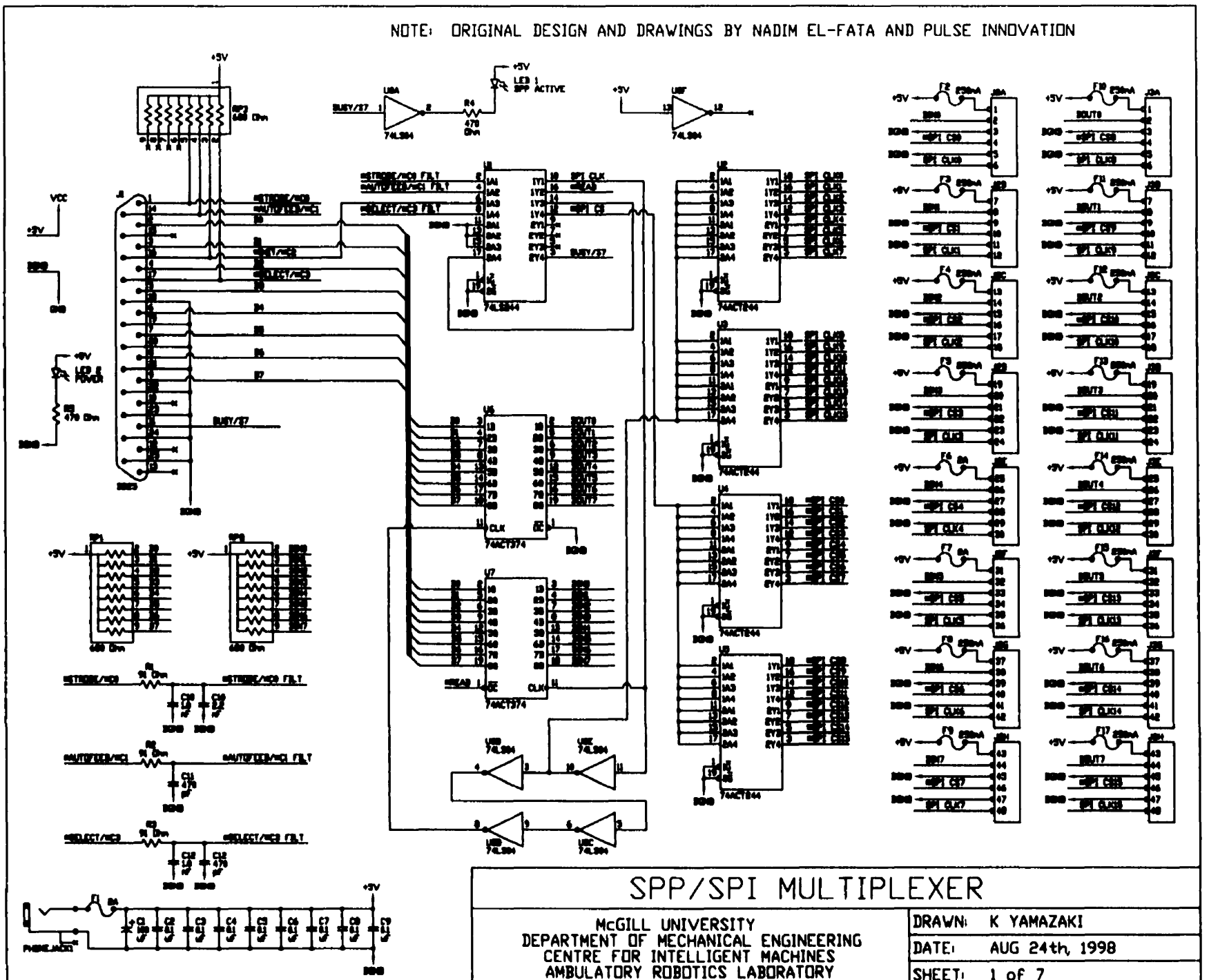
NOTE: ORIGINAL DESIGN AND DRAWINGS BY NADIM EL-FATA AND PULSE INNOVATION
SPP/SPI MULTIPLEXER
McGILL UNIVERSITY
DEPARTMENT OF MECHANICAL ENGINEERING
CENTRE FOR INTELLIGENT MACHINES
AMBULATORY ROBOTICS LABORATORY
DRAWN: K YAMAZAKI
DATE: AUG 24th, 1998
SHEET: 1 of 7

NOTE: ORIGINAL DESIGN AND DRAWINGS BY NADIM EL-FATA AND PULSE INNOVATION

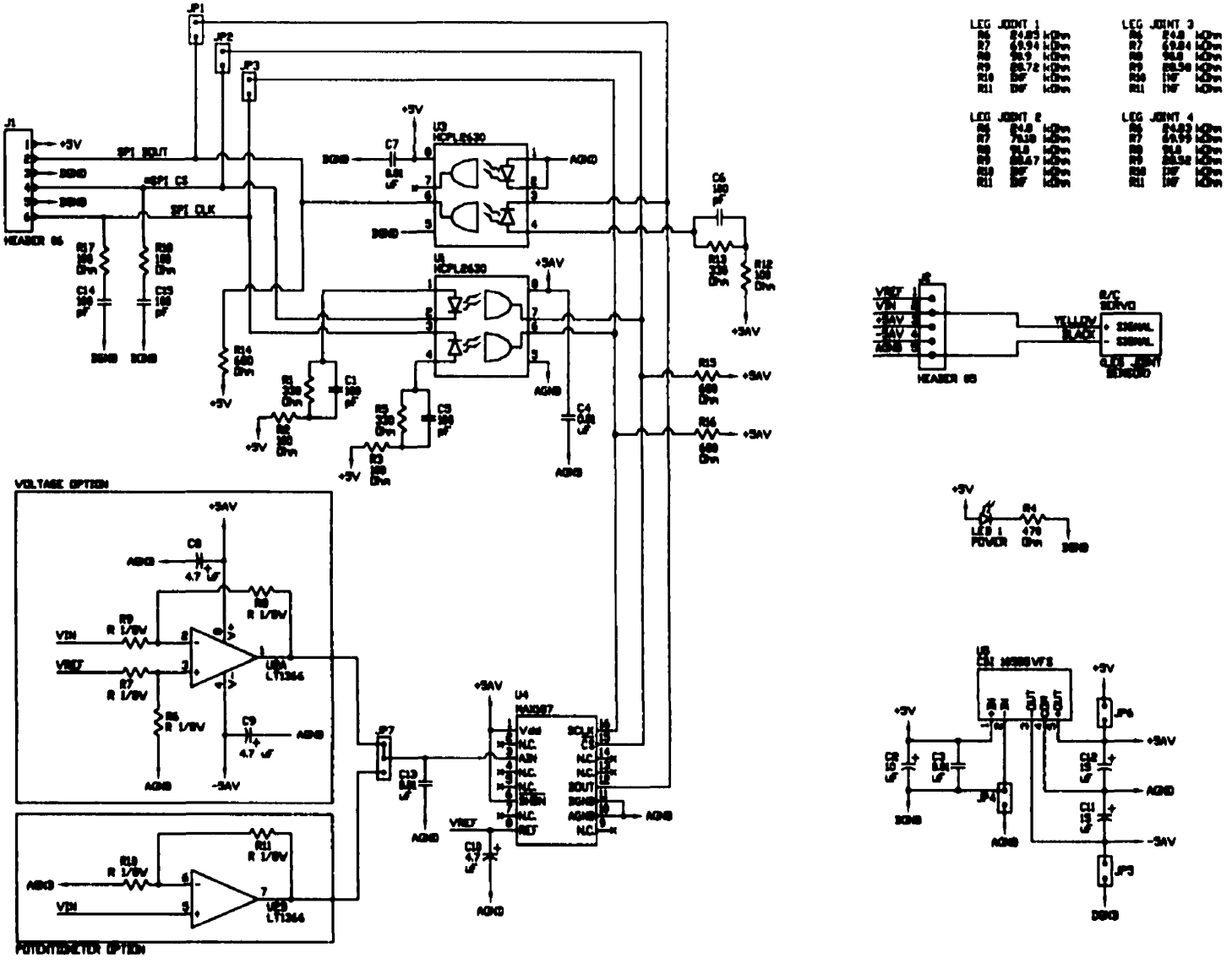

ADIO (ISOLATED) WITH R/C SERVO

McGILL UNIVERSITY DEPARTMENT OF MECHANICAL ENGINEERING CENTRE FOR INTELLIGENT MACHINES AMBULATORY ROBOTICS LABORATORY	DRAWN: K YAMAZAKI DATE: AUG 21st, 1998 SHEET: 2 of 7

NOTES: ORIGINAL DESIGN AND DRAWINGS BY NADIM EL-FATA AND PULSE INNOVATION
GYRO MODIFICATION BY SAMI OBAID

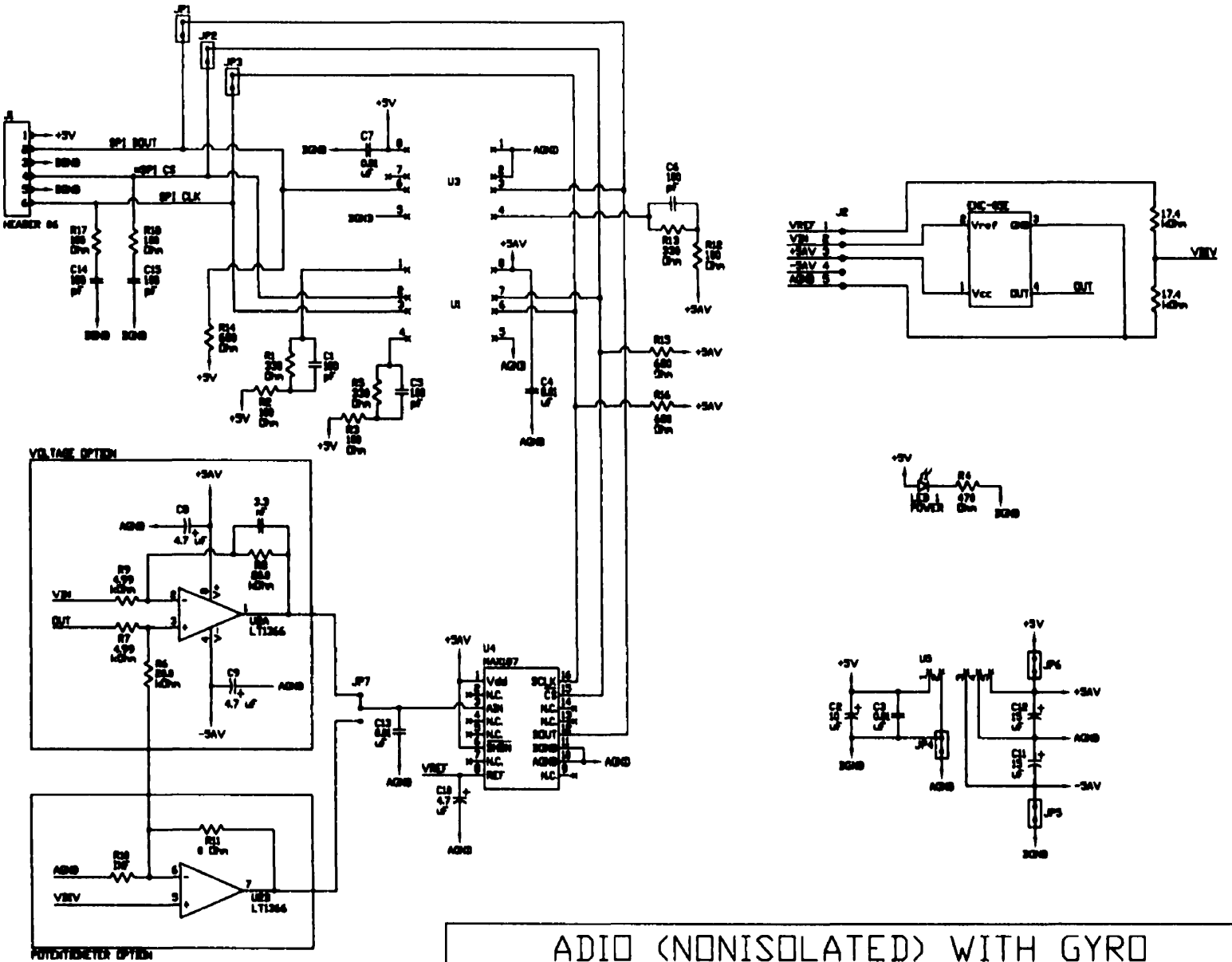

ADIO (NONISOLATED) WITH GYRO

McGILL UNIVERSITY
DEPARTMENT OF MECHANICAL ENGINEERING
CENTRE FOR INTELLIGENT MACHINES
AMBULATORY ROBOTICS LABORATORY

DRAWN:	K YAMAZAKI
DATE:	NOV 14th, 1998
SHEET:	3 of 7

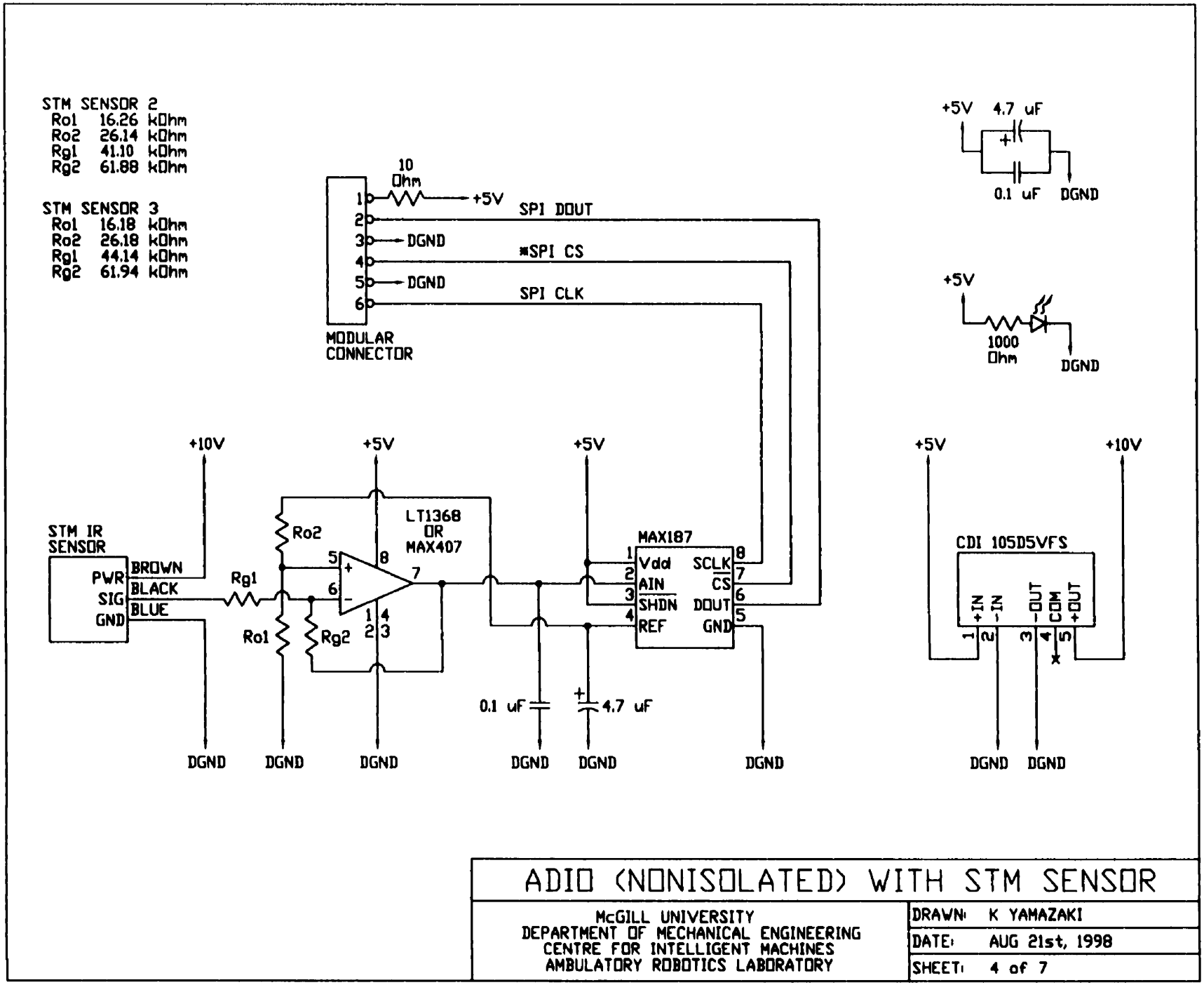

ADIO (NONISOLATED) WITH STM SENSOR		
McGILL UNIVERSITY DEPARTMENT OF MECHANICAL ENGINEERING CENTRE FOR INTELLIGENT MACHINES AMBULATORY ROBOTICS LABORATORY	DRAWN:	K YAMAZAKI
	DATE:	AUG 21st, 1998
	SHEET:	4 of 7

NOTE: ORIGINAL DESIGN AND DRAWINGS BY NADIM EL-FATA AND PULSE INNOVATION

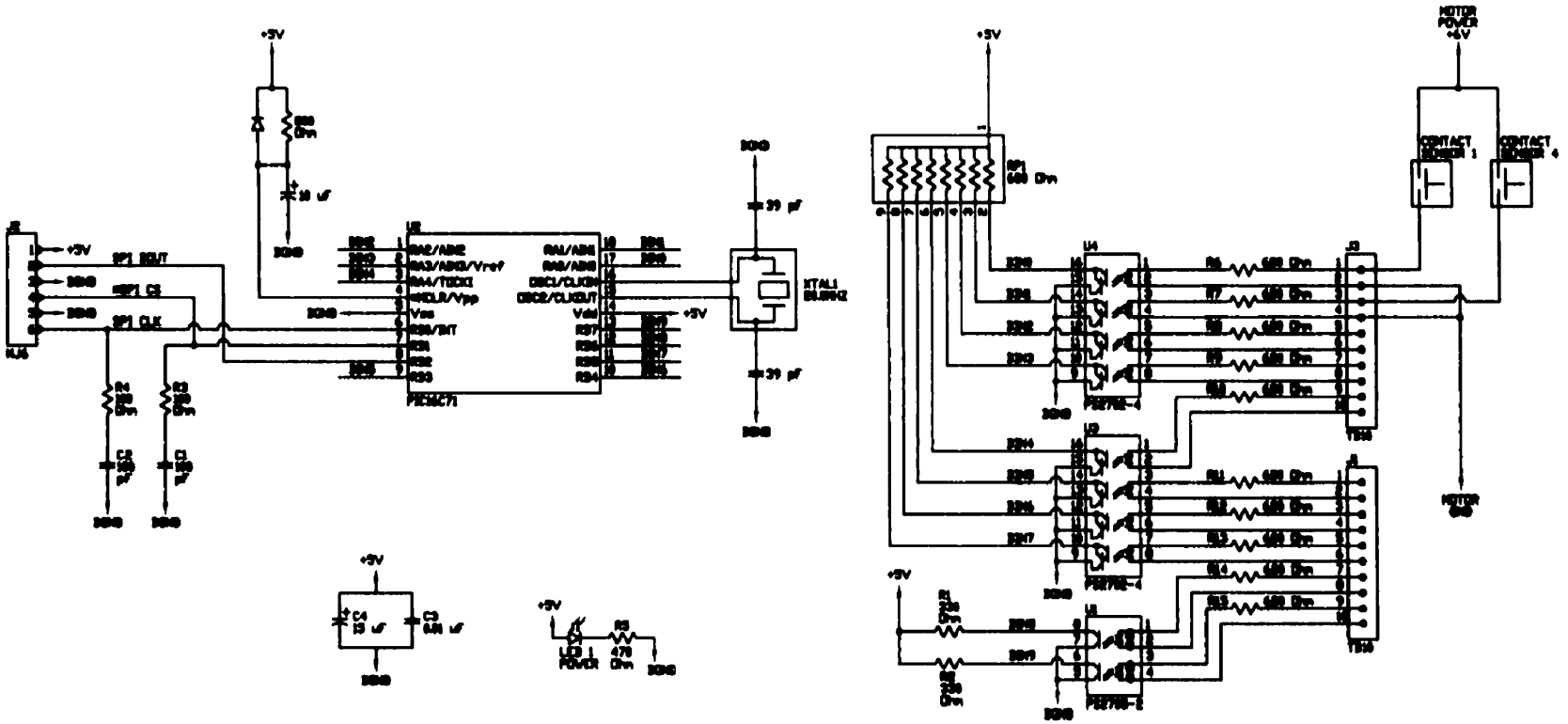

DIN WITH CONTACT SENSORS		
McGILL UNIVERSITY DEPARTMENT OF MECHANICAL ENGINEERING CENTRE FOR INTELLIGENT MACHINES AMBULATORY ROBOTICS LABORATORY	DRAWN:	K YAMAZAKI
	DATE:	AUG 26th, 1998
	SHEET:	5 of 7

NOTE: ORIGINAL DESIGN AND DRAWINGS BY NADIM EL-FATA AND PULSE INNOVATION

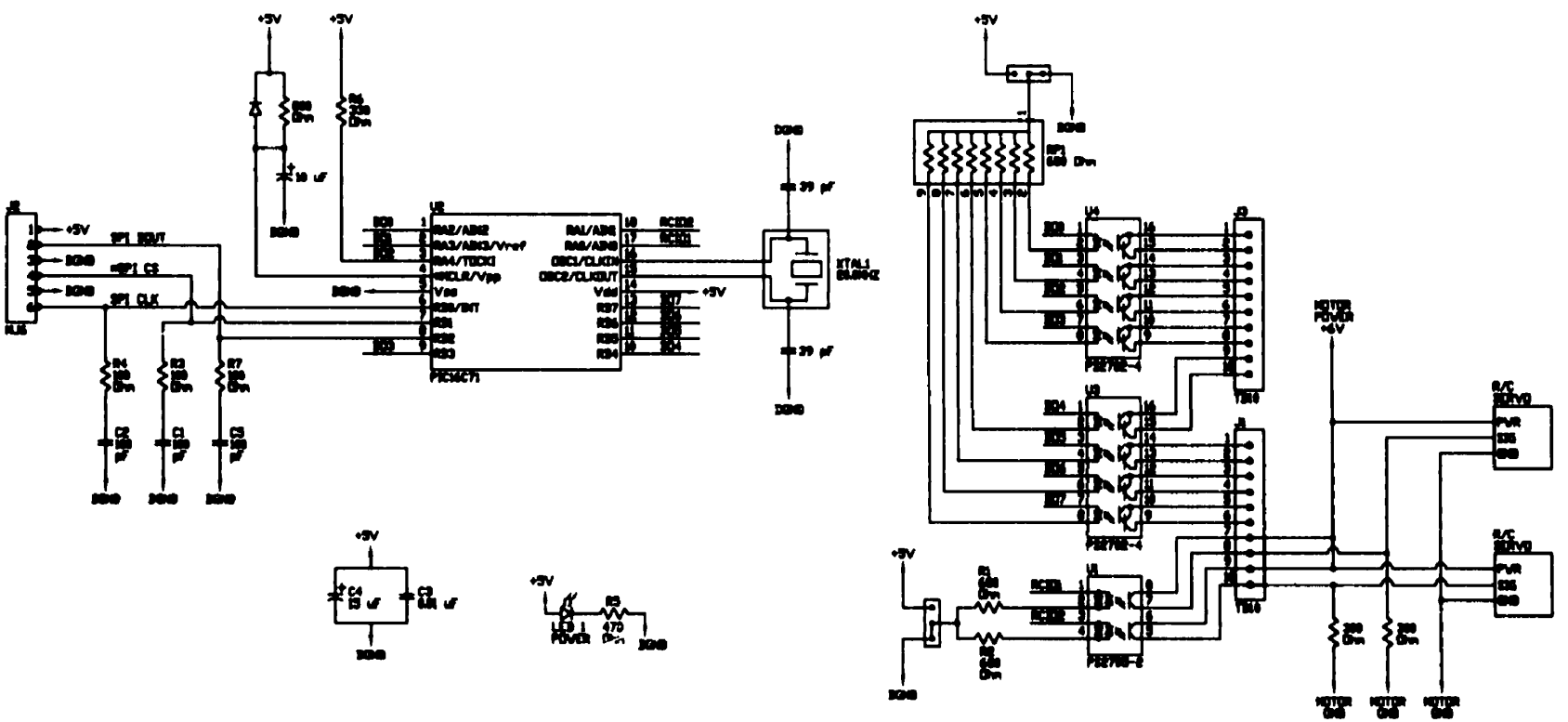

RCIO WITH R/C SERVOS		
McGILL UNIVERSITY DEPARTMENT OF MECHANICAL ENGINEERING CENTRE FOR INTELLIGENT MACHINES AMBULATORY ROBOTICS LABORATORY	DRAWN:	K YAMAZAKI
	DATE:	AUG 26th, 1998
	SHEET:	6 of 7

NOTE: ORIGINAL DESIGN AND DRAWINGS BY NADIM EL-FATA AND PULSE INNOVATION

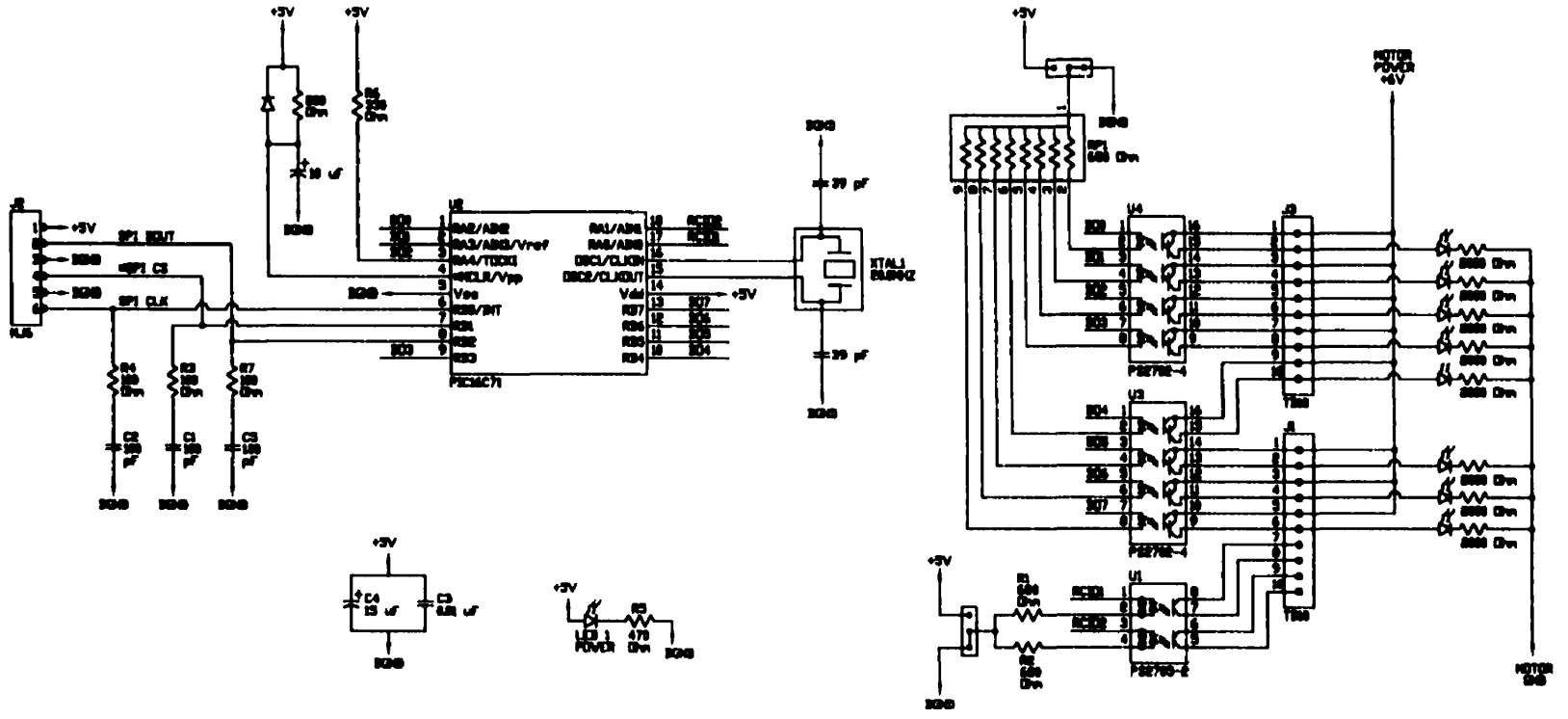

DOUT WITH LED BANK

McGILL UNIVERSITY DEPARTMENT OF MECHANICAL ENGINEERING CENTRE FOR INTELLIGENT MACHINES AMBULATORY ROBOTICS LABORATORY	DRAWN: K YAMAZAKI DATE: AUG 26th, 1998 SHEET: 7 of 7

Appendix B

Mechanical Drawings

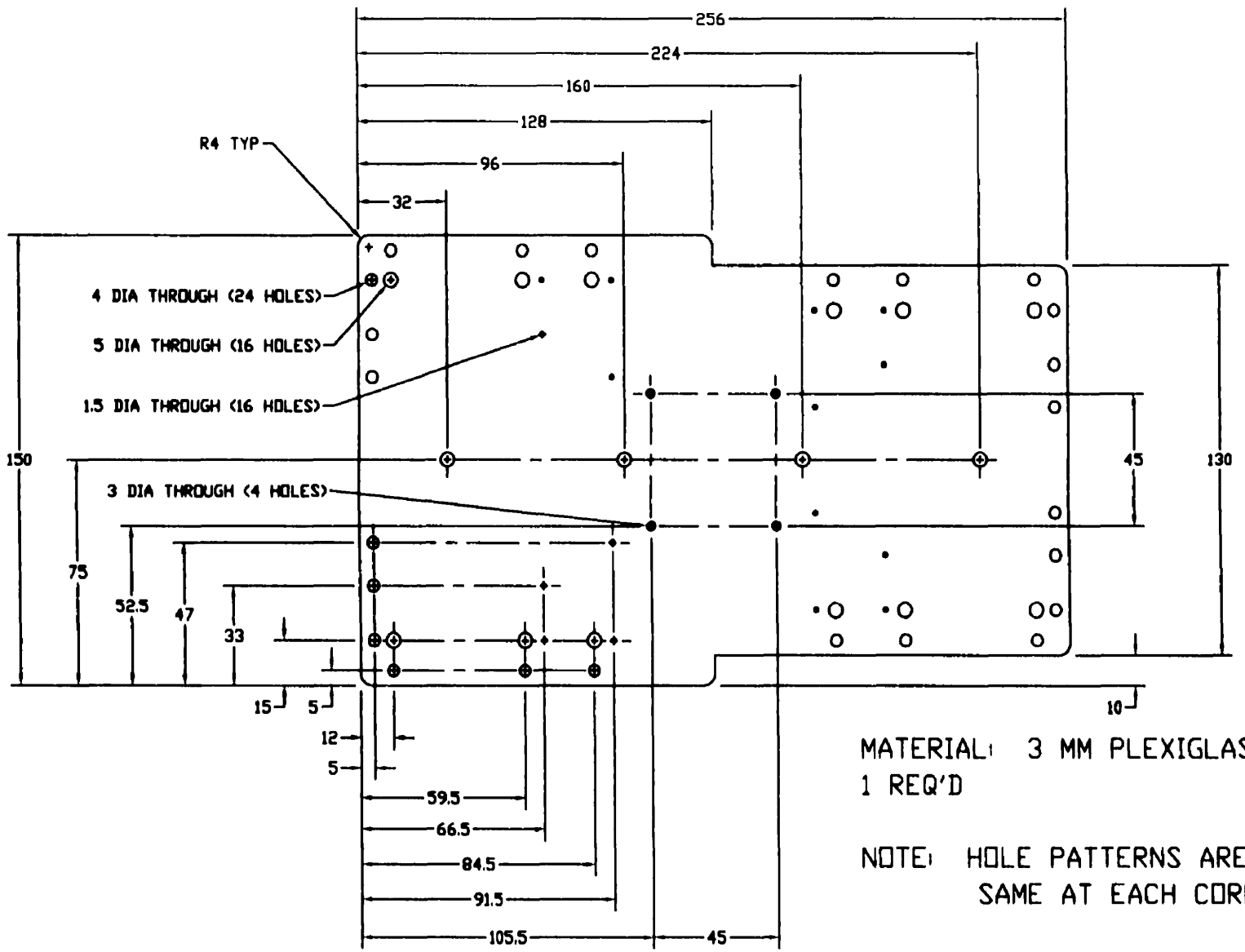

MAIN PLATFORM	DRAWN: K YAMAZAKI
	DATE: SEPT 7th, 1998
McGILL UNIVERSITY DEPARTMENT OF MECHANICAL ENGINEERING CENTRE FOR INTELLIGENT MACHINES AMBULATORY ROBOTICS LABORATORY	UNITS: MM
	SCALE: 1:2 (APPROX)
	SHEET: 1 of 15

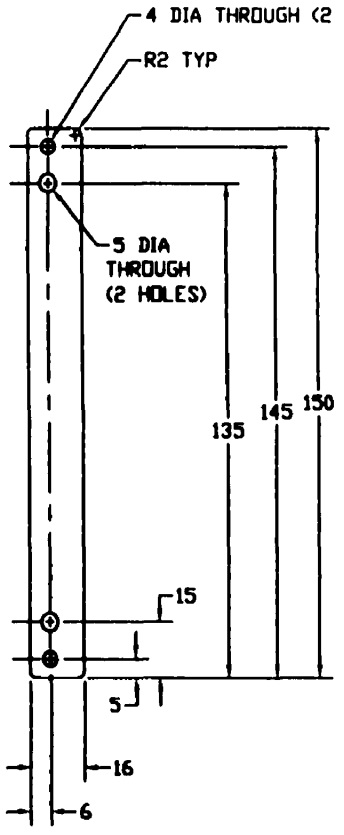

BACK CROSS SUPPORT
2 REQ'D

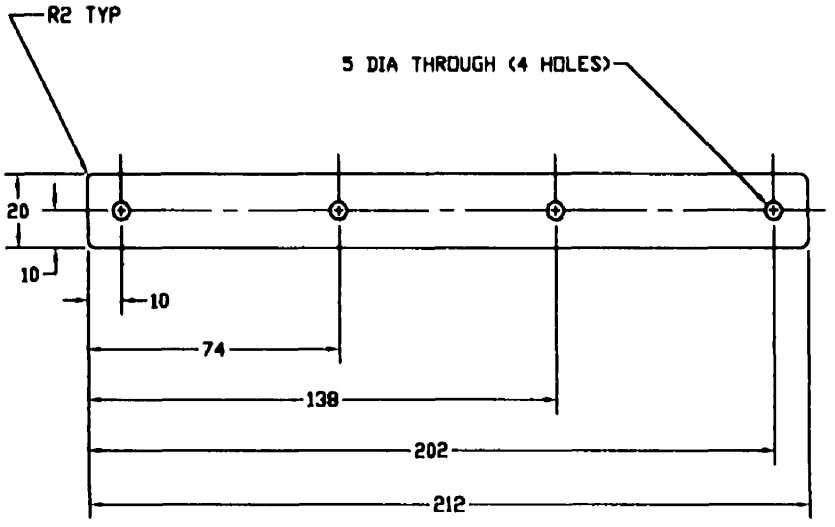

LONGITUDINAL SUPPORT
2 REQ'D

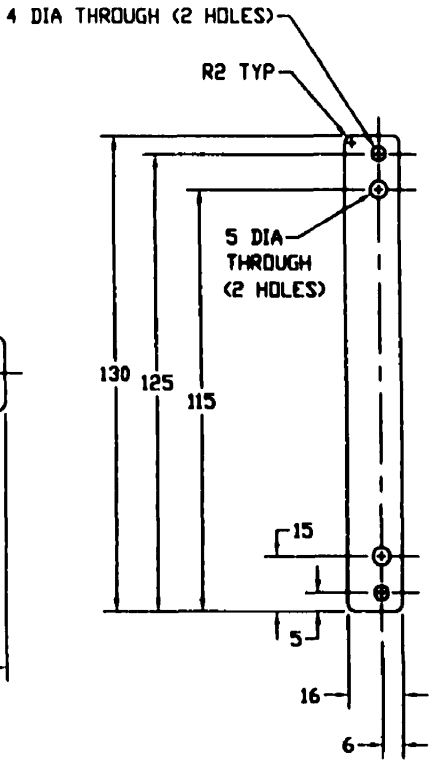

FRONT CROSS SUPPORT
2 REQ'D

MAT'L: 3 MM PLEXIGLASS (ALL PIECES ON THIS SHEET)

MAIN PLATFORM SUPPORTS	DRAWN: K YAMAZAKI
	DATE: SEPT 7th, 1998
McGILL UNIVERSITY DEPARTMENT OF MECHANICAL ENGINEERING CENTRE FOR INTELLIGENT MACHINES AMBULATORY ROBOTICS LABORATORY	UNITS: MM
	SCALE: 1:2 (APPROX)
	SHEET: 2 of 15

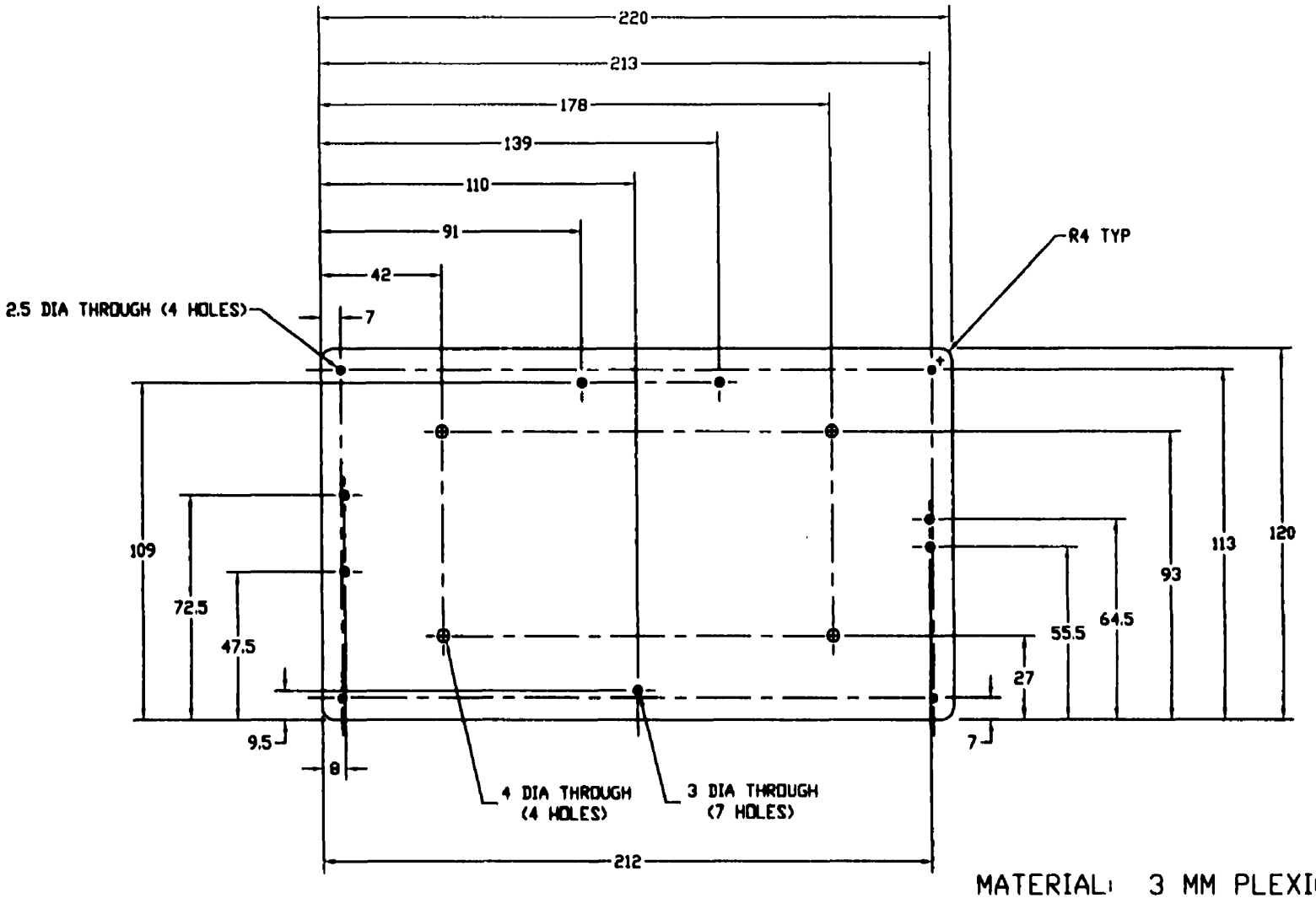

MATERIAL: 3 MM PLEXIGLASS
1 REQ'D

MIDDLE PLATFORM	DRAWN: K YAMAZAKI
	DATE: SEPT 7th, 1998
McGILL UNIVERSITY DEPARTMENT OF MECHANICAL ENGINEERING CENTRE FOR INTELLIGENT MACHINES AMBULATORY ROBOTICS LABORATORY	UNITS: MM
	SCALE: 1:2 (APPROX)
	SHEET: 3 of 15

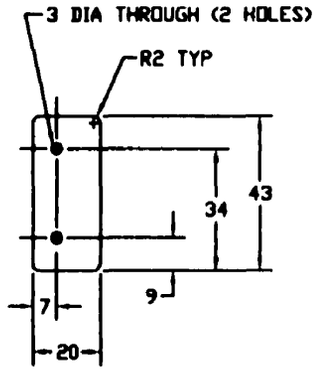

BACK ALIGNMENT PIECE
1 REQ'D

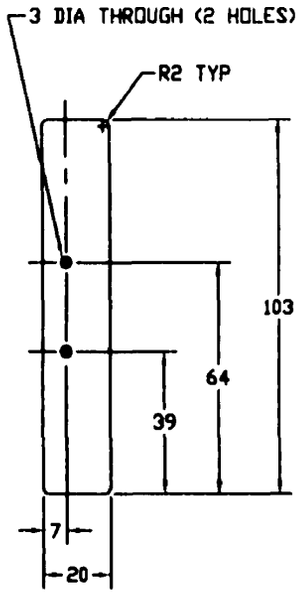

BACK SPACER
1 REQ'D

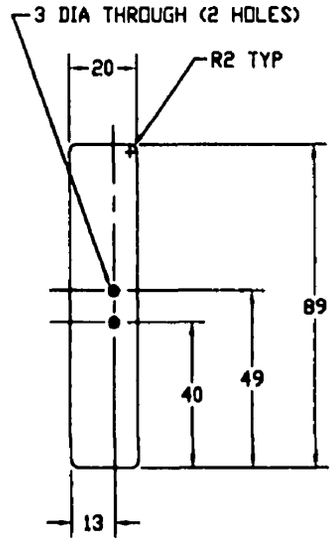

FRONT SPACER
1 REQ'D

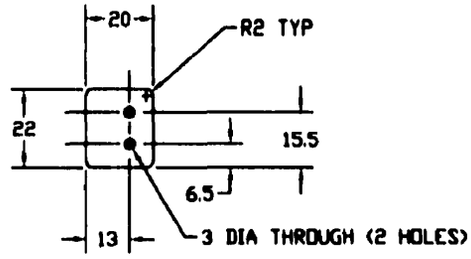

FRONT ALIGNMENT PIECE
1 REQ'D

MAT'L: 6 MM PLEXIGLASS (ALL PIECES ON THIS SHEET)

MIDDLE PLATFORM SPACERS	DRAWN: K YAMAZAKI
	DATE: SEPT 7th, 1998
McGILL UNIVERSITY DEPARTMENT OF MECHANICAL ENGINEERING CENTRE FOR INTELLIGENT MACHINES AMBULATORY ROBOTICS LABORATORY	UNITS: MM
	SCALE: 1:2 (APPROX)
	SHEET: 4 of 15

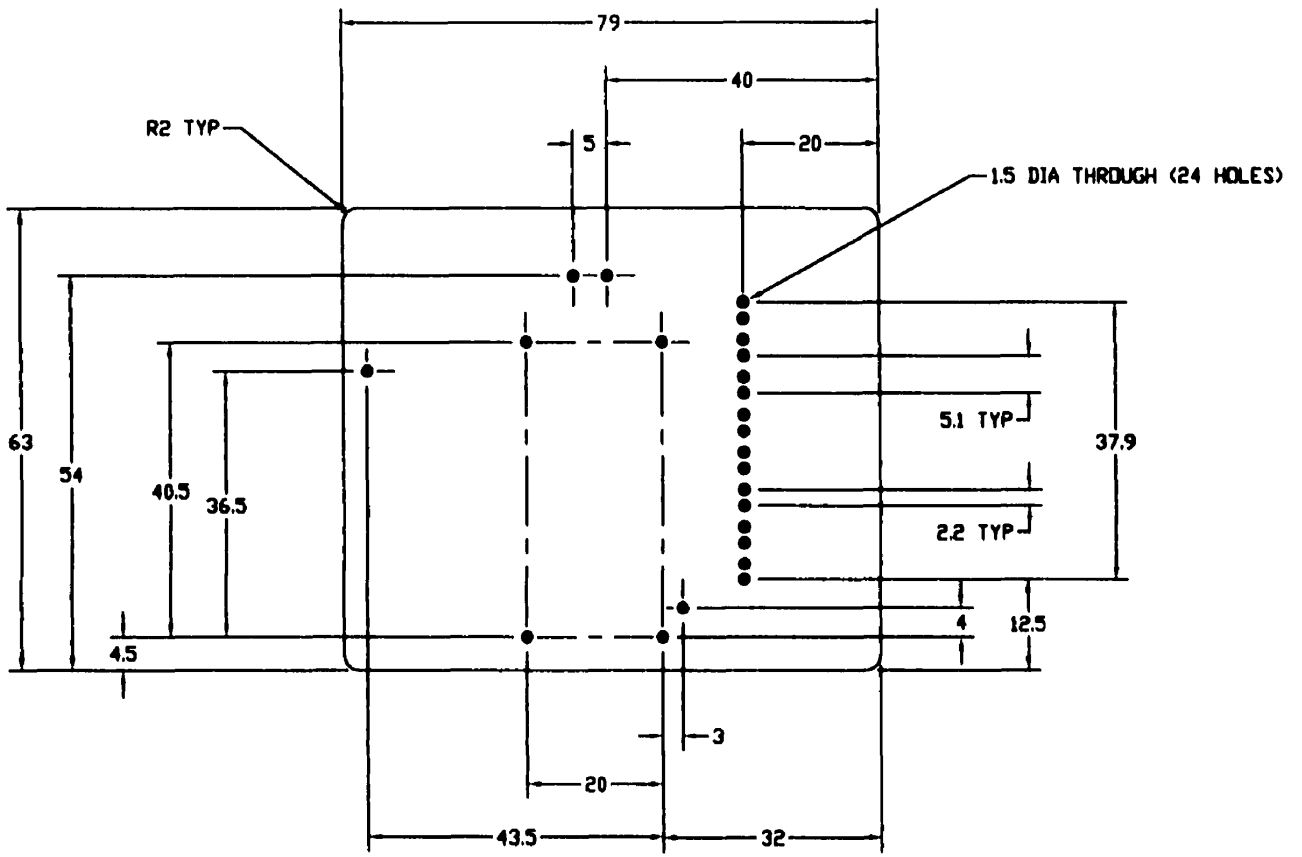

MATERIAL: 3 MM PLEXIGLASS
1 REQ'D

UPPER PLATFORM	DRAWN: K YAMAZAKI
	DATE: AUG 13th, 1998
McGILL UNIVERSITY DEPARTMENT OF MECHANICAL ENGINEERING CENTRE FOR INTELLIGENT MACHINES AMBULATORY ROBOTICS LABORATORY	UNITS: MM
	SCALE: 1:1 (APPROX)
	SHEET: 5 of 15

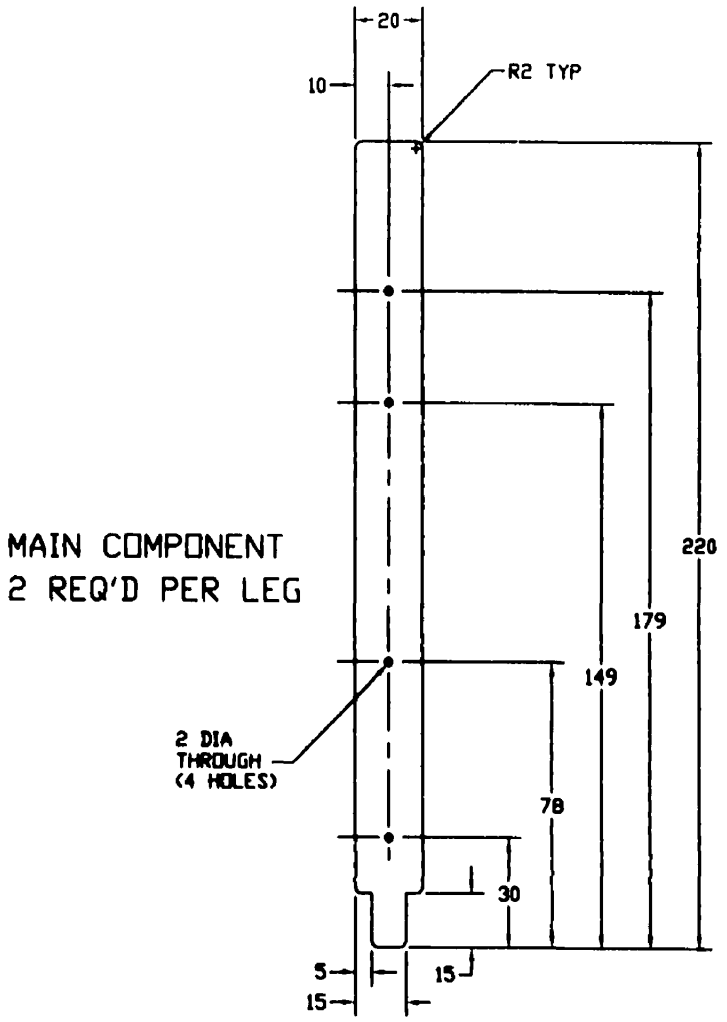

MAIN COMPONENT
2 REQ'D PER LEG

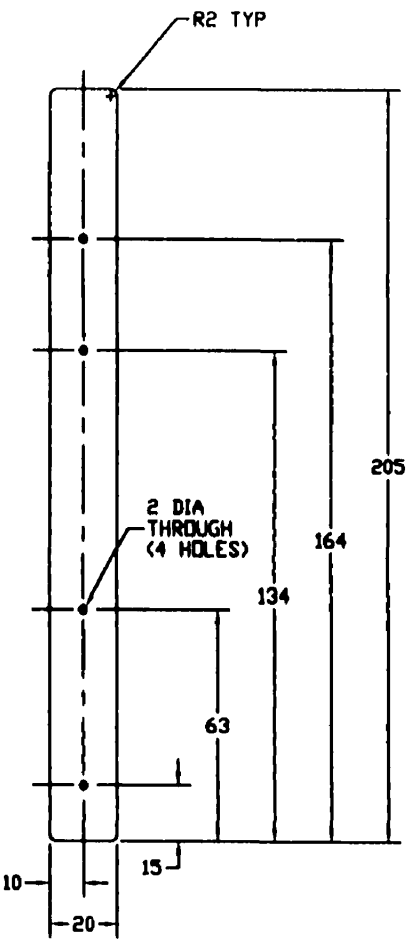

SUPPORT COMPONENT
1 REQ'D PER LEG

MAT'L: 3 MM PLEXIGLASS (ALL PIECES ON THIS SHEET)
2 LEGS REQ'D

LEG (TYPE 1)	DRAWN: K YAMAZAKI
	DATE: SEPT 7th, 1998
McGILL UNIVERSITY DEPARTMENT OF MECHANICAL ENGINEERING CENTRE FOR INTELLIGENT MACHINES AMBULATORY ROBOTICS LABORATORY	UNITS: MM
	SCALE: 1:2 (APPROX)
	SHEET: 6 of 15

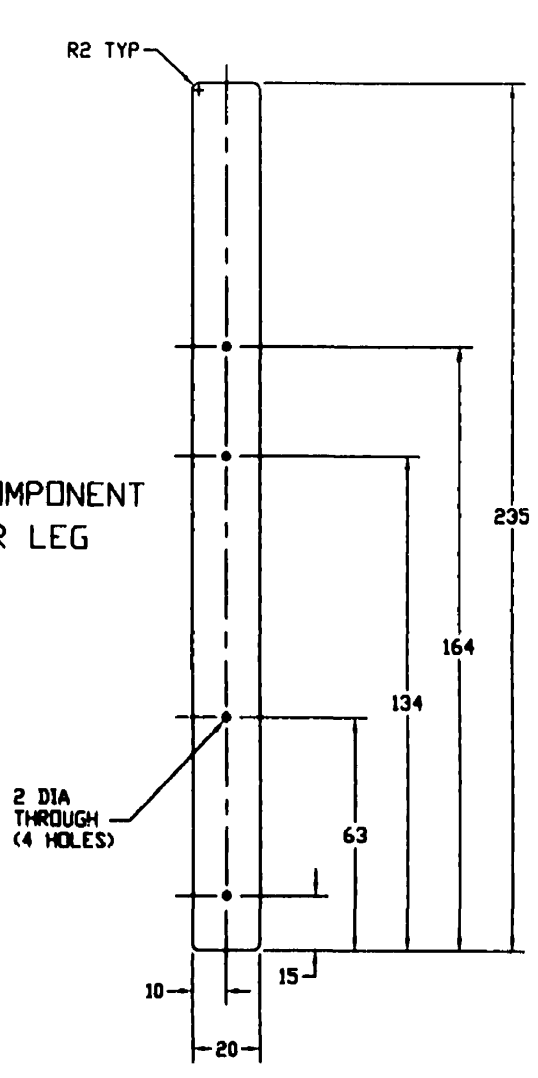

SUPPORT COMPONENT
1 REQ'D PER LEG

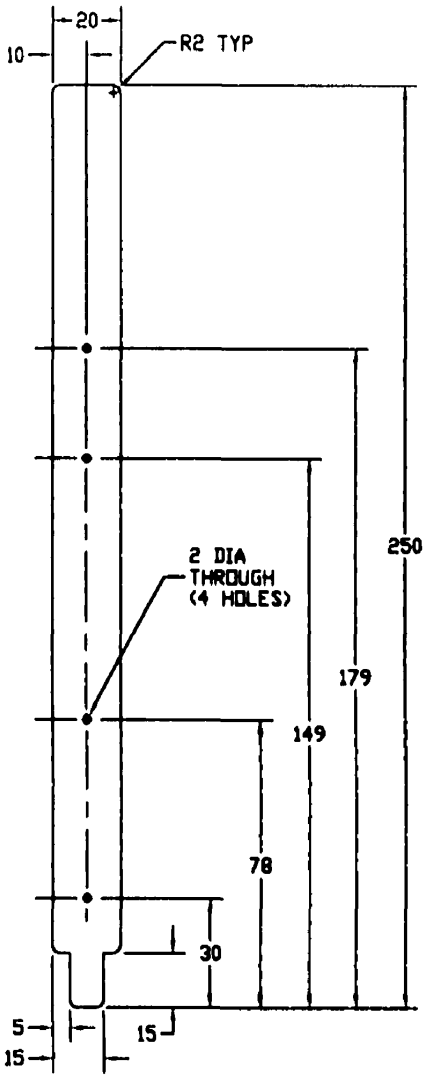

MAIN COMPONENT
2 REQ'D PER LEG

MAT'L: 3 MM PLEXIGLASS (ALL PIECES ON THIS SHEET)
2 LEGS REQ'D

LEG (TYPE 2)	DRAWN: K YAMAZAKI
	DATE: SEPT 7th, 1998
McGILL UNIVERSITY DEPARTMENT OF MECHANICAL ENGINEERING CENTRE FOR INTELLIGENT MACHINES AMBULATORY ROBOTICS LABORATORY	UNITS: MM
	SCALE: 1:2 (APPROX)
	SHEET: 7 of 15

SENSOR SUPPORT
1 REQ'D PER HOUSING

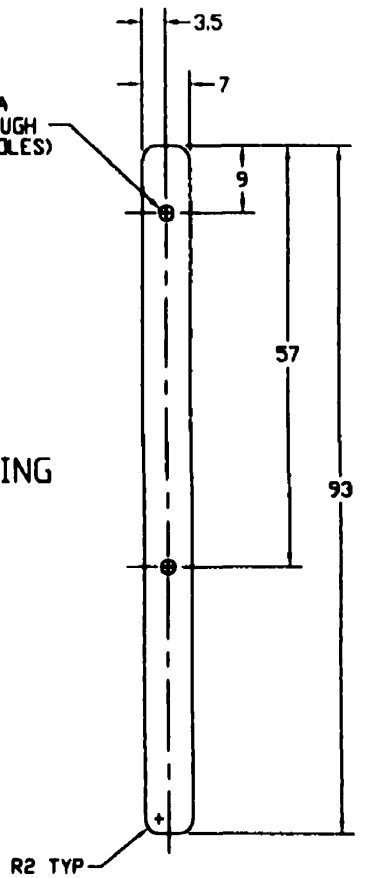

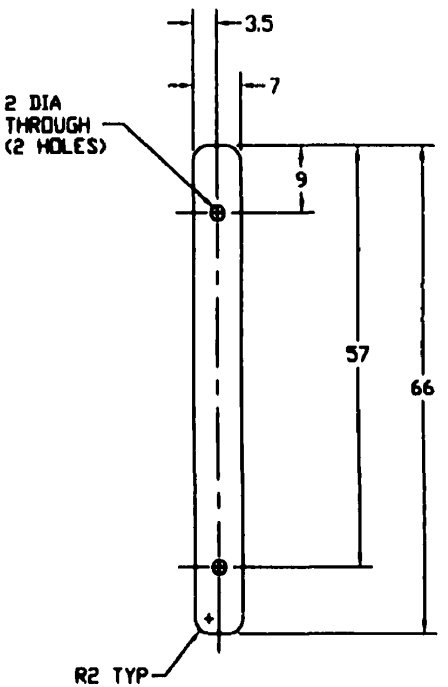

SPACER
1 REQ'D PER HOUSING

MAT'L: 3 MM PLEXIGLASS (ALL PIECES ON THIS SHEET)
2 HOUSINGS REQ'D

SENSOR HOUSING (TYPE 1)	DRAWN: K YAMAZAKI
	DATE: SEPT 7th, 1998
McGILL UNIVERSITY DEPARTMENT OF MECHANICAL ENGINEERING CENTRE FOR INTELLIGENT MACHINES AMBULATORY ROBOTICS LABORATORY	UNITS: MM
	SCALE: 1:1 (APPROX)
	SHEET: 8 of 15

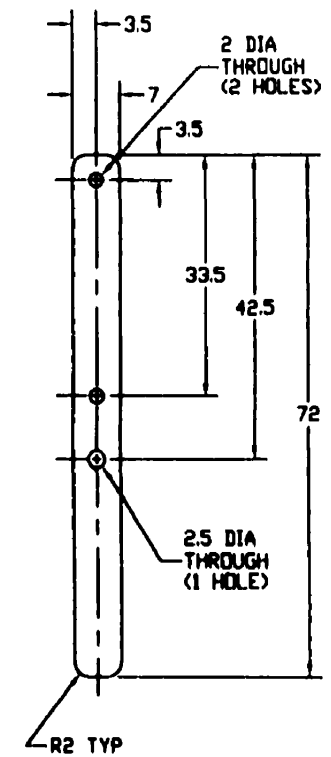

SENSOR SUPPORT
1 REQ'D PER HOUSING

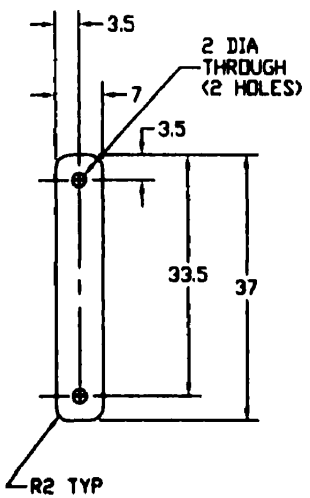

SPACER A
2 REQ'D PER HOUSING

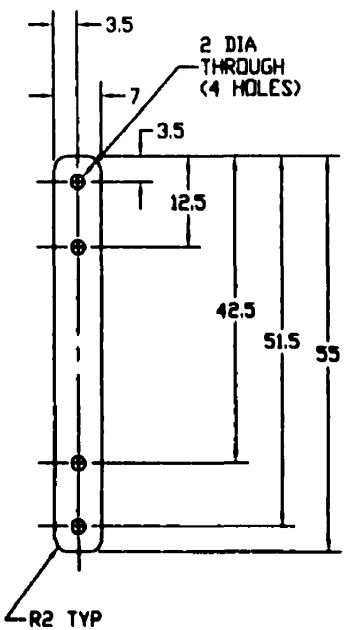

SPACER B
1 REQ'D PER HOUSING

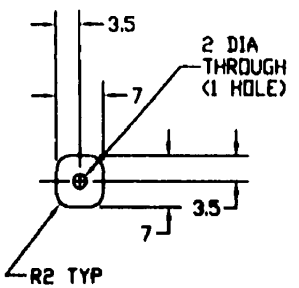

SPACER C
2 REQ'D PER HOUSING

MAT'L: 3 MM PLEXIGLASS (ALL PIECES ON THIS SHEET)
2 HOUSINGS REQ'D

SENSOR HOUSING (TYPE 2)	DRAWN: K YAMAZAKI
	DATE: SEPT 8th, 1998
McGILL UNIVERSITY DEPARTMENT OF MECHANICAL ENGINEERING CENTRE FOR INTELLIGENT MACHINES AMBULATORY ROBOTICS LABORATORY	UNITS: MM
	SCALE: 1:1 (APPROX)
	SHEET: 9 of 15

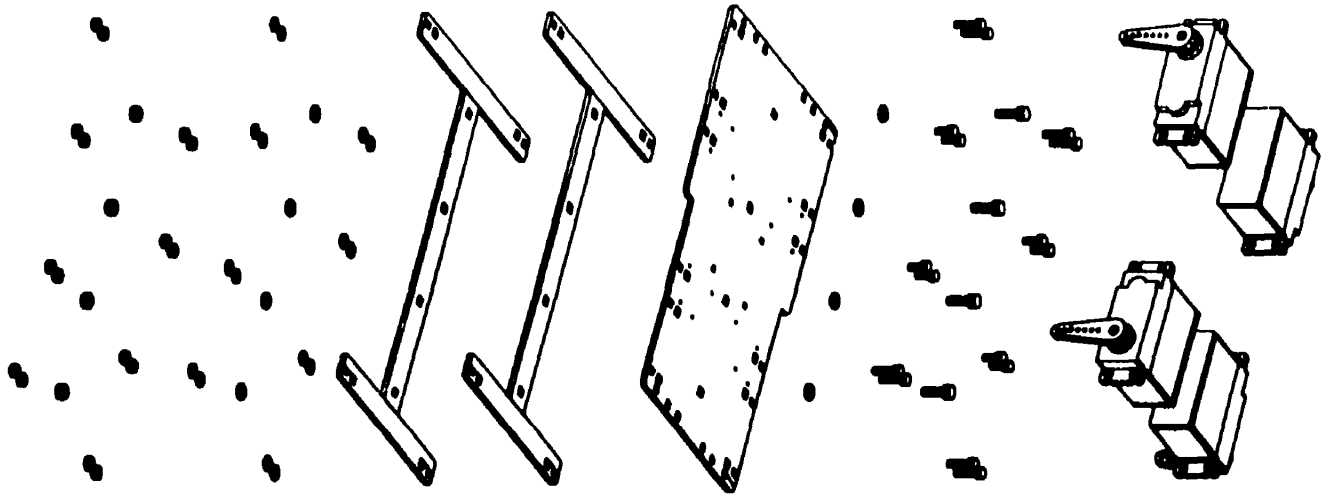

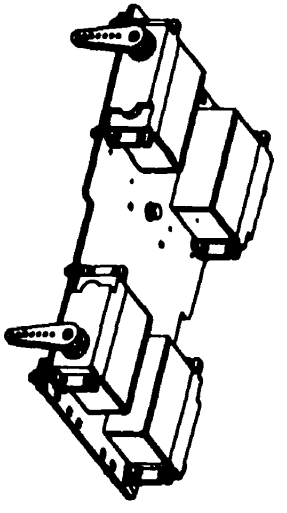

HARDWARE

1	MAIN PLATFORM (SHEET 1)
2	FRONT CROSS SUPPORTS (SHEET 2)
2	LONGITUDINTAL SUPPORTS (SHEET 2)
2	BACK CROSS SUPPORTS (SHEET 2)
4	HITEC R/C SERVOS
4	M5x16 CAP SCREWS
8	M5 WASHERS
4	M5 NUTS
8	M4X16 CAP SCREWS
8	M4X10 CAP SCREWS
16	M4 WASHERS
16	M4 NUTS
	SPECTRA STRING (FOR SECURING R/C SERVOS)

ASSEMBLY, MAIN PLATFORM

McGILL UNIVERSITY
DEPARTMENT OF MECHANICAL ENGINEERING
CENTRE FOR INTELLIGENT MACHINES
AMBULATORY ROBOTICS LABORATORY

DRAWN:	K YAMAZAKI
DATE:	OCT 1st, 1998
SHEET:	10 of 15

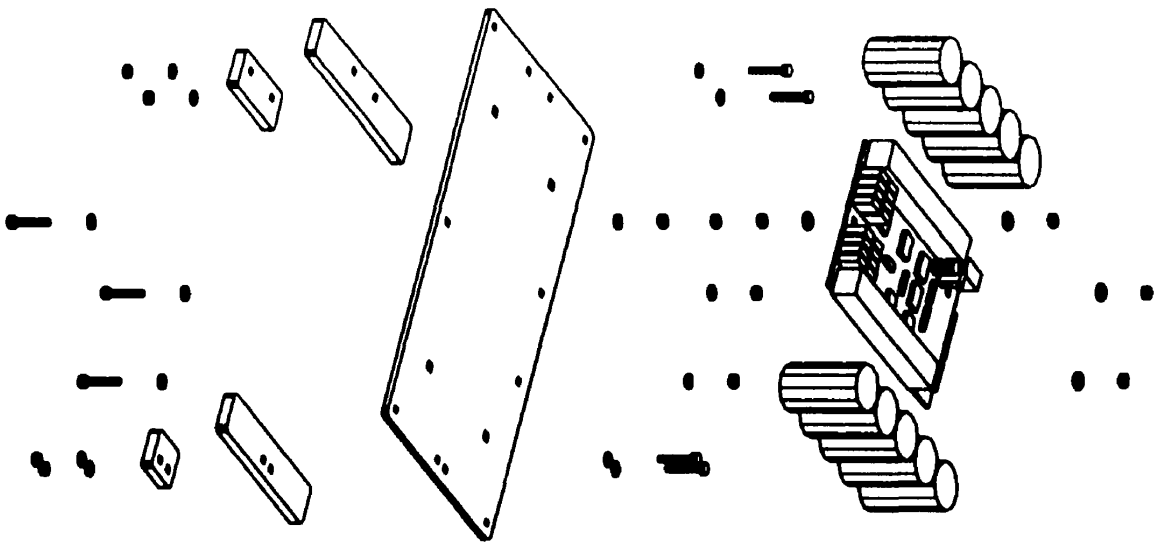

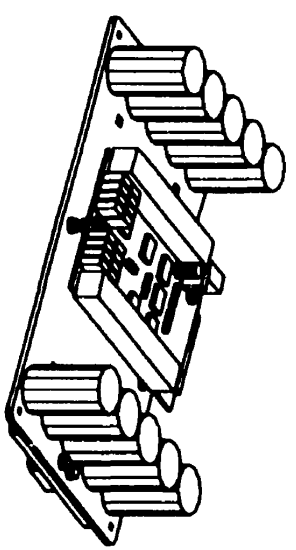

HARDWARE

1	MIDDLE PLATFORM (SHEET 3)
1	FRONT ALIGNMENT PIECE (SHEET 4)
1	FRONT SPACER (SHEET 4)
1	BACK SPACER (SHEET 4)
1	BACK ALIGNMENT PIECE (SHEET 4)
10	NICAD BATTERIES
1	SPP/SPI MULTIPLEXER
7	M3x20 CAP SCREWS
14	M3 WASHERS
4	M3 WASHERS (NYLON)
12	M3 NUTS
4	CABLE TIES (FOR SECURING BATTERIES)

ASSEMBLY, MIDDLE PLATFORM

McGILL UNIVERSITY
DEPARTMENT OF MECHANICAL ENGINEERING
CENTRE FOR INTELLIGENT MACHINES
AMBULATORY ROBOTICS LABORATORY

DRAWN:	K YAMAZAKI
DATE:	OCT 1st, 1998
SHEET:	11 of 15

HARDWARE

1	UPPER PLATFORM (SHEET 5)
1	DC-DC CONVERTER (LAMBDA AS10-5-5)
8	LEDS
1	FUSE (2A) WITH FUSE HOLDER

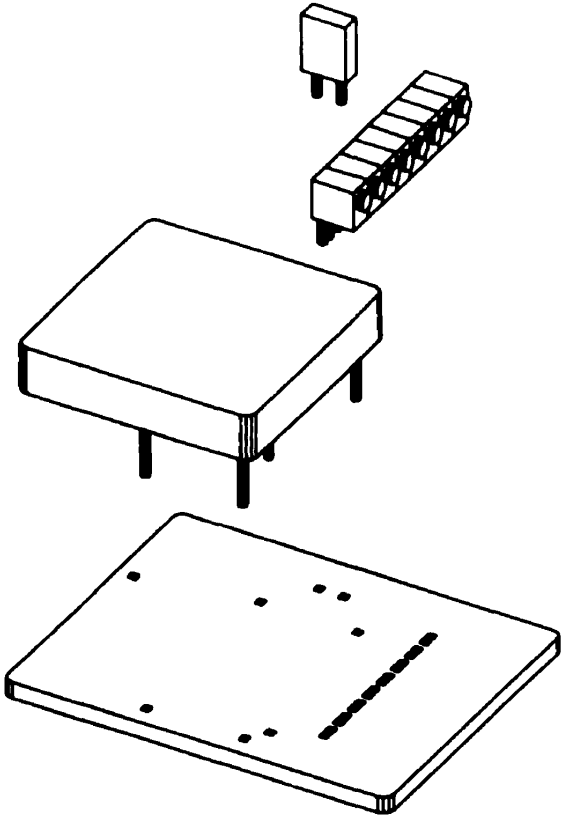

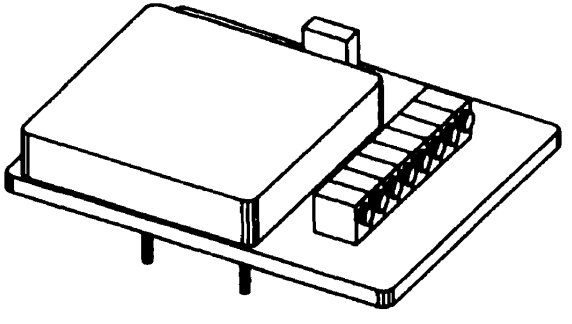

ASSEMBLY, UPPER PLATFORM

McGILL UNIVERSITY
DEPARTMENT OF MECHANICAL ENGINEERING
CENTRE FOR INTELLIGENT MACHINES
AMBULATORY ROBOTICS LABORATORY

DRAWN:	K YAMAZAKI
DATE:	OCT 1st, 1998
SHEET:	12 of 15

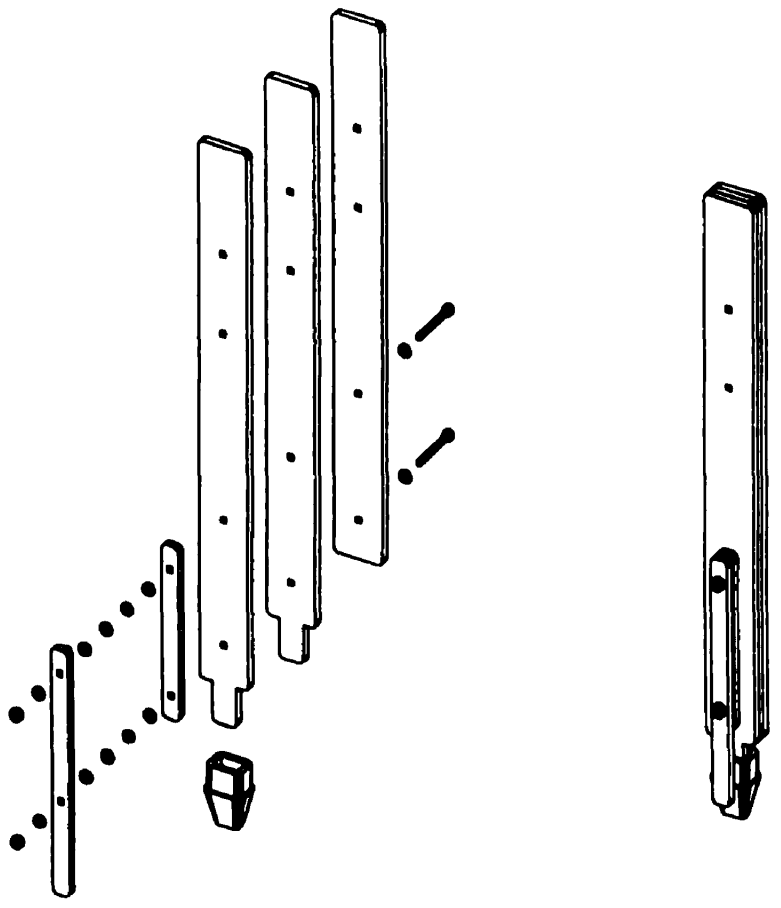

HARDWARE

TYPE 1 LEG
- 2 MAIN COMPONENTS (SHEET 6) PER LEG
- 1 SUPPORT COMPONENT (SHEET 6) PER LEG
- 1 FOOT (ERASER) PER LEG

TYPE 1 SENSOR HOUSING
- 1 SENSOR SUPPORT (SHEET 8) PER HOUSING
- 1 SPACER (SHEET 8) PER HOUSING
- 2 M2x20 CAP SCREWS PER HOUSING
- 12 M2 WASHERS PER HOUSING
- 2 M2 NUTS PER HOUSING

ASSEMBLY, TYPE 1 LEG AND SENSOR HOUSING

McGILL UNIVERSITY
DEPARTMENT OF MECHANICAL ENGINEERING
CENTRE FOR INTELLIGENT MACHINES
AMBULATORY ROBOTICS LABORATORY

DRAWN:	K YAMAZAKI
DATE:	OCT 1st, 1998
SHEET:	13 of 15

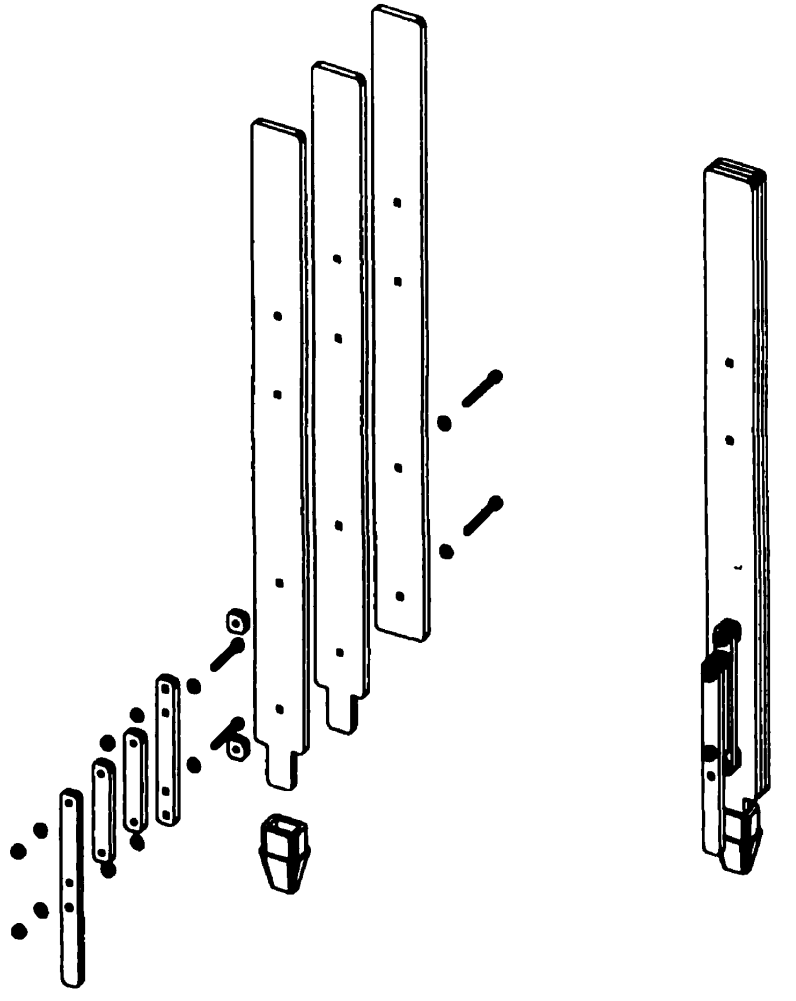

HARDWARE

TYPE 2 LEG
- 2 MAIN COMPONENTS (SHEET 7) PER LEG
- 1 SUPPORT COMPONENT (SHEET 7) PER LEG
- 1 FOOT (ERASER) PER LEG

TYPE 2 SENSOR HOUSING
- 1 SENSOR SUPPORT (SHEET 9) PER HOUSING
- 2 SPACER A'S (SHEET 9) PER HOUSING
- 1 SPACER B (SHEET 9) PER HOUSING
- 2 SPACER C'S (SHEET 9) PER HOUSING
- 2 M2x16 CAP SCREWS PER HOUSING
- 2 M2x20 CAP SCREWS PER HOUSING
- 8 M2 WASHERS PER HOUSING
- 4 M2 NUTS PER HOUSING

ASSEMBLY, TYPE 2 LEG AND SENSOR HOUSING

McGILL UNIVERSITY
DEPARTMENT OF MECHANICAL ENGINEERING
CENTRE FOR INTELLIGENT MACHINES
AMBULATORY ROBOTICS LABORATORY

DRAWN:	K YAMAZAKI
DATE:	OCT 1st, 1998
SHEET:	14 of 15

HARDWARE

1	MAIN PLATFORM ASSEMBLY (SHEET 10)
1	MIDDLE PLATFORM ASSEMBLY (SHEET 11)
1	UPPER PLATFORM ASSEMBLY (SHEET 12)
1	TYPE 1 LEG WITH TYPE 1 SENSOR HOUSING (SHEET 13)
1	TYPE 1 LEG WITH TYPE 2 SENSOR HOUSING (SHEETS 13 & 14)
1	TYPE 2 LEG WITH TYPE 1 SENSOR HOUSING (SHEETS 13 & 14)
1	TYPE 2 LEG WITH TYPE 2 SENSOR HOUSING (SHEET 14)
8	M2x20 CAP SCREWS
20	M2 NUTS
16	M2 WASHERS
16	M5 WASHERS
	SPECTRA STRING (FOR SECURING MAIN AND MIDDLE PLATFORMS)

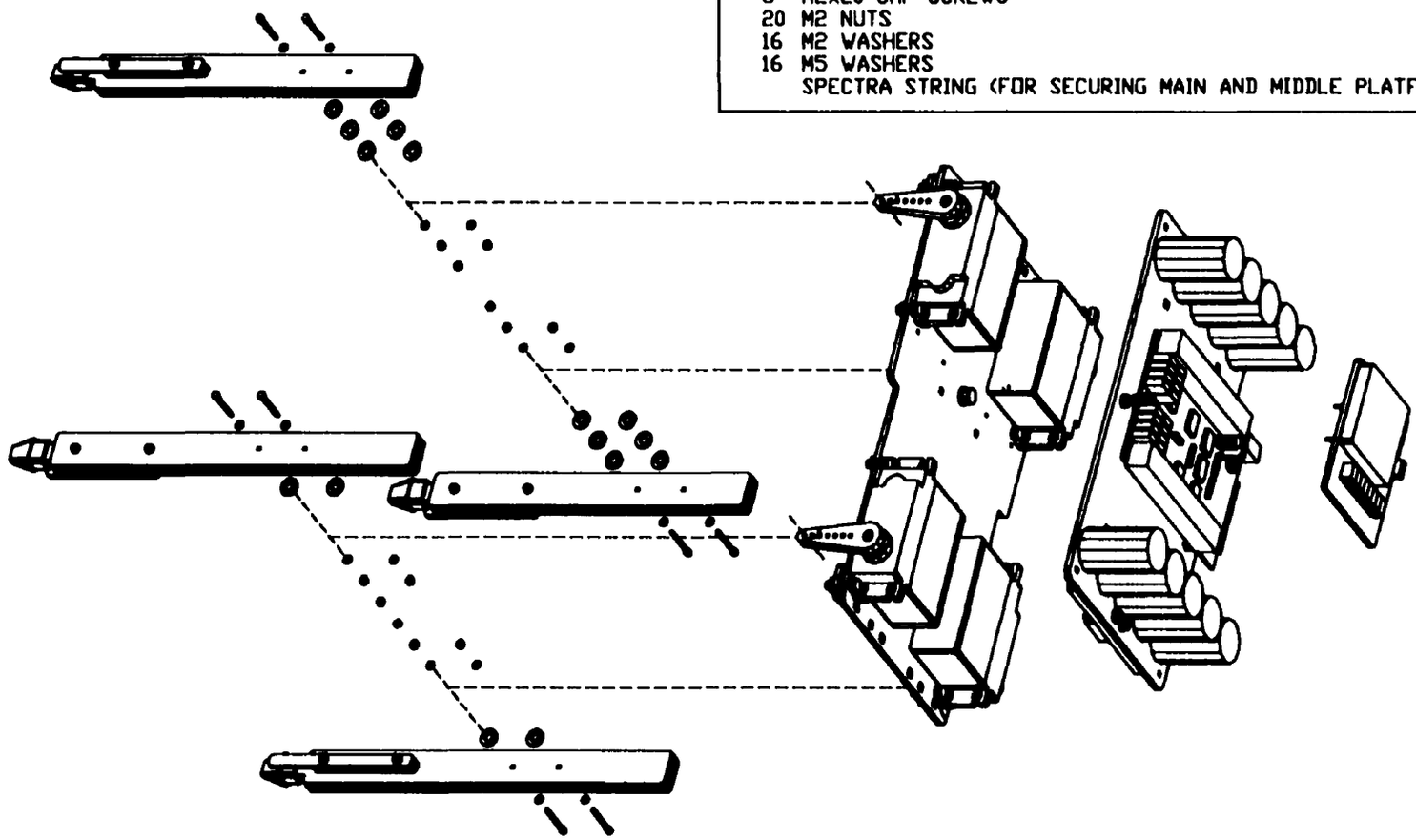

FINAL ASSEMBLY

McGILL UNIVERSITY
DEPARTMENT OF MECHANICAL ENGINEERING
CENTRE FOR INTELLIGENT MACHINES
AMBULATORY ROBOTICS LABORATORY

DRAWN:	K YAMAZAKI
DATE:	OCT 1st, 1998
SHEET:	15 of 15

Appendix C

Inertia Calculations

C.1 Theory

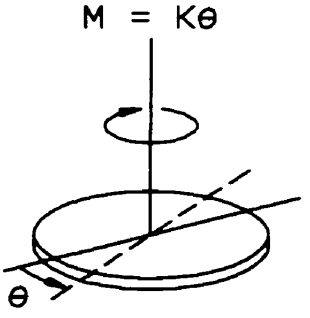

Figure C.1: A Torsional Pendulum

If we are given an object supported by a wire that acts like a torsional spring (Figure C.1) and the object is displaced from its equilibrium angle and then released, the object will oscillate at its natural frequency. Assuming that the mass of the wire is small in comparison to the mass of the object and that the wire generates a restorative moment $M = K\theta$, then the natural frequency of oscillation is

$$\omega_n = \sqrt{\frac{K}{I}}, \tag{C.1}$$

where ω_n is the natural frequency in $\frac{rad}{s}$, K is the spring constant in $\frac{Nm}{rad}$, and I is

the moment of inertia in kgm^2. Assuming that K is a constant, then

$$\omega_n^2 I = Constant. \tag{C.2}$$

This relationship can be used to determine the inertia of an object using a known inertia as reference. This is done by measuring ω_n for both cases using the same wire. The two results can then be compared using (C.2) and the unknown inertia calculated.

C.2 Experimental Validation

The above theory was validated using a Plexiglas plate supported by a guitar wire. The plate had a mass of 0.121 kg with the dimensions shown in Figure C.2.

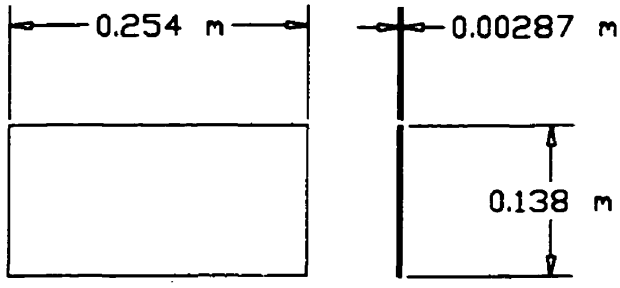

Figure C.2: Plate Dimensions For Inertia Experiments

Figure C.3 details the two setups used for the validation. For setup 1, the calculation of the relevant inertia was

$$\begin{aligned} \mathrm{I} &= \tfrac{1}{12} m(b^2 + l^2) \\ \mathrm{I} &= \tfrac{1}{12}(0.121kg)((0.254m)^2 + (0.00287m)^2) \\ \mathrm{I} &= 0.000651 kgm^2. \end{aligned}$$

The inertia for setup 2 was similarly calculated to be $I = 0.000843 kgm^2$. The time for 8 oscillations was then measured for each setup. Tables C.1 and C.2 detail the results.

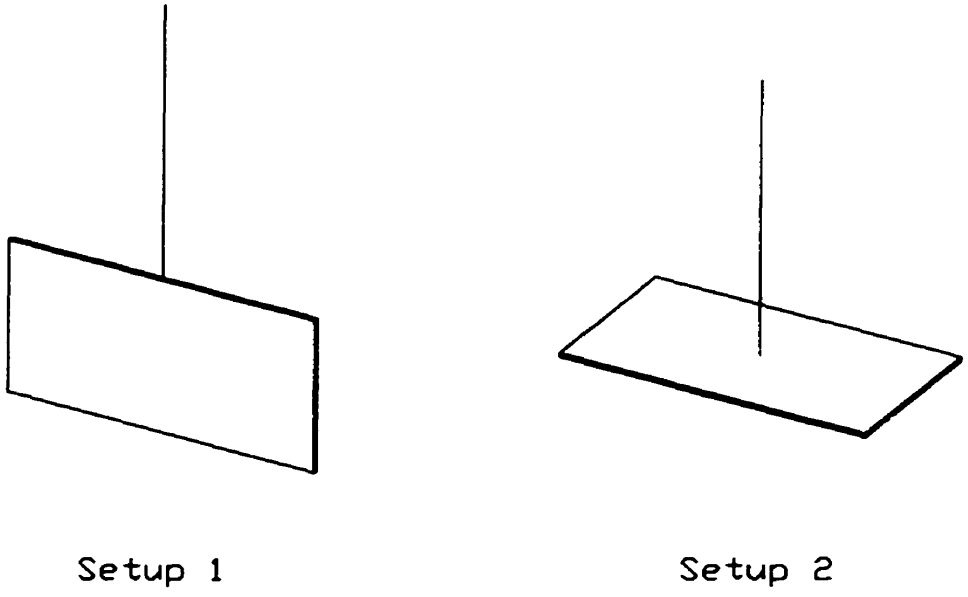

Figure C.3: Inertia Experimental Setup 1

TRIAL	TIME FOR 8 CYCLES	FREQUENCY
1	116 seconds	0.433 $\frac{rad}{s}$
2	117 seconds	0.430 $\frac{rad}{s}$
3	116 seconds	0.433 $\frac{rad}{s}$
Average	116.3 seconds	0.432 $\frac{rad}{s}$

Table C.1: Results of Inertia Experiments With Setup 1

TRIAL	TIME FOR 8 CYCLES	FREQUENCY
1	133 seconds	0.378 $\frac{rad}{s}$
2	133 seconds	0.378 $\frac{rad}{s}$
3	133 seconds	0.378 $\frac{rad}{s}$
Average	133 seconds	0.378 $\frac{rad}{s}$

Table C.2: Results of Inertia Experiments With Setup 2

For setup 1, $\omega_n^2 I = 0.000121 \frac{kgm^2}{s^2}$ and for setup 2, $\omega_n^2 I = 0.000120 \frac{kgm^2}{s^2}$. This is a difference of less than 1%, verifying the technique.

C.3 Experimental Calculation of Scout I's Inertia

The same experiment was performed using Scout I with its legs folded up near its body. Table C.3 details the results.

TRIAL	TIME FOR 8 CYCLES	FREQUENCY
1	545 seconds	0.0922 $\frac{rad}{s}$
2	545 seconds	0.0922 $\frac{rad}{s}$
3	546 seconds	0.0921 $\frac{rad}{s}$
Average	545.3 seconds	0.0922 $\frac{rad}{s}$

Table C.3: Results of Inertia Experiments With Scout I

Comparing the results of setup 2 with the results using Scout I yields

$$\begin{aligned} \omega_{n,Scout}^2 I_{Scout} &= 0.000120 \frac{kgm^2}{s^2} \\ (0.0922 \frac{rad}{s})^2 I_{Scout} &= 0.000120 \frac{kgm^2}{s^2} \\ I_{Scout} &= 0.014 kgm^2 \end{aligned}$$

C.4 Theoretical Calculation of Scout I's Inertia

Referring Table 2.3, the inertia of Scout I's body was calculated theoretically. The actuators, batteries, and electronics were treated as lumped masses located a distance from the center of gravity (CG) of Scout I's body. The structure was simplified to a slim rod passing through Scout I's CG. The results agree very closely with the experimental calculation of the inertia.

$$
\begin{aligned}
I_{Scout} &= I_{Actuators} + I_{Batteries} + I_{Electronics} + I_{Structure} \\
I_{Scout} &= (0.58kg)(0.1m)^2 + (0.50kg)(0.1m)^2 + (0.53kg)(0.04m)^2 + \\
&= \tfrac{1}{12}(0.58kg)(0.25m)^2 \\
I_{Scout} &= 0.015kgm^2
\end{aligned}
$$

Appendix D

Equations of Motion

This appendix presents a detailed derivation of the equations of motion for Scout I during both the front and back leg support cases. The notations used were defined in Figure (3.2) and Table (3.1).

D.1 Back Leg Support

Using the Lagrange technique, the equations of motion for the back leg support phase were derived.

$$\mathbf{x}_2 = \begin{bmatrix} l\cos(\theta+\phi_2) + L\cos(\theta) - H\sin(\theta) \\ l\sin(\theta+\phi_2) + L\sin(\theta) + H\cos(\theta) \end{bmatrix}$$

$$\dot{\mathbf{x}}_2 = \begin{bmatrix} -l(\dot{\theta}+\dot{\phi}_2)\sin(\theta+\phi_2) - L\dot{\theta}\sin(\theta) - H\dot{\theta}\cos(\theta) \\ l(\dot{\theta}+\dot{\phi}_2)\cos(\theta+\phi_2) + L\dot{\theta}\cos(\theta) - H\dot{\theta}\sin(\theta) \end{bmatrix}$$

$$\begin{aligned} \mathrm{T} &= \frac{1}{2}m\dot{\mathbf{x}}_2^T\dot{\mathbf{x}}_2 + \frac{1}{2}mr^2\dot{\theta}^2 \\ &= \frac{1}{2}m\Big[[l^2+L^2+H^2+r^2+2Ll\cos(\phi_2)+2Hl\sin(\phi_2)]\dot{\theta}^2 + l^2\dot{\phi}_2^2 \\ &\quad +2l[l+L\cos(\phi_2)+H\sin(\phi_2)]\dot{\theta}\dot{\phi}_2\Big] \end{aligned}$$

$$
\begin{aligned}
\mathrm{V} &= mg[l\sin(\theta+\phi_2) + L\sin(\theta) + H\cos(\theta)] \\
\mathcal{L} &= \mathrm{T} - \mathrm{V}
\end{aligned}
$$

$$
\begin{aligned}
\frac{\partial \mathcal{L}}{\partial \dot{\theta}} &= m\Big[[l^2 + L^2 + H^2 + r^2 + 2Ll\cos(\phi_2) + 2Hl\sin(\phi_2)]\dot{\theta} \\
&\quad + l[l + L\cos(\phi_2) + H\sin(\phi_2)]\dot{\phi}_2\Big] \\
\frac{\partial \mathcal{L}}{\partial \dot{\phi}_2} &= m\Big[l^2\dot{\phi}_2 + l[l + L\cos(\phi_2) + H\sin(\phi_2)]\dot{\theta}\Big] \\
\frac{d}{dt}\frac{\partial \mathcal{L}}{\partial \dot{\theta}} &= m\Big[[l^2 + L^2 + H^2 + r^2 + 2Ll\cos(\phi_2) + 2Hl\sin(\phi_2)]\ddot{\theta} - 2l[L\sin(\phi_2) - H\cos(\phi_2)]\dot{\theta}\dot{\phi}_2 \\
&\quad + l[l + L\cos(\phi_2) + H\sin(\phi_2)]\ddot{\phi}_2 - l[L\sin(\phi_2) - H\cos(\phi_2)]\dot{\phi}_2^2\Big] \\
\frac{d}{dt}\frac{\partial \mathcal{L}}{\partial \dot{\phi}_2} &= m\Big[l^2\ddot{\phi}_2 + l[l + L\cos(\phi_2) + H\sin(\phi_2)]\ddot{\theta} - l[L\sin(\phi_2) - H\cos(\phi_2)]\dot{\theta}\dot{\phi}_2\Big] \\
\frac{\partial \mathcal{L}}{\partial \theta} &= mg[-l\cos(\theta+\phi_2) - L\cos(\theta) + H\sin(\theta)] \\
\frac{\partial \mathcal{L}}{\partial \phi_2} &= ml\Big[[-L\sin(\phi_2) + H\cos(\phi_2)]\dot{\theta}^2 - [L\sin(\phi_2) - H\cos(\phi_2)]\dot{\theta}\dot{\phi}_2 - g\cos(\theta+\phi_2)\Big]
\end{aligned}
$$

Thus the equations of motion for the back leg support phase were found to be

$$
\begin{aligned}
&[l^2 + L^2 + H^2 + r^2 + 2Ll\cos(\phi_2) + 2Hl\sin(\phi_2)]\ddot{\theta} \\
&+l[l + L\cos(\phi_2) + H\sin(\phi_2)]\ddot{\phi}_2 - 2l[L\sin(\phi_2) - H\cos(\phi_2)]\dot{\theta}\dot{\phi}_2 \\
&+l[-L\sin(\phi_2) + H\cos(\phi_2)]\dot{\phi}_2^2 \\
&+g[l\cos(\theta+\phi_2) + L\cos(\theta) - Hsin(\theta)] = 0 \qquad \text{(D.1)}
\end{aligned}
$$

$$
\begin{aligned}
&l^2\ddot{\phi}_2 + l[l + L\cos(\phi_2) + H\sin(\phi_2)]\ddot{\theta} \\
&+l[L\sin(\phi_2) - Hcos(\phi_2)]\dot{\theta}^2 + gl\cos(\theta+\phi_2) = \frac{\tau_2}{m} \qquad \text{(D.2)}
\end{aligned}
$$

D.2 Front Leg Support

The above procedure was repeated for the front leg support phase, allowing the equations of motion for this phase to be derived.

$$\mathbf{x}_1 = \begin{bmatrix} l\cos(\theta+\phi_1) - L\cos(\theta) - H\sin(\theta) \\ l\sin(\theta+\phi_1) - L\sin(\theta) + H\cos(\theta) \end{bmatrix}$$

$$\dot{\mathbf{x}}_1 = \begin{bmatrix} -l(\dot\theta+\dot\phi_1)\sin(\theta+\phi_1) + L\dot\theta\sin(\theta) - H\dot\theta\cos(\theta) \\ l(\dot\theta+\dot\phi_1)\cos(\theta+\phi_1) - L\dot\theta\cos(\theta) - H\dot\theta\sin(\theta) \end{bmatrix}$$

$$\begin{aligned} \mathrm{T} &= \frac{1}{2}m\dot{\mathbf{x}}_1^T\dot{\mathbf{x}}_1 + \frac{1}{2}mr^2\dot\theta^2 \\ &= \frac{1}{2}m\Big[[l^2+L^2+H^2+r^2-2Ll\cos(\phi_1)+2Hl\sin(\phi_1)]\dot\theta^2 \\ &\quad +l^2\dot\phi_1^2 + 2l[l - L\cos(\phi_1)+H\sin(\phi_1)]\dot\theta\dot\phi_1\Big] \\ \mathrm{V} &= mg[l\sin(\theta+\phi_1) - L\sin(\theta) + H\cos(\theta)] \\ \mathcal{L} &= \mathrm{T} - \mathrm{V} \end{aligned}$$

$$\begin{aligned} \frac{\partial\mathcal{L}}{\partial\dot\theta} &= m\Big[[l^2+L^2+H^2+r^2-2Ll\cos(\phi_1)+2Hl\sin(\phi_1)]\dot\theta \\ &\quad +l[l - L\cos(\phi_1)+H\sin(\phi_1)]\dot\phi_1\Big] \\ \frac{\partial\mathcal{L}}{\partial\dot\phi_1} &= m\Big[l^2\dot\phi_1 + l[l - L\cos(\phi_1)+H\sin(\phi_1)]\dot\theta\Big] \\ \frac{d}{dt}\frac{\partial\mathcal{L}}{\partial\dot\theta} &= m\Big[[l^2+L^2+H^2+r^2-2Ll\cos(\phi_1)+2Hl\sin(\phi_1)]\ddot\theta + 2l[L\sin(\phi_1)+H\cos(\phi_1)]\dot\theta\dot\phi_1 \\ &\quad +l[l - L\cos(\phi_1)+H\sin(\phi_1)]\ddot\phi_1 + l[L\sin(\phi_1)+H\cos(\phi_1)]\dot\phi_1^2\Big] \\ \frac{d}{dt}\frac{\partial\mathcal{L}}{\partial\dot\phi_1} &= m\Big[l^2\ddot\phi_1 + l[l - L\cos(\phi_1)+H\sin(\phi_1)]\ddot\theta + l[L\sin(\phi_1)+H\cos(\phi_1)]\dot\theta\dot\phi_1\Big] \\ \frac{\partial\mathcal{L}}{\partial\theta} &= mg[-l\cos(\theta+\phi_1) + L\cos(\theta) + H\sin(\theta)] \\ \frac{\partial\mathcal{L}}{\partial\phi_1} &= ml\Big[[L\sin(\phi_1)+H\cos(\phi_1)]\dot\theta^2 + [L\sin(\phi_1)+H\cos(\phi_1)]\dot\theta\dot\phi_1 - g\cos(\theta+\phi_1)\Big] \end{aligned}$$

Thus the equations of motion for the front leg support phase were found to be

$$\begin{aligned}
&[l^2 + L^2 + H^2 + r^2 - 2Ll\cos(\phi_1) + 2Hl\sin(\phi_1)]\ddot{\theta} \\
&+l[l - L\cos(\phi_1) + H\sin(\phi_1)]\ddot{\phi}_1 + 2l[L\sin(\phi_1) + H\cos(\phi_1)]\dot{\theta}\dot{\phi}_1 \\
&+l[L\sin(\phi_1) + H\cos(\phi_1)]\dot{\phi}_1^2 \\
&+g[l\cos(\theta + \phi_1) - L\cos(\theta) - H\sin(\theta)] = 0 \qquad \text{(D.3)}
\end{aligned}$$

$$\begin{aligned}
&l^2\ddot{\phi}_1 + l[l - L\cos(\phi_1) + H\sin(\phi_1)]\ddot{\theta} \\
&-l[L\sin(\phi_1) + H\cos(\phi_1)]\dot{\theta}^2 + gl\cos(\theta + \phi_1) = \frac{\tau_1}{m} \qquad \text{(D.4)}
\end{aligned}$$

Appendix E

Impact Models

This appendix presents a detailed derivation of the impact equations for Scout I during the transfer of support from the front to back and back to front legs. The notations used were defined in Figure (3.2) and Tables (3.1) and (3.2).

E.1 Back Leg Impact

From Meriam and Kraige [29], the angular momentum of a body about a fixed point O was

$$\mathbf{I}\omega + \mathbf{r} \times \mathbf{mv}.$$

Thus, the angular momentums of the planar Scout I model just before and just after back leg impact were

$$\begin{aligned} H^- &= I\dot{\theta}^{B-} + m(x_2\dot{z}_1 - \dot{x}_1 z_2) \\ &= m\Big[[r^2 - L^2 + H^2 + l^2\cos(\phi_1^B - \phi_2^B) + Ll[\cos(\phi_1^B) - \cos(\phi_2^B)] \\ &\quad + Hl[\sin(\phi_1^B) + \sin(\phi_2^B)]]\dot{\theta}^{B-} + l[l\cos(\phi_1^B - \phi_2^B) + L\cos(\phi_1^B) + H\sin(\phi_1^B)]\dot{\phi}_1^B\Big] \\ H^+ &= I\dot{\theta}^{B+} + m(x_2\dot{z}_2 - \dot{x}_2 z_2) \end{aligned}$$

$$= m\left[[r^2 + l^2 + L^2 + H^2 + 2Ll\cos(\phi_2^B) + 2Hl\sin(\phi_2^B)]\dot{\theta}^{B+} + l[l + L\cos(\phi_2^B) + H\sin(\phi_2^B)]\dot{\phi}_2^B\right].$$

Assuming that angular momentum was conserved at impact, then $H^- = H^+$ and the back impact was governed by

$$\begin{aligned}\left[r^2 - L^2 + H^2 + l^2\cos(\phi_1^B - \phi_2^B) + Ll[\cos(\phi_1^B) - \cos(\phi_2^B)] + Hl[\sin(\phi_1^B) + \sin(\phi_2^B)]\right]\dot{\theta}^{B-} \\ + l[l\cos(\phi_1^B - \phi_2^B) + L\cos(\phi_1^B) + H\sin(\phi_1^B)]\dot{\phi}_1^B = \\ \left[r^2 + L^2 + H^2 + l^2 + 2l[L\cos(\phi_2^B) + H\sin(\phi_2^B)]\right]\dot{\theta}^{B+} \\ + l[l + L\cos(\phi_2^B) + H\sin(\phi_2^B)]\dot{\phi}_2^B.\end{aligned} \tag{E.1}$$

E.2 Front Leg Impact

The momentum transfer equation for the front leg impact was derived in a similar manner. The angular momentums just before and just after front leg impact were

$$\begin{aligned}H^- &= I\dot{\theta}^{F-} + m(x_1\dot{z}_2 - \dot{x}_2 z_1) \\ &= m\left[[r^2 - L^2 + H^2 + l^2\cos(\phi_1^F - \phi_2^F) + Ll[\cos(\phi_1^F) - \cos(\phi_2^F)]\right. \\ &\quad \left. + Hl[\sin(\phi_1^F) + \sin(\phi_2^F)]]\dot{\theta}^{F-} + l[l\cos(\phi_1^F - \phi_2^F) - L\cos(\phi_2^F) + H\sin(\phi_2^F)]\dot{\phi}_2^F\right] \\ H^+ &= I\dot{\theta}^{F+} + m(x_1\dot{z}_1 - \dot{x}_1 z_1) \\ &= m\left[[r^2 + l^2 + L^2 + H^2 - 2Ll\cos(\phi_1^F) + 2Hl\sin(\phi_1^F)]\dot{\theta}^{F+}\right. \\ &\quad \left. + l[l - L\cos(\phi_1^F) + H\sin(\phi_1^F)]\dot{\phi}_1^F\right].\end{aligned}$$

With $H^- = H^+$, the impact was found to be governed by

$$\left[r^2 - L^2 + H^2 + l^2\cos(\phi_1^F - \phi_2^F) + Ll[\cos(\phi_1^F) - \cos(\phi_2^F)] + Hl[\sin(\phi_1^F) + \sin(\phi_2^F)]\right]\dot{\theta}^{F-}$$
$$+l[l\cos(\phi_1^F - \phi_2^F) - L\cos(\phi_2^F) + H\sin(\phi_2^F)]\dot{\phi}_2^F =$$
$$\left[r^2 + L^2 + H^2 + l^2 - 2l[L\cos(\phi_1^F) - H\sin(\phi_1^F)]\right]\dot{\theta}^{F+}$$
$$+l[l - L\cos(\phi_1^F) + H\sin(\phi_1^F)]\dot{\phi}_1^F. \tag{E.2}$$